Novel Electroanalytical Methods.

By

John O'Gorman

A Thesis Presented to

Dublin City University

for the award of MSc.

Prepared under the supervision of Dr. John Cassidy,

School of Chemistry, Dublin Institute of Technology, Kevin Street.

October 1998.

To my father

Declaration:

I hereby certify that this material, which I now submit for assessment on the programme of study leading to the award of M.Sc. is entirely my own work and has not been taken from the work of others save and to the extent that such work has been cited and acknowledged within the text of this work.

Signed: John O'Gorman ID No.:_____

Date: 16/10/98

Novel Electroanalytical Methods

John O'Gorman.

Abstract

This work involves the characterisation of novel electroanalytical techniques, and the combined use of these and more standard methods in studying different electrochemical systems. Ferrocene carboxylic acid (FCA) was studied extensively using cyclic voltammetry, rotating disk electrochemistry, differential pulse voltammetry, a microelectrode, UV-Vis and I.R. spectroelectrochemistry, and convolution.

In chapter 2, various qualitative and quantitative studies were performed on aqueous solutions of FCA using the above techniques in an effort to explain the occurrence of an oxidation post-peak in the cyclic voltammogram. It was found that the conditions necessary for the post-peak to occur were; high pH (>9), and the presence of oxygen. Although attempts to gain spectral characterisation of the species responsible were unsuccessful, it is proposed that the post-peak is a result of the oxidation of oxygen to ozone - a reaction which is mediated by the ferrocene carboxylate.

In chapter 3, a three-electrode electrochemical cell with a platinum microelectrode of radius 5×10^{-6}m as the working electrode was used for the study of ferrocyanide. This system was examined using both direct and differential pulse voltammetry experiments. Theory was postulated for applying a differential pulse waveform to a microelectrode and simulations were carried out and compared with the experimental results. While Cottrell behaviour was assumed for the first set of simulations, it later became necessary to modify the theory to allow for a steady state current occurring at the microelectrode after the pulse. This modified theory concurred well with the experimental results, and the sensitivity of the experiment was found to be $8.1\times10^{-7}\,AM^{-1}$, while that predicted from the simulations was $8.4\times10^{-7}\,AM^{-1}$. Concentrations as low as 5×10^{-5}M $\left[Fe(CN)_6\right]^{4-}$ were clearly observed.

In chapter 4, a ferrocyanide system was examined using both direct and differential pulse voltammetry experiments at a rotating disk electrode. Two theoretical models were postulated for applying a differential pulse waveform to a rotating disk electrode, and simulations were carried out and compared with the experimental results. It was found that Model 1 applies when pulse widths are short and/or when rotation rates are low, and conversely, Model 2 applies when pulse widths are long and/or when rotation rates are high. In this case the experimental results seemed to be governed by an overlap of both models.

In chapter 5, the semidifferentiation of cyclic voltammograms for the further elucidation of electrochemical processes was explored, with ferrocyanide and FCA as the analytes. Many simulations were carried out and compared to experimental data. The simulation of a bulk species with a subsequent catalytic current and an irreversible adsorbed species seemed to fit the experimental cyclic voltammogram and semiderivative of FCA in 0.2M Na_2HPO_4/H_2O best. Also in chapter 5, HPLC experiments using an electrochemical detector for the detection of ascorbic acid were carried out. Both direct and differential currents were applied, with the direct current experiments being used as a standard technique for the characterisation of the differential current experiments. Although both techniques did yield peaks for ascorbic acid, a much larger signal was observed for the direct current experiments.

ACKNOWLEDGEMENTS

I would like to thank Dr. John Cassidy for supervising this project, and for all his help and guidance throughout.

I would also like to thank my mother for all the support she has given me over the last two years.

I also wish to thank my girlfriend, Derval, for all her help and encouragement.

I gratefully acknowledge a postgraduate scholarship grant from the Dublin Institute of Technology.

TABLE OF CONTENTS

1 Introduction

1.1 General Introduction

Electrochemistry is a very important tool in the modern world. The ramifications of the subject extend into areas diverse as batteries, fuel cells, clean technology, electrosynthesis of organic and inorganic compounds, semiconductors, material corrosion, conversion and storage of solar energy, effluent re-cycling, biological transfer processes and a wide range of highly specific analytical techniques.

Electrochemistry is, strictly speaking, a branch of surface science as it is specifically concerned with the electrified interface. It is the study of behaviour of surfaces in contact with a liquid and in the presence of an electrical field, and includes the effect of the field on the structural and chemical properties of the interface. The chemical reactivity of the surface as a function of the electrical field is central to the subject of electrochemistry.

Amperometry is one area of electrochemistry which has long been applied to analytical chemistry. This is based on the principle that when a species is oxidised or reduced at an electrode, the resulting current is directly proportional to the concentration of the species. The analytical usefulness of this technique coupled with the developments in potentiometry and polarography, has led to a wide range of instrumental applications for analysis. However Faradaic electrochemistry has long been plagued with problems associated with electrode instability, as many electrochemical processes cause passivation of the electrode surface. The advent of the dropping mercury electrode heralded a new dawn in the world of electrochemistry,

as it provided electrochemists with a renewable electrode surface. Unfortunately the inherent difficulties associated with mercury electrodes (toxicity, liquid and limited potential range), along with the advances made in selective spectroscopic techniques (Atomic Absorption Spectroscopy), caused a decline in interest in Faradic electrochemistry as an analytical tool. However there has been a revival in electroanalysis recently, with the development of new pulsed techniques coupled with increasingly user friendly computer driven equipment. Other important developments include the first enzyme electrode in the late 1960's [1] and the introduction of chemically modified electrodes in the early 1970's [2]. These developments have succeeded in improving the selectivity of analytical techniques by creating analyte – specific surfaces. Hence the concept of tailoring the properties of conventional electrode surfaces has evolved, and this has helped in the reestablishment of electrochemistry as a powerful analytical tool. Also, the financial rewards reaped from commercial applications of chemical and biological sensors, have fuelled modified electrode research.

There are many popular voltammetric methods for analysis, which involve different types of applied waveforms and cell configurations. Perhaps the simplest applied waveform is that of the potential step in chronoamperometry. This is a useful technique for ascertaining the electrode area, A, as when the magnitude of the current is plotted against $1/\sqrt{t}$ the slope of this line is directly proportional to A. Linear sweep voltammetry involves the application of a regularly changing waveform to the working electrode. The potential is swept in a positive/negative direction, and when a certain species in solution is oxidised/reduced at the working electrode, the current begins to decay. Thus a peak current appears when a linear potential profile is applied

to a stationary electrode in solution. This technique can be used for analytical purposes, as the peak current is proportional to concentration.

Furthermore it is possible to apply a reverse potential ramp in order to re-reduce/re-oxidise an oxidised/reduced species for a reversible system. This is termed cyclic voltammetry (see section 1.3.1) and is useful in obtaining important information about a redox couple. However, there is a problem with double layer charging current, which occurs due to the gradual changing of electrode potential. This is also true of linear sweep voltammetry and chronoamperometry.

Another important analytical technique is that of rotating disk electrochemistry (see section 1.3.2). This consists of a linear potential ramp waveform, applied to a rotating disk electrode. However instead of a peak current as in voltammetry, the current reaches a limiting value. This results in a sigmoidal response. This happens due to convective mass transport, where reagent is being continuously swept towards the electrode. This limiting, or steady-state, current is directly proportional to $\sqrt{\omega}$, where ω is the rotation rate and concentration of electroactive species in solution. The rotating disk electrode may also be used for the measurement of heterogeneous rate constants.

DC polarography is another popular method of electroanalysis [3] and, as mentioned above, its arrival was seen as a major breakthrough in electrochemistry. In fact Heyrovsky received the Nobel Prize for pioneering the method. This method consists of a linear potential ramp applied to a dropping mercury electrode. New drops of mercury enter the analyte solution at regular time intervals and these help to stir the solution continuously, which results in the direct current (DC) response taking a sigmoidal shape, as in the case of rotating disk electrochemistry. There are several

advantages associated with the use of mercury for trace metal analysis. Firstly, as each drop appears the electrode surface is new and well defined, unlike at solid electrodes which may contain surface oxides and frequently need to be pre-treated before use. Secondly, the reduction and subsequent deposition of trace metals on a solid electrode requires a nucleation step, whereas for a range of heavy metal cations such as Cd^{2+}, Cu^{2+} and Pb^{2+}, the reduced form of the metal dissolves in the mercury, forming an amalgam. This is a much simpler process and more reproducible current profiles are obtained. Another advantage is that it is difficult to reduce H^{+} at mercury, and this makes the analysis of metals in acidic solutions possible. However there are a number of problems associated with the use of mercury as an electrode material. These include its reasonably high vapour pressure, clogging of the capillary, and the presence of non-faradaic 'peak maxima' currents. Furthermore, as each drop enters the analyte solution, a new double layer has to be formed. This results in a high residual current, which limits the detection limit of this technique. Lastly, there is also the difficulty of measuring the limiting currents at low analyte concentrations and sloping baselines. The original technique has been modified by the use of pulse waveforms to lower the detection limit [4].

As mentioned above there is a large residual current in polarography due to the new double layer required for each drop. Pulse methods have since been developed to discriminate against the double layer charging current and thus improve the sensitivity of the technique. This is done by taking advantage of the fact that the time scale to form the double layer is much shorter than that of the faradaic current, as is shown in figure 1.1. Also, as each drop grows the magnitude of the faradaic current increases due to the larger surface area.

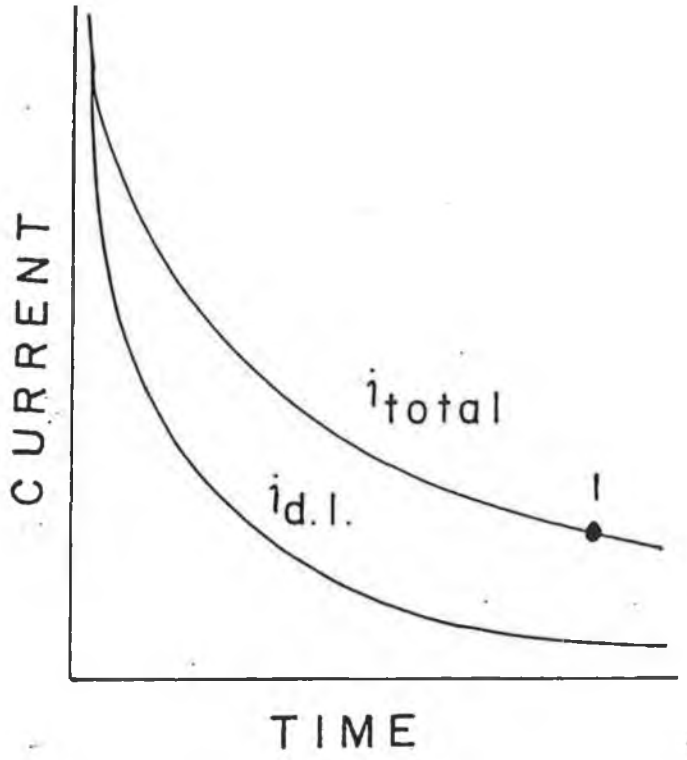

Figure 1.1: The decay in total current (i_{total}) and double layer charging current ($i_{d..l.}$) after the application of a potential step. When the current is sampled at the point 1, there is very little contribution from the double layer charging current. This fact is used widely in pulse techniques to achieve lower limits of detection.

Normal pulse polarography (NPP) involves applying a slightly more complicated waveform than a linear ramp. Pulses are applied in phase with the drop lifetime. The current is then sampled at a point long enough after the pulse is applied to allow the double layer charging to decay and the faradaic contribution to dominate. The current is also sampled at the end of the drop lifetime - when the drop area is largest, unlike in polarography, where the current is monitored continuously giving rise to noise that has to be filtered out. In addition to its use with the dropping mercury electrode, this waveform has been employed at microelectrodes for *in vivo* analysis as the applied pulses serve to clean the electrode from the interference caused by adsorbed organic species [5].

Another important pulse method – differential pulse polarography (DPP), involves the application of a series of pulses to a slowly increasing linear potential ramp. Like NPP, the pulses are in phase with the drop lifetime and the current is sampled at two points on the waveform; once just before the pulse is applied and again at a sufficient time interval after the pulse has been applied. The main advantage over DC polarography that DPP shares with other pulse methods is that there is little double layer charging contribution to the overall response, which allows the achievement of a lower detection limit. An advantage that DPP has over both DC polarography and other pulse methods is that due to the differential measurement sequence, the output of this technique takes the form of a symmetrical peak, which is more useful from an analytical perspective.

Staircase and square wave voltammetry techniques have been used extensively for solid electrodes. The staircase voltammetric method involves the application of a digitised linear ramp. The advantage of this technique over cyclic voltammetry is that

discrimination against double layer charging can be achieved by sampling the current at a short time interval after the step has been applied, as can be seen in figure 1.2(a). Under conditions where the pulse width and the height of the potential step are small, the current response for this technique is identical to that of linear scan voltammetry. This technique has been used for analysis in flowing streams and in liquid chromatography. Square wave voltammetry is an allied technique where the waveform is shown in figure 1.2(b). Currents can be sampled at points 1 and 2, and either these or the difference between them can be used as the response. Rather than being a ramp based technique it is closer to a digitised step (figure 1.2(a)), with increasing and decreasing pulses. This technique has been used at small solid electrodes, or at a dropping mercury electrode [6]. Square wave voltammetry is one of the fastest techniques compared to differential and normal pulse methods. Indeed the application of complex waveforms under computer control has progressed to the extent that most of the problems associated with these techniques are due to mercury delivery and cell design.

Stripping methods such as anodic stripping voltammetry are often employed to achieve a lower detection limit. This technique accumulates metal as amalgams into a hanging mercury drop or a mercury film. By subsequently applying one of the waveforms mentioned above, the metal can be stripped out. Rather than using mercury it is possible to accumulate the analyte in a coating on the electrode surface by depositing a polycationic/polyanionic layer on the electrode surface. Direct adsorption of particular compounds can also be used to accumulate them on electrode surfaces where then can be subsequently oxidised. Very low concentrations of amalgam forming metals can be detected using stripping methods (as low as 10^{-10}mol dm^{-3}) [7].

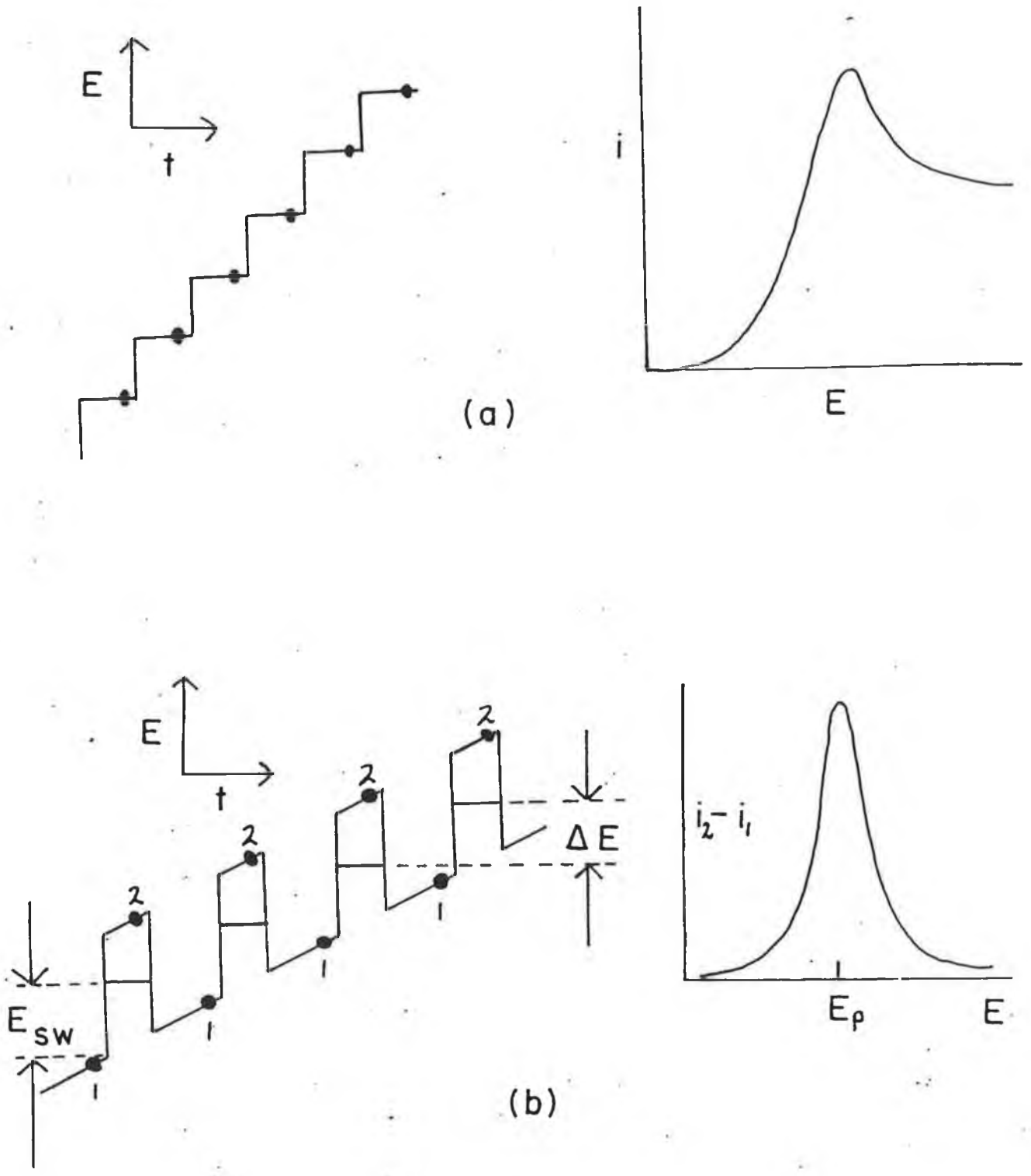

Figure 1.2: (a) Staircase voltammetry. Note that the resulting current is not symmetrical as in the case of linear scan voltammetry. (b) Square wave voltammetry. E_{SW} is the applied pulse amplitude (up and down) to a staircase voltammetric waveform where ΔE is the regularly increasing step in potential. The difference between the current sampled at the point 2 and at the point 1 results in a symmetrical waveform.

Electroanalysis in flowing streams is an important area in which amperometric methods of detection can be applied. Electrochemical detectors in flowing streams such as in flow injection analysis (FIA), or high performance liquid chromatography (HPLC) may be used to detect a wider range of compounds than UV-Visible methods. Flow injection analysis involves the introduction of a sample into a carrier of reagent, which allows the analysis of a certain analyte in the plug. It is a very simple technique and is easily adaptable to portable instruments. The cell configuration may take the form of a thin layer or a wall jet where the effluent from the column impinges perpendicularly onto the surface of the working electrode. The thin layer planar electrode configuration is normally operated at a constant potential in order to prevent the occurrence of a double layer charging current. Recent advances in this area have been centred around the use of coated electrodes in order to enhance selectivity. For example Nafion may be used to selectively exclude anions and include cations from a flowing stream [8]. In a wall jet configuration the sensitivity depends on the working electrode area to nozzle diameter ratio [9]. Steroids and copper have been detected using this configuration [10]. Also, reticulated vitreous carbon electrodes have been shown to yield an enhanced signal to noise ratio compared to planar electrodes, when used in a flow injection analysis configuration [11].

Pulsed amperometric detection involves the use of cleaning desorption waveforms on a regular basis as shown in figure 1.3. E_2 and E_3 are used for cleaning and the signal is accumulated at E_1. The current may be sampled (a), or integrated (b), or integrated over a small cyclic ramp as shown in (c). Species may be determined at bare electrodes or else by adsorption at oxide coated electrodes. These two methods depend on the choice of E_2. This waveform can be applied at a high enough frequency to be used as a detector in HPLC. The waveform in figure 1.3(c) is termed

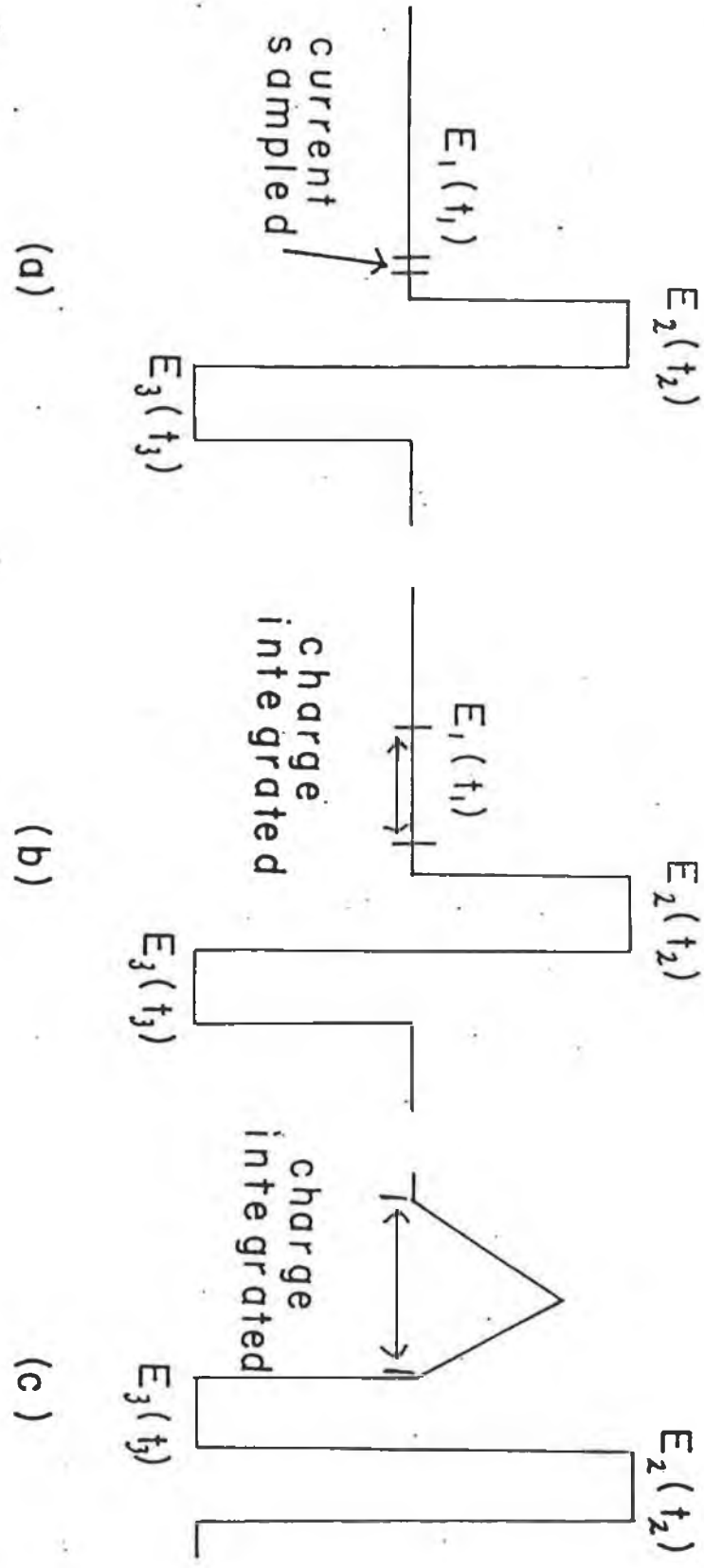

Figure 1.3: (a) Pulsed amperometric detection (PAD). The current is sampled towards the end of E_1. (b) The current is integrated over a short time at E_1. (c) The current is integrated while the cyclic scan is being applied.

integrated pulsed amperometric detection (IPAD) and this technique is more sensitive than PAD. Both are useful means of detection in HPLC where UV-Visible spectroscopy is inadequate.

Technological advances in electrode construction have opened up many new possibilities in the field of electroanalysis. The ability to make tiny electrodes such as microelectrodes has made living cell *in vivo* analysis possible. They can be used in a two-electrode configuration with a conventional sized reference electrode. As a microelectrode's electrochemical area is so small, the current output will also be tiny and therefore will not significantly change the composition of the reference electrode, and consequently there will be no significant potential drop through the solution. Another advantage of the microelectrode over the macroelectrode is that it has a greater faradaic to double layer charging current ratio. Difficulties associated with microelectrodes include the requirement for a low noise means of current measurement along with practical problems of polishing and manipulation.

There have been many unusual applications of microelectrodes, e.g. the use of microelectrodes in recent studies aimed at time-resolved probing of processes (e.g. secretion) in single cells [12], the in-vivo monitoring of neurochemical events (e.g. stimulated dopamine release), or high resolution characterisation of surfaces as in scanning probe microscopy.

Arrays of microelectrodes can exploit further the enhanced diffusion as well as being capable of providing a greater and more easily measurable current. They have also been used as detectors in HPLC and FIA [13, 14].

This work is concerned with the use of amperometric methods of detection in electroanalysis. The two main methods of detection used were cyclic voltammetry

and rotating disk electrochemistry, and these are discussed in detail in sections 1.3.1 and 1.3.2 respectively. Chapter 2 deals mainly with the use of cyclic voltammetry for the characterisation of the electrochemical reactions of ferrocenecarboxylic acid (FCA), occurring both at the electrode and in bulk solution, between the potential limits applied. The rotating disk electrode is also employed in studying the mediation of ascorbic acid oxidation by FCA, which is incorporated in a polymer coating on the electrode surface. Chapters 3 and 4 are concerned with the characterisation of the response from the application of differential pulse voltammetry to the microelectrode and rotating disk electrode respectively, with ferrocyanide as the model analyte. In chapter 5 the advantages of using convolution for the further elucidation of cyclic voltammograms are explored, with both ferrocyanide and FCA as the analytes. Also in chapter 5, ascorbic acid is used as the analyte in comparing the analytical usefulness of direct current and differential pulse HPLC experiments, using an electrochemical detector.

1.2 General Electrochemical Introduction

This section of the introduction is concerned with providing the reader with an insight into some of the fundamentals of electrochemistry.

1.2.1 Electrochemical reactions and measurements

Electrochemical measurements may be made on a system for a number of reasons. These include the analysis of a solution for traces of metal ions or organic species, the gathering of thermodynamic or kinetic data on a certain reaction, the generation of an intermediate or the electrosynthesis of a product of interest. All of these processes

require an understanding of the basic principles of electrode reactions and the electrical properties of electrode/solution interfaces.

In order to understand the two main applications of electrochemistry for analysis, it is necessary to understand what happens when an electrode is placed in an electrolyte solution. However before discussing this, the term potential (E) must be defined. The potential of a solution containing both the oxidised (Ox) and reduced (Red) forms of a redox couple, is simply represented by the Nernst equation, which is shown in equation 1.1.

$$E = E^{0'} + \frac{RT}{nF} \ln\left\{\frac{[Ox]}{[Red]}\right\} \qquad 1.1$$

where $E^{0'}$ is the formal potential, which is characteristic of each particular redox couple and all the other symbols have their usual meaning.

In potentiometric experiments, the current is equal to zero and potential is determined as a function of concentration. As no current flows in the experiment, no net faradaic reaction occurs. When there is zero current the Nernst equation applies. Potentiometry (the relation of potential to analyte concentration) suffers from the problem of specificity. The potential of a solution with a mixture of two couples would be averaged out since it depends on both couples. In order to introduce a degree of selectivity, the interfacial potential difference can be measured across an ion selective membrane using a pair of reference electrodes [15].

Rather than obtaining analytical information from a system at equilibrium, as described in potentiometry, the concentration of analyte can be determined by relating it to the number of electrons transferred across an electrode solution interface as

current. Shifting the equilibrium of the system generates this current. For example, consider the following reaction for ferrocene, Fc.

$$Fc^{+} + e^{-} \leftrightarrow Fc^{0} \qquad E^{\circ'} \qquad 1.2.$$

It is possible to shift this reaction to the left by applying a potential more positive than that of the formal potential to the working electrode. The resulting current is directly proportional to the concentration of ferrocene. However this approach introduces its own difficulties as the analyte is consumed at the electrode as can be seen in figure 1.4. When such a potential is applied to the electrode, any ferrocene close to the electrode will be oxidised, and the current will decay gradually with time as all the ferrocene close to the electrode is consumed. Therefore at first sight this technique does not seem to be analytically useful, as the current decreases with time.

In order to relate current to concentration the following two limiting cases are considered. When ferrocene is oxidised at an electrode, either the kinetics of electron transfer at the electrode, or mass transport of ferrocene towards the electrode surface, or both may limit the current. It is possible to develop an equation for current under conditions where the kinetics is the rate-determining step. This is represented as the net current difference between cathodic and anodic processes: $i = i_{cathodic} - i_{anodic}$. This may be expanded to give equation 1.3.

$$i = nFAk^{0}\left\{\exp\left(\frac{-\alpha nF\left(E - E^{0'}\right)}{RT}\right)C_{o}(0,t) - \exp\left(\frac{(1-\alpha)nF\left(E - E^{0'}\right)}{RT}\right)C_{r}(0,t)\right\} \qquad 1.3$$

where k^0 is the standard heterogeneous rate constant for the redox process at the electrode surface, α is the transfer coefficient which is a measure of how the applied

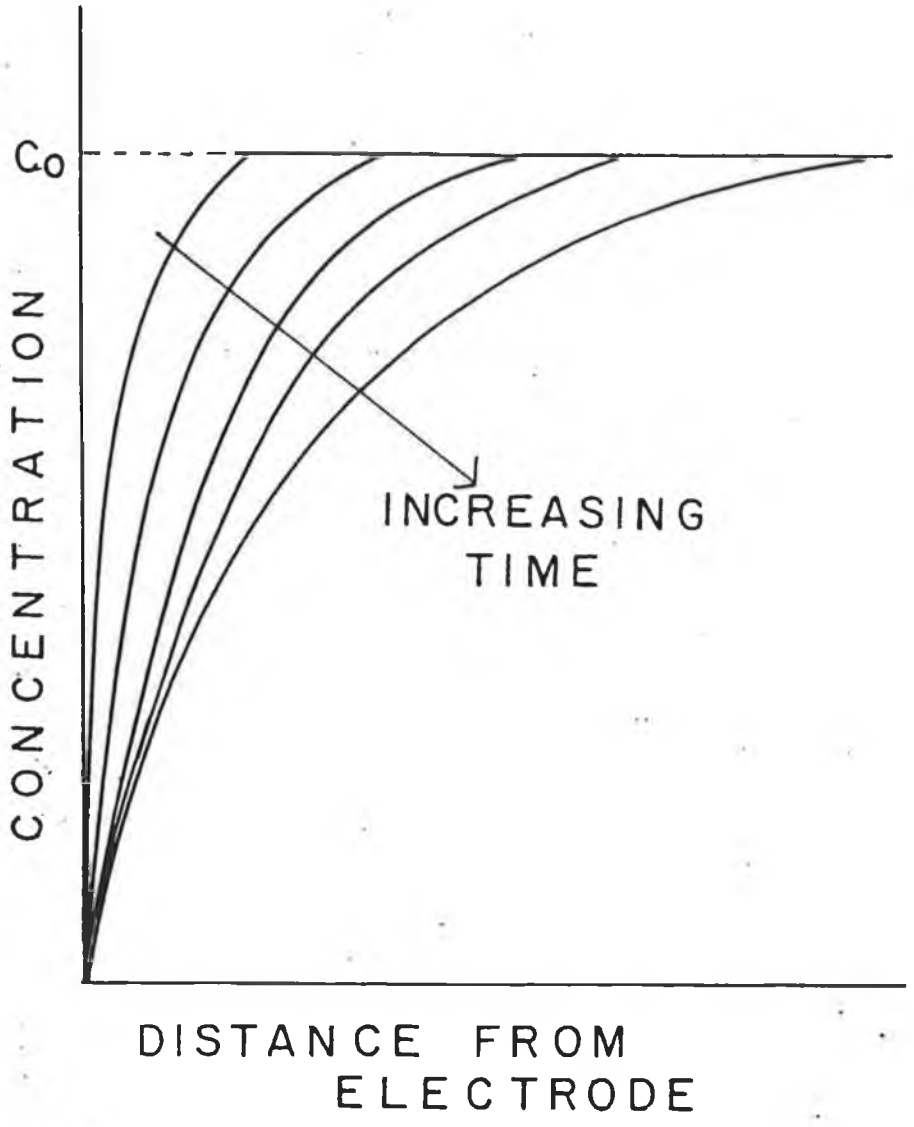

Figure 1.4: Representation of concentration distance profiles when a potential step is applied so that the concentration of ferrocene at the electrode surface falls to zero. This leads to a difference in concentration, and the ferrocene diffuses in from bulk solution to remove this concentration difference. Over a period of time this process can be seen as an expanding depletion (or diffusion) layer.

potential is helping the forward reaction and hindering the backward reaction, C(x,t) is the general term for concentration at a distance x from the electrode at time t, o and r represent the oxidised and reduced states, and all the other symbols have their usual meaning. Both the magnitude of $E - E^{0'}$ and the value of k^0 (which is characteristic of the analyte and the electrode) are important in determining the rate of electron transfer at the electrode. Equation 1.3 contains information about whether the current is limited by kinetics or mass transport of analyte. Mass transport limits the current when k^0 is sufficiently large, or when the value of E is such that the rate of reaction is sufficiently high. This can be controlled experimentally, and under these conditions the current is given by the following equation.

$$i = nFAD \left.\frac{dC}{dx}\right|_{x=0} \qquad 1.4$$

Here the derivative term represents the slope of the concentration profile at the electrode surface. This derivative term may be thought of as the tangent of the concentration distance plot at the electrode surface. D, the diffusion coefficient, is a constant characteristic of the analyte, which usually takes a value between 10^{-6} and 10^{-5} cm^2 sec^{-1}.

There are two types of processes which occur at electrodes. In one type, electrons are transferred across the metal/solution interface. This electron transfer causes oxidation or reduction to occur. These reactions are governed by Faraday's law and hence are termed faradaic processes. Some reactions are thermodynamically or kinetically unfavourable and as such no charge transfer will occur. Processes such as adsorption and desorption can occur however, and the structure of the solution/electrode interface

can change with changing potential or solution composition. These processes are termed non-faradaic processes.

1.2.2 Electrochemical cells and cell configurations

When the potential of an electrode of interest is measured against a non-polarizable reference electrode, a voltage drop of iRs, by Ohm's Law, is observed during the passing of current. Rs is the resistance of the solution which lies between the two electrodes, and is therefore dependent on the distance between the electrodes.

The simplest electrode system is the two–electrode system. This consists of a working electrode and a reference electrode and works reasonably well for aqueous polarography, where Rs is low and the current is small. If non-aqueous solvents are used or if the experiment generates a large current, iRs drop can become a serious problem. In these cases it is necessary to switch to a three-electrode configuration. This involves the introduction of a counter or auxiliary electrode. The function of this auxiliary electrode is to act as a sink for any current passed.

The device used to measure the potential difference between the working and reference electrodes must have high input impedance, so that a negligible current is drawn through the reference. This means that the potential of the reference electrode will remain constant, as relatively little current is passed. However even such an arrangement does not remove all of the iRs drop from the reading observed by the potential controlling device (potentiostat). For the reference electrode placed anywhere but exactly at the working electrode surface, some fraction of iRs, called the uncompensated resistance, will be observed in the measured potential. This can minimised by using a very fine capillary tip called a Luggin capillary.

1.2.3 Factors affecting mass transport

It is routine practice to use the three-electrode configuration in modern electrochemical techniques. Most electrochemical experiments involve mass transport or electrode kinetics, since either or both limit current. There are three forms of mass transport and each one is described below:

1 Migration – this is the transport of ions through an electrical potential gradient. To minimise migration the analyte solution should contain a high concentration of inert electrolyte, called the supporting or background electrolyte. This ensures a nearly constant electric potential throughout the solution.

2 Convection – this is the transport of ions or molecules by mechanical motion of the solution. Convection may occur either through gravity operating on a density gradient or through stirring of the solution or motion of the electrode. Convection can be minimised by maintaining a controlled temperature, or defined by using a rotating disk electrode.

3 Diffusion – this is the transport of ions or molecules through a chemical potential gradient. In stagnant solutions with excess electrolyte, the predominant form of mass transport is diffusion.

1.3 Electrochemical Techniques

1.3.1 Cyclic voltammetry

Cyclic voltammetry is a potential sweep technique, which is commonly used in determining the kinetic parameters of a wide variety of electrochemical systems. It is particularly useful in the area of preliminary mechanistic investigations.

Cyclic voltammetry is an extension of linear sweep voltammetry. This involves applying a potential ramp as a function of time to the working electrode. An "electrochemical spectrum", indicating potentials at which redox processes occur, can be swiftly and easily obtained. In cyclic voltammetry, the potential is cycled between two potentials (measured in volts), and the cell current (measured in amps) is recorded as a function of the applied potential.

To see what form cyclic voltammograms take it is convenient to look at the following reversible reaction, where O and R are soluble solution bound species:

$$O + ne^{-} \leftrightarrow R \qquad E^{\circ`} \tag{1.5}$$

The formal potential, $E^{\circ`}$, is the potential of the cell when

$$\frac{[O]}{[R]} = 1 \tag{1.6}$$

where [O] represents the concentration of species O, and [R] corresponds to the concentration of species R.

The ratio of O:R for a given reversible reaction occurring at the electrode surface, is dictated by the applied potential, E, and given by the Nernst equation [16]. The

region next to the electrode is known as the "Nernst Diffusion Layer". Once reduction of species O occurs due to a negative ramp, this diffusion layer develops and increases in magnitude and begins to extend out into the solution, resulting in a greater distance across which the reactant must travel. As the potential applied is more negative, a stage is reached when the concentration of O at the electrode surface falls to zero. At this stage, increasing thickness of the diffusion layer gives rise to a peak in the cyclic voltammogram, as is shown in figure 1.5. As the potential is swept back, oxidation occurs.

For a reversible system the peak to peak separation, ΔE_p, is approximately 57/n mV at 25°C, where n is equal to the number of electrons transferred. However, uncompensated resistance in the cell may induce a larger ΔE_p than expected. Varying the scan rate has no effect on the peak potential for a reversible system, but does cause a change in the peak current. Randles and Sevcik developed the following equation to relate peak current to scan rate for a reduction process at 25°C [17]:

$$i_p = 2.69 \times 10^5 n^{3/2} A \sqrt{D_O} \sqrt{\nu} C_O \qquad 1.7$$

where i_p = peak current in amps

n = number of electrons transferred

A = electrode area

D_O = diffusion coefficient of species O ($cm^2\ s^{-1}$)

ν = scan rate ($V\ s^{-1}$)

C_O = concentration of electroactive species O ($mol\ cm^{-3}$).

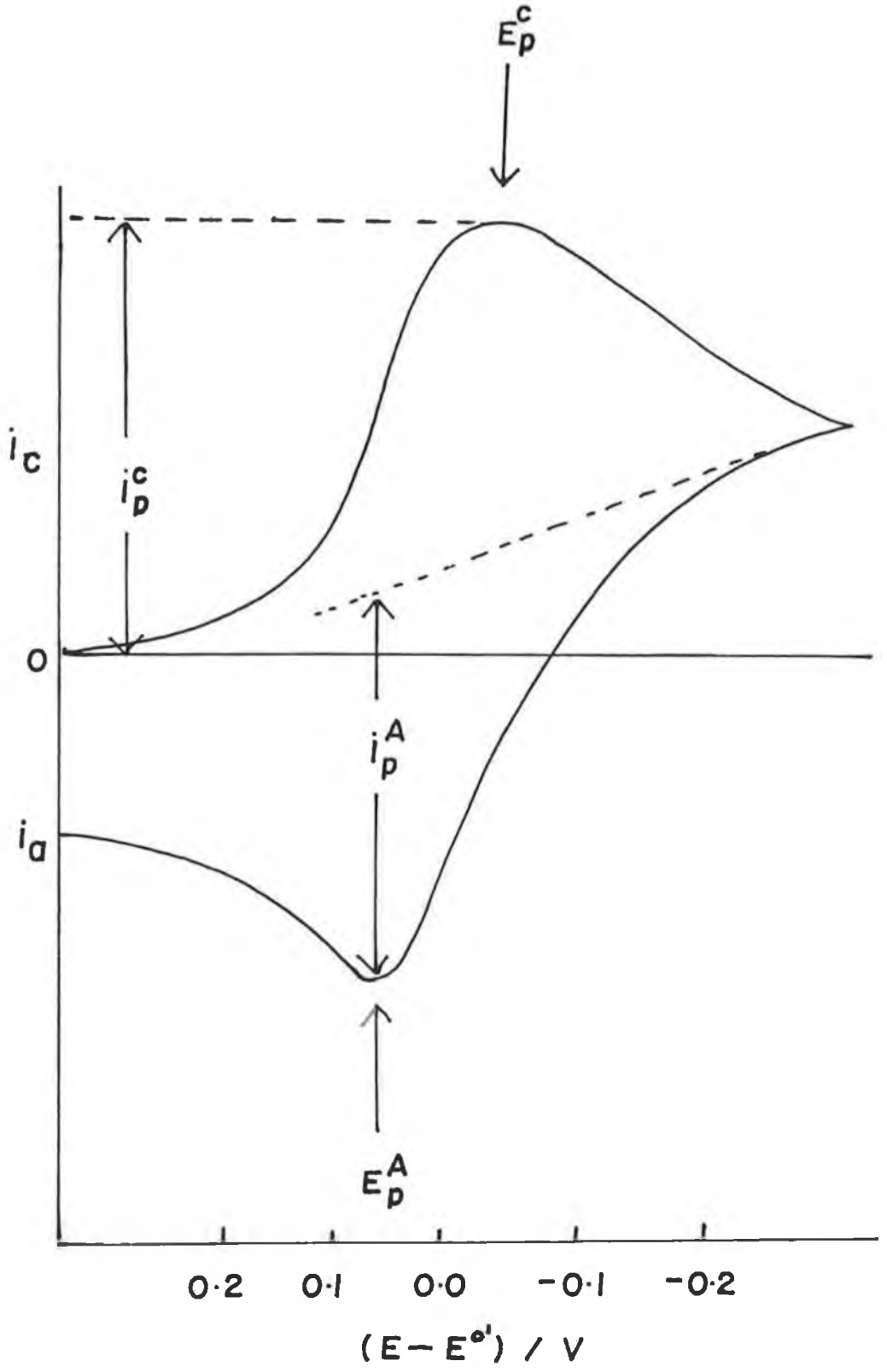

Figure 1.5: Typical cyclic voltammetric response for a reversible electrochemical process, showing the cathodic (i^C_p) and anodic (i^A_p) peak currents and also the cathodic (i^C_p) and anodic (i^A_p) peak potentials.

Nicholson developed a relation between anodic and cathodic peak currents [18]:

$$\frac{i_{pa}}{i_{pc}} = \frac{(i_{pa})_O}{i_{pc}} + 0.485\frac{(i_{sp})_O}{i_{pc}} + 0.086 \qquad 1.8$$

where i_{pa} = anodic peak current

i_{pc} = cathodic peak current

$(i_{pa})_O$ = uncorrected anodic current

$(i_{sp})_O$ = uncorrected current at the switching potential.

Figure 1.5 also illustrates how the anodic and cathodic currents can be determined from a cyclic voltammogram.

For a reversible system, the rate of electron transfer is greater than the rate of mass transport. As a result of this, Nernstian equilibrium is maintained at the electrode surface. As the rate of electron transfer lowers, the electrochemistry is said to be quasi-reversible. For a quasi-reversible system, the peak to peak separation is greater than 57/n mV and it increases with increasing scan rate. Due to the slower kinetics there is a slower rate of change in concentration at the electrode surface. This gives rise to a somewhat broader peak in the cyclic voltammogram of a quasi-reversible system.

The absence of a reverse peak suggests a totally irreversible system. This may be due to a purely irreversible mechanism, or as a result of the product undergoing a further chemical reaction. For a true irreversible mechanism the relationship between the peak current and the scan rate is as follows [19]:

$$i_p = 2.99 \times 10^5 n(\alpha n_a)^{1/2} A\sqrt{D_O}\sqrt{\nu}C_O \qquad 1.9$$

where α = transfer coefficient

n = number of electrons involved in the overall process

n_a = number of electrons involved in the rate determining step

(The other symbols have been defined previously.)

For a given system, more than one set of peaks may appear in the cyclic voltammogram. These systems may be analysed by varying the initial, switching and final potentials. This can facilitate the detection of subsequent reactions, and provide important information on the relationship between peaks in cyclic voltammograms.

The main application of cyclic voltammetry is in the preliminary electrochemical characterisation of a system. Hence, cyclic voltammetry is often the chosen technique in studying a particular system for the first time. Its main advantage is that a cyclic voltammogram provides instant information on the reversibility of a system, and on the potential regions in which the species in question is electrochemically active.

1.3.2 Rotating disk electrochemistry

As the potential is swept past the equilibrium potential, the diffusion layer thickness increases, which results in the diffusion of the analyte towards the electrode surface

becoming longer. The diffusion layer thickness can be maintained at a constant value by rotating the electrode. This results in the forced convection of the analyte in solution. To allow formation of sufficient product to achieve a steady-state, the scan rate must be slow (typically $\leq$ 10mV sec^{-1}). The rotating disk electrode (RDE) is relatively simple to construct. It consists of a disk of the electrode material encased in Teflon. This electrode is then screwed onto a steel shaft, which is then rotated by the rotating mechanism. A schematic diagram of the components in a rotating disk electrode is shown in below figure 1.6.

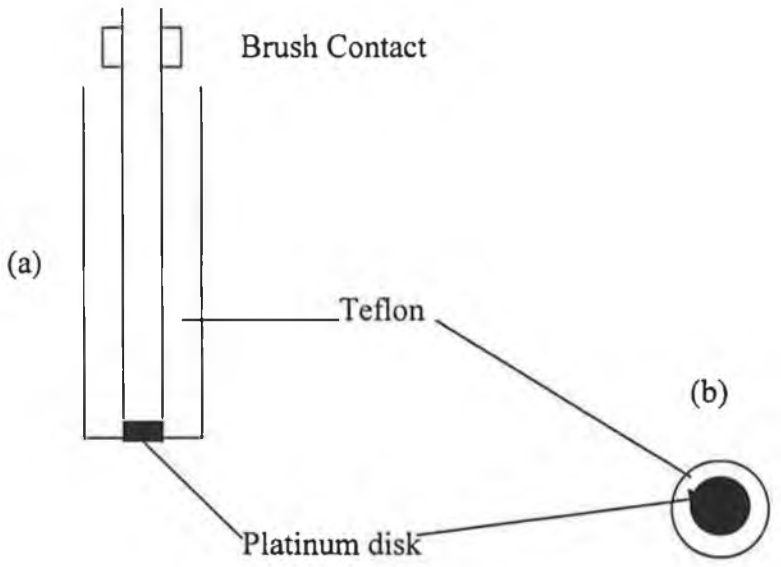

Figure 1.6: Schematic representation of a rotating disk electrode. (a) represents a cross-section of the electrode and (b) represents the electrode surface.

The electrode is rotated at a certain frequency, f, which is measured in revolutions per minute. This is then related to the angular velocity, ω (radians sec^{-1}), by the following; $\omega = 2\pi f/60$. As the rotation rate is lowered the diffusion layer thickness increases.

A schematic diagram of the solution flow due to forced convection at a RDE is shown below in figure 1.7.

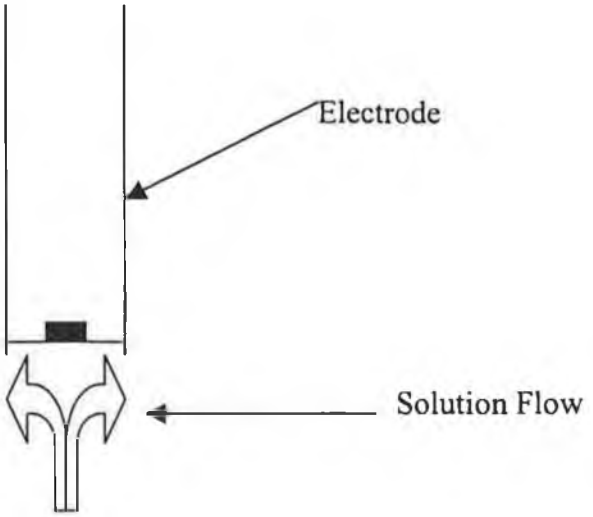

Figure 1.7: Representation of solution flow at a rotating disk electrode.

As the electrode rotates, adjacent solution is pulled along by viscous drag and thrown away from the axis of rotation by the centrifugal force. The expelled solution is replaced by flow normal to the electrode surface. The rotating disk acts as a pump in sucking solution up from below and then flushing it out, away from the electrode.

The characteristic response from a rotating disk electrode is sigmoidal in shape, as seen in figure 1.8. An electrode redox process yields a limiting current, i_L, as opposed to a peak current as in cyclic voltammetry. Fick's Law can be solved analytically for such a system and the limiting current can be related to the rotation rate for an oxidation process by the Levich equation:

$$i_L = 0.62nFAD^{2/3}\nu^{-1/6}C^*\omega^{1/2} \qquad 1.10$$

where C* is the bulk concentration in mol cm^{-3}, v is the kinematic velocity (cm^2 sec^{-1})

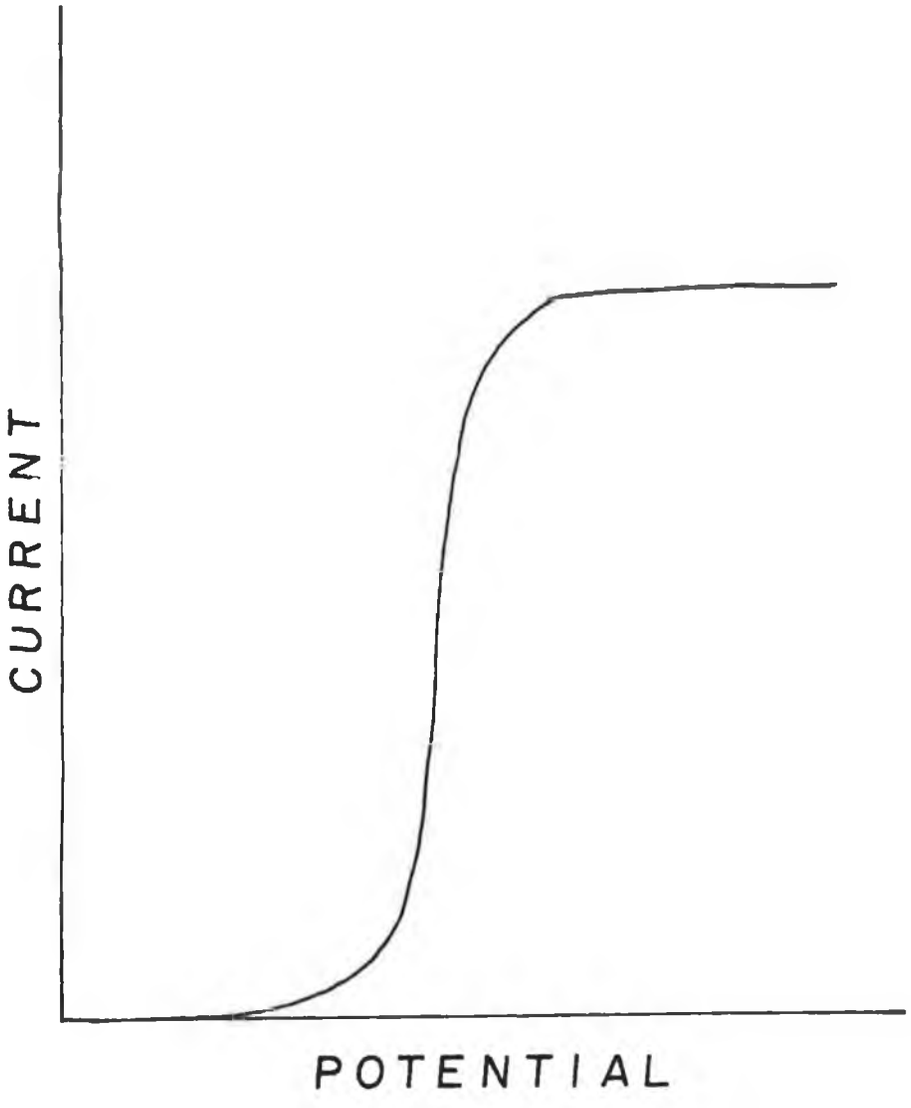

Figure 1.8: Typical sigmoidal-shaped response from a rotating disk electrode.

and ω is the rotation rate in radians per second. A plot of i_L versus $\omega^{1/2}$ should be linear, if the system is under mass transport control. If electron transfer kinetics are slow, this yields a lower current than expected by the Levich equation. Where slow electron transfer occurs, the Levich equation is modified to take kinetics into account. Then the following equation is obtained;

$$\frac{1}{i} = \frac{1}{nFAk_f C^*} + \left(\frac{1.61\nu^{-1/6}}{nFAC^* D^{1/2}}\right)\left(\frac{1}{\omega^{1/2}}\right) \qquad 1.11$$

where k_f is the rate constant for the forward reaction, and all the other symbols have their usual meaning. A plot of 1/i versus $1/\omega^{1/2}$ should be linear with a slope that is independent of potential, but due to the presence of k_f, the intercept is very dependent on potential.

1.4 References

1. L.C. Clark, and C. Lyons, 'Electrode systems for continuous monitoring in cardiovascular surgery', Ann. N.Y. Acad. Sci., (1962), **102**, 29.

2. G.G. Guilbault and J. Montalvo, J. Am. Chem. Soc., (1969), **91**, 2164.

3. J. Wang, 'Analytical Electrochemistry', VCH New York, (1994), p29.

4. G.C. Barker, and I.L. Jenkin, Analyst, (1952), **77**, 685.

5. J.F. Cassidy, and M.B. Foley, 'Chemistry in Britain', (1993), **9**, 764.

6. J. Osteryoung, and R.A. Osteryoung, Anal. Chem., (1985), **57**, 101A.

7. J. Wang, 'Analytical Electrochemistry', VCH New York, (1994), p45.

8. E.W. Kristensen, W.G. Kuhr, and R.M. Wightman, Anal. Chem., (1987), **59**, 1752.

9. J.N. Bariscari, and G.G. Wallace, Electroanalysis, (1994), **6**, 209-215.

10. H. Gunasingham, B.T. Tay, and K.P. Ang, Anal. Chim. Acta, (1985), **176**, 143.

11. J. Wang, Electrochim. Acta, (1981), **26**,1721.

12. R. Kennedy, L. Luang, M. Atkinson, and P. Dush, Anal. Chem., (1993), **65**,1882.

13. R.M. Penner, and C.R. Martin, Anal. Chem., (1987), **59**, 2625.

14. R.J. Tait, P.C. Bury, B.C. Finnin, B.L. Reed, and A.M. Bond, J. Electroanal. Chem., (1993), **356**, 25.

15. P.P. Buck, CRC Crit. Rev. Anal. Chem., (1976), **5**, 323.

16. A.J. Bard and L.R. Faulkner, 'Electrochemical Methods - Fundamentals and Applications', Wiley, NewYork, (1980), p51.

17. A.J. Bard and L.R. Faulkner, 'Electrochemical Methods - Fundamentals and Applications', Wiley, NewYork, (1980), p218.

18. A.J. Bard and L.R. Faulkner, 'Electrochemical Methods - Fundamentals and Applications', Wiley, NewYork, (1980), p229.

19. A.J. Bard and L.R. Faulkner, 'Electrochemical Methods - Fundamentals and Applications', Wiley, NewYork, (1980), p222.

2 The Electrochemistry of Ferrocene monocarboxylic acid

2.1 Introduction

The electrochemical properties of ferrocene and its derivatives have long since been identified as having numerous advantageous applications to the world of electrochemistry. These properties have been exploited extensively in a large number of molecular electronic applications such as molecular switches [1], metal probes [2], molecular magnets [3], non-linear optics [4] and more commonly in biosensor construction [5-10].

The wide use of ferrocene and its derivatives in biosensors cannot solely be attributed to its ability to mediate in redox protein electrochemical reactions, as a large number of simpler metal complexes such as ferrocyanide [11-13] can also perform this function adequately. This apparent preference for ferrocenes in the development of biosensors, as in other applications, is instead largely due to the unrivalled versatility offered by its derivatives.

The structure of ferrocene consists of an iron atom sandwiched between two cyclopentadienyl rings. The addition of functional substituents to this basic structure can significantly alter the physical and chemical properties of the molecule. It follows that through the addition of specific substituent groups, these ferrocene mediators can be tailored to carry out the diverse biological and chemical functions encountered in sensor development. During the early development of sensors which relied on solution based mediation, modifications of the solubilities and electrochemical

properties of these derivatives by altering functional substituents were a primary concern. The recent pursuit of reagentless biosensors has meant that it has been necessary to immobilise the mediator, through the various functionalities of the different substituents, either onto a polymer [14,15], the electrode [16], or even the protein itself [17-19].

Although ferrocene is known to be relatively inert in most solvents, with the notable exception of chlorocarbons [20], certain derivatives have been known to decompose rapidly when exposed to light in various different solvents [20-23]. The relationship between decomposition rate and solvent appears to be complex [21], but it is thought that the contributing factor to the decomposition process is the presence of water - even in trace amounts. The effect of this photodegradation process on the electrochemical properties and the direct implications for biosensor design and development is particularly important given the popularity of ferrocenes as mediators and the fact that water is the most common operational medium for biosensors. Therefore both the functionality offered by a substituent and the effect, if any, that it may have on the stability of the molecule, should be considered when choosing a particular ferrocene derivative for use in any molecular electronic application.

The high reversibility of the ferrocene/ferricinium redox couple facilitates the use of ferrocenes as model electrochemical systems. One such system, based on the ferrocene derivative of ferrocene carboxylic acid (FCA), was investigated in this work. FCA consists of a carboxylic acid group attached to one of the cyclopentadienyl rings in the basic ferrocene structure and is often used as a mediator in biosensors, with its role in glucose mediation being the most common example [24]. The structure of FCA is illustrated below in figure 2.1. The presence of the

carboxylic acid group serves to enhance the solubility of the molecule in water, and therefore allows for its use in studying redox reactions in aqueous media. This, coupled to the fact that FCA has been found to be stable to photodecomposition in aqueous solution [25], led to the decision to use FCA as the model electrochemical system in this work.

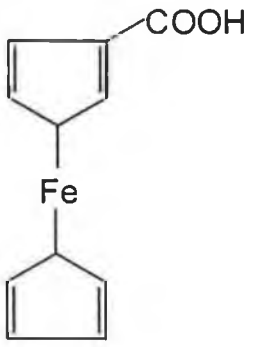

Figure 2.1: The structure of ferrocene carboxylic acid.

2.1.1 Spectroelectrochemistry

Not all important information about electrode processes can be obtained from experiments that involve only the usual electrochemical variables of current, charge and potential. This has led to the development of other experimental techniques, such as spectroelectrochemistry which use extra parameters or variables in order to gain information about a particular electrochemical system. Spectroelectrochemistry, which is the coupling of optical and electrochemical methods, has been employed for over two decades in the investigation of a wide variety of inorganic, organic and biological redox systems [26, 27].

Perhaps the simplest spectroelectrochemical experiment is one which involves directing a beam of light through a transparent electrode, and then measuring the

changes in absorbance resulting from species being consumed or produced in the electrode process. This would require an optically transparent electrode (OTE), such as a doped SnO_2 layer on glass or quartz. The OTE is placed in the spectrometer so that the light beam is passed directly through the transparent electrode and the solution [28]. The primary advantage of spectroelectrochemistry is the cross-correlation of information from the simultaneous electrochemical and optical measurements. In a typical experiment, the changes in absorbance are related to concentration and optical path length. Evaluation of the absorbance versus time curve can yield extremely useful information on reaction mechanisms and kinetics.

Another technique, which is also the one employed in this work, involves directing a Fourier Transform infrared beam through a transparent cell window and onto a reflective electrode surface, which then directs the beam into the detector.

The interaction of infrared radiation with surface species depends on the polarisation of light with respect to the plane of the electrode surface. The relative contributions of *s*-polarised and *p*-polarised light to the overall light intensity can be predicted using Fresnel's equations [29].

S-polarised radiation undergoes a phase shift of nearly 180° at all angles of incidence, and therefore has virtually no electric field strength at the electrode surface due to destructive interface between the reflected and incident beams. Hence *s*-polarised light gives no information about the species adsorbed on the electrode surface, and is usually filtered out, since it increases the overall noise of the system.

However *p*-polarised light undergoes a phase shift that is a function of the incident angle and as a result, has a high electric field strength at the surface at high incident

angles. Thus *p*-polarised light is the only radiation that gives information on the nature of species at the electrode surface. For studies of solution species, both *s*-polarised and *p*-polarised light can give useful information on dissolved infrared absorbers.

Information on the orientation of molecules adsorbed on electrode surfaces can be obtained by studying the relationship between the *p*-polarised radiation intensity and the direction of the molecular (or ionic) dipole with respect to the surface. Optimal absorption of infrared light occurs when the component of the dipole moment derivative, with respect to the normal co-ordinate, is in the same direction as the incident radiation. A dipole derivative, parallel to the surface, is infrared inactive due to the absence of any component of the incident electromagnetic field parallel to the surface. As the dipole derivative moves from the parallel to the perpendicular position, with respect to the surface, the probability of infrared absorption increases. This distinction between absorbances due to vibrating species orientated either parallel or perpendicular to the surface, is known as the surface selection rule.

The technique used in this work is known as Subtractively Normalised Fourier Transform Infrared Reflectance Spectroscopy (SNFTIRS). This technique is very useful in characterising both electrochemical products and intermediates by examining the spectral peaks which either disappear or appear during the course of an electrochemical reaction. The experimental details of this technique are given in section 2.2.2.

2.2 Experimental Procedure

2.2.1 Instrumentation, electrodes and chemicals

Cyclic voltammetry, potential control and charge and current measurement was performed using an Edt potentiostat Model ECP 100 linked to a H.B. Thompson ramp generator. A J.J.Lloyd X-Y chart recorder Model PL3 was used to chart the response.

A three electrode one compartment system was employed for all electrochemical experiments. The working electrode was a platinum, gold or glassy carbon disk sealed in Teflon with an exposed surface area of approximately $0.07cm^2$. The reference was a saturated calomel electrode and the auxiliary was a carbon rod. The surface of the working electrode was polished regularly with 0.3μm alumina and then rinsed with de-ionised water to keep it clean.

All chemicals used were of reagent grade and all aqueous solutions were prepared using de-ionised water. Both nitrogen and oxygen were bubbled through solutions using a Dreschler bottle. All organic solvents used were of HPLC grade. The temperature for all experiments was ambient (20 ± 4°C).

2.2.2 Spectroelectrochemistry

Changes in the UV-Vis spectrum of the oxidised form of FCA were monitored using a Shimadzu UV-Vis spectrometer.

SNFTIRS was performed using the cell depicted in figure 2.2 and a schematic drawing of the instrumentation used is shown in figure 2.3. The working electrode in this cell was a platinum disk electrode (radius = 0.5cm). The auxiliary electrode was

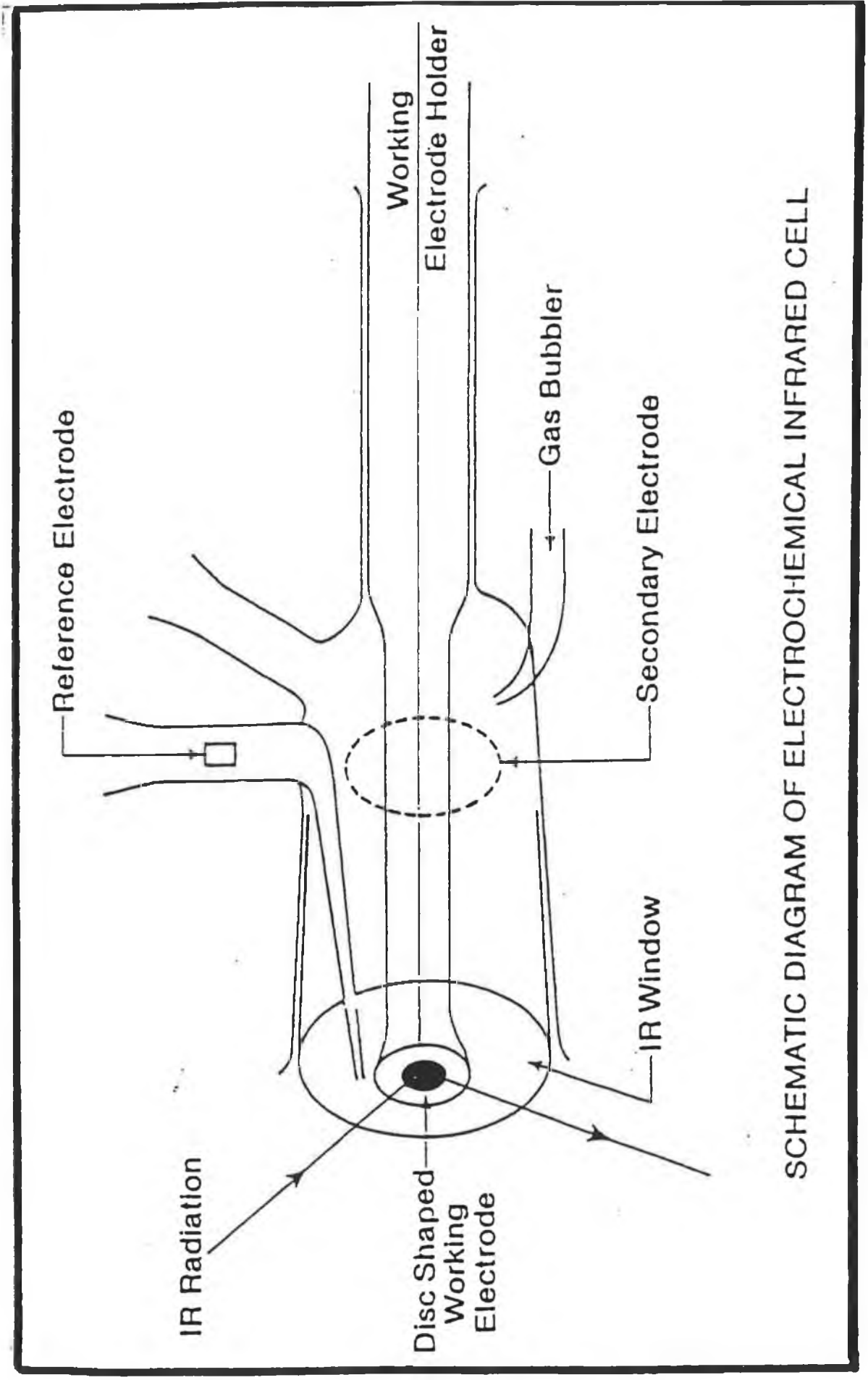

Figure 2.2: Schematic drawing of electrochemical cell.

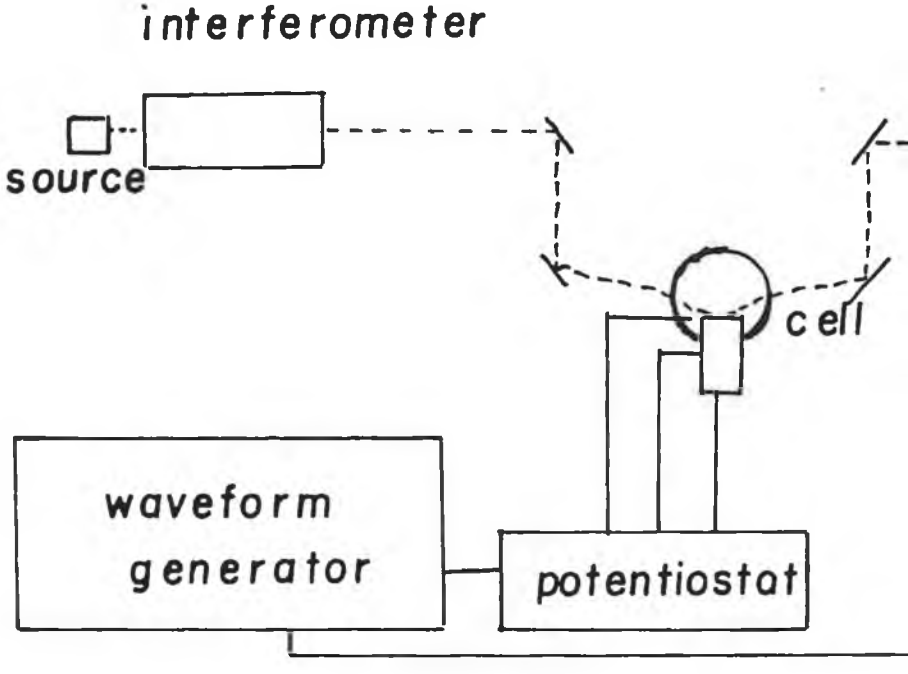
interferometer
source
cell
waveform
generator
potentiostat

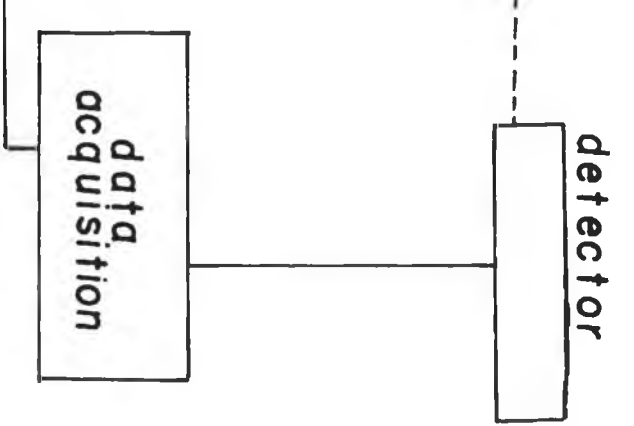

Figure 2.3: Schematic drawing of the instrumentation for infrared spectroelectrochemistry.

a piece of platinum wire, while the reference electrode was a saturated calomel electrode. Species at the electrode were analysed by reflecting the infrared beam of light through the transparent CaF_2 cell window, onto the electrode surface and then into the detector. This was done with the aid of two mirrors where one directed the beam onto the electrode, and the other one directed the reflected beam into the detector. A potential at which no electrochemical reaction occurs was then applied to the cell using a potentiostat. The difference spectra were collected by running a background scan at this potential (0.0V) followed by a sample scan at 0.6V. The background scan was then automatically subtracted from the sample scan.

2.2.3 Coating and loading of electrodes

Polyvinylpyridine (PVP) was dissolved in methanol (0.3% w/v) and 1,6-dibromohexane was added in excess as the cross-linker. A drop of this solution was then applied to the surface of the electrode and evaporated to dryness with the aid of a hairdryer. This resulted in a layer of PVP being deposited on the surface of the electrode. This layer was then cross-linked by heating in an oven at 90°C for 8 hours.

After cross-linking the layer was loaded with FCA by using the electrode as the working electrode in a saturated solution of FCA and continuously sweeping the potential between 0.0V and 0.6V. This resulted in the FCA molecules diffusing into the layer but being unable to diffuse back into the solution. This happens due to the ferrocene carboxylate acting as an anion to the quaternised PVP.

2.3 Results and Discussion

2.3.1 Cyclic voltammetry of FCA under various conditions

As mentioned in the introduction to this chapter, FCA is widely used as a model electrochemical system. Indeed, for this reason, it was the first system studied in this project. Also its greater solubility in water over that of most other ferrocene derivatives, was an added advantage in studying the electrochemistry of aqueous systems. In the first instance it was employed to test the equipment through direct comparison of its cyclic voltammograms to those previously documented [30].

In this project, the cyclic voltammetry of FCA was first investigated, in the presence of air, in 0.2M Na_2HPO_4/H_2O (pH = 9.2). Different scan rates were applied and the resulting cyclic voltammograms are shown in figure 2.4. At the faster scan rates (40 - 100mVsec^{-1}) the FCA exhibits highly reversible behaviour ($\Delta Ep \cong 60mV$). However while this peak to peak separation is similar at the slower scan rates (5 - 20mVsec^{-1}), there is also an example of non-ideal behaviour in the presence of a "bump" or oxidative post-peak, which is not seen at the faster scan rates. After being unable to find any previously documented evidence of this unusual phenomenon, it was decided to investigate further in an effort to account for its occurrence.

The first step in doing so was to look at even slower scan rates as can be seen in figure 2.5. It is clear that the post-peak increases in magnitude relative to the bulk oxidation peak with increasingly slower scan rates. This happened at Pt, Au and glassy carbon electrodes to the same extent. This seemed to indicate that the reason the post-peak was not seen at high scan rates was that it was obscured by the much larger bulk oxidation peak. A more likely explanation is the presence of a catalytic

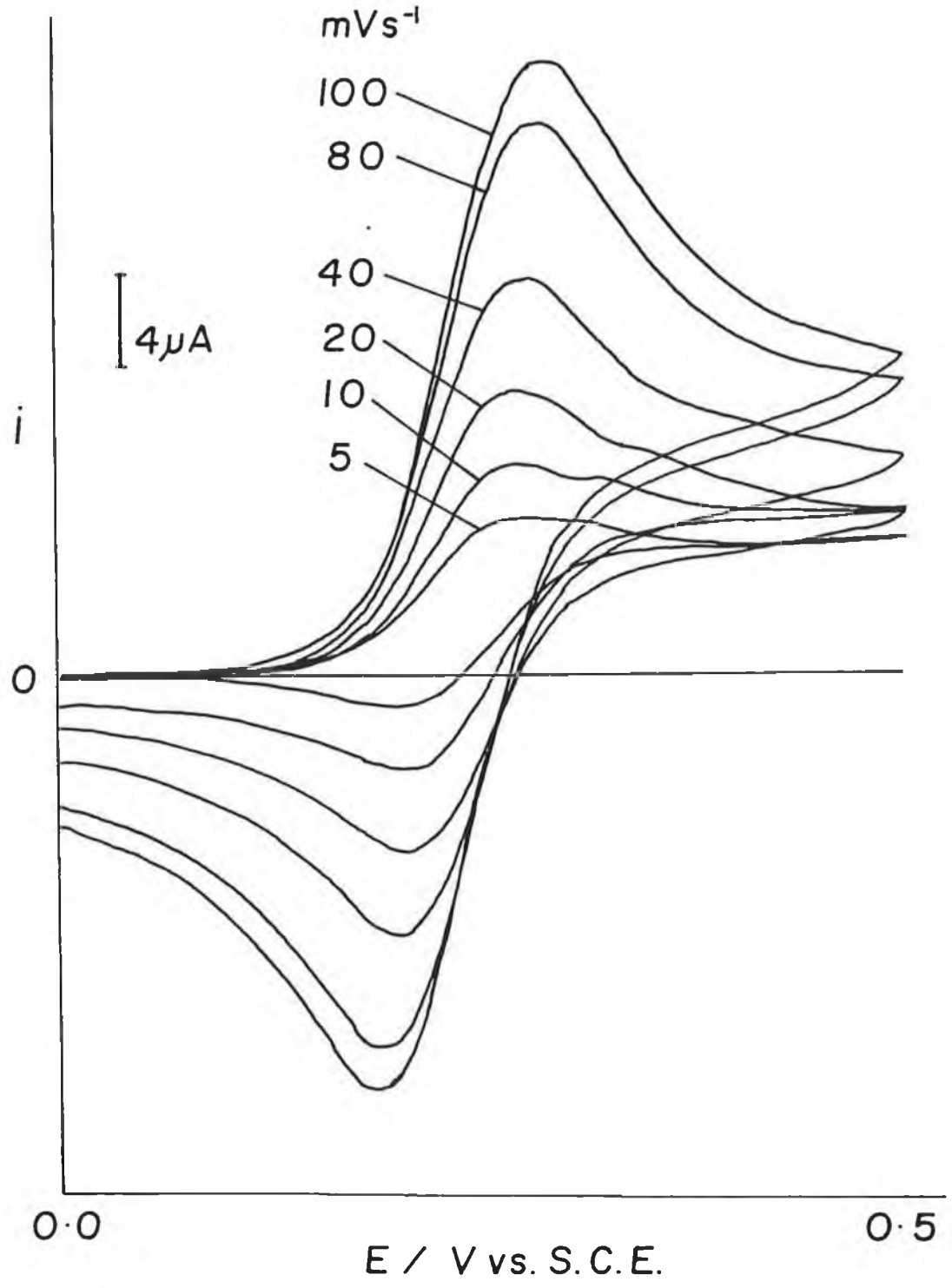

Figure 2.4: Cyclic voltammograms of 1mM FCA in 0.2M Na_2HPO_4/H_2O at the gold working electrode, and in the presence of air.

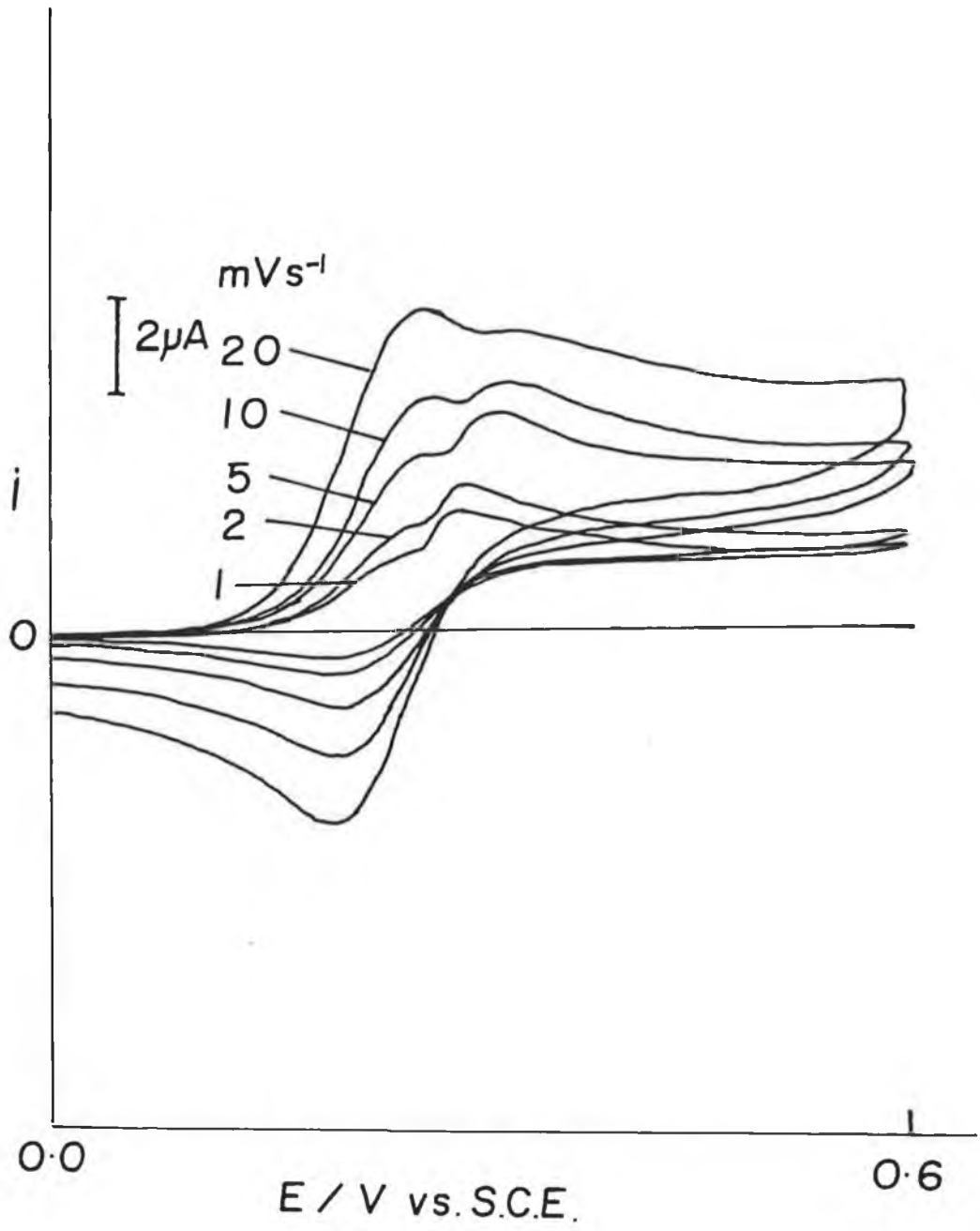

Figure 2.5: Cyclic voltammograms of 1mM FCA in 0.2M Na_2HPO_4/H_2O at the gold working electrode, and in the presence of air.

chemical reaction which is subsequent to the electrochemical step; an EC mechanism. It also suggested that perhaps this post-peak was the result of a species being adsorbed onto the working electrode and itself being oxidised after the bulk oxidation. However the absence of a corresponding re-reduction peak was curious. It is interesting that the post-peak occurred at the three different electrode types. This makes a surface adsorbed species less likely since the adsorption would depend on the electrode nature.

An effort was made to further discount the possibility that the post-peak could be the result of some molecules of FCA adsorbing on the surface of the electrode, and being oxidised just after the bulk oxidation. Should this be the case, the peak current of the adsorbed species would increase with sweep rate. In fact, the opposite occurs. Also, electrodes were left for longer periods in the FCA solution and no post-peak was observed at fast sweep rates. This indicates that if adsorption is occurring, it is the adsorption of an intermediate. In an effort to clarify whether or not the underivatised ring of the FCA molecule is adsorbed, β-cyclodextrin was added to the solution. As β-cyclodextrin has a bucket-like structure [30], it forms an inclusion complex with FCA and ensures that the underivatised ring of FCA is shielded, thus preventing adsorption. Figure 2.6 shows the results of scanning a 2mM solution of FCA in 0.2M Na_2HPO_4/H_2O at $100mVs^{-1}$ and $20mVs^{-1}$ (solid lines) and the same solution again but with β-cyclodextrin added (dotted line). When the β-cyclodextrin was added the current decreased at both scan rates. This is due to the inclusion complex being more bulky than the FCA molecules alone, and therefore its movement in solution is somewhat more restricted. The $20mVs^{-1}$ scan shows that the post-peak does not disappear when the β-cyclodextrin is added, and therefore the post-peak cannot be attributed to a delay in the oxidation of some FCA molecules due to their adsorption

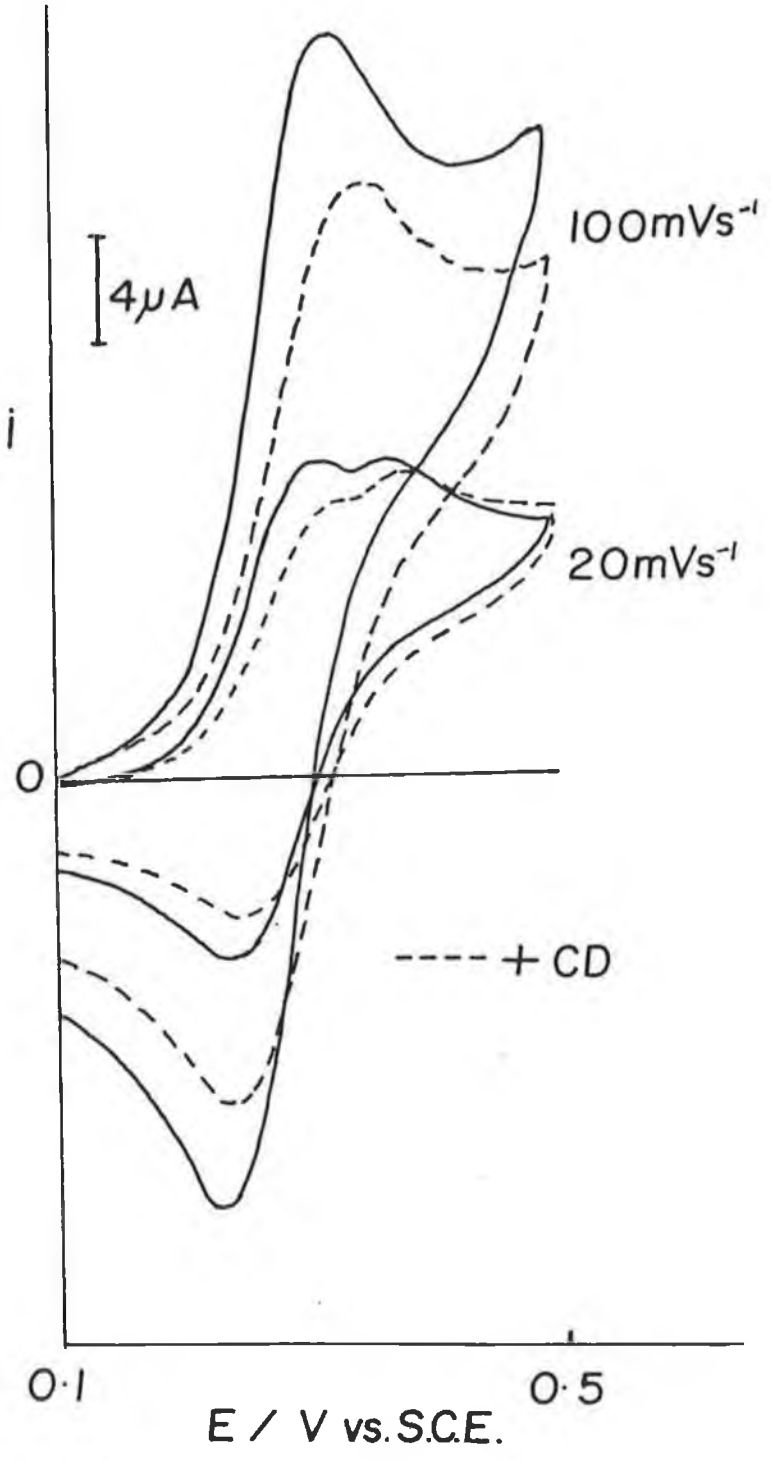

Figure 2.6: Cyclic voltammograms of 2mM FCA in 0.2M Na_2HPO_4/H_2O at $100mVs^{-1}$ and $20mVs^{-1}$ (solid lines) and the same solution with β-cyclodextrin added (dotted lines), at a platinum electrode.

on the electrode surface. This also shows that the presence of β-cyclodextrin does not prevent a subsequent catalytic mediation from occurring.

A concentration study was then carried out, where the FCA concentration was varied from 0.1mM to solution saturation (≅10mM), and it was found that the higher the concentration of FCA the smaller the post-peak was relative to the diffusion controlled peak, and that for a saturated solution of FCA there was no post-peak at all. At this time however, the reason for the appearance of the post-peak was still unclear.

In order to see if the presence of oxygen was having an effect, the solution was then deoxygenated with nitrogen. This produced a dramatic result in that the post-peak disappeared completely, as can be seen in figure 2.7. Equally dramatic observations were made when oxygen was then bubbled through the same solution. These are represented in figure 2.8. Here the post-peak not only returns, but its magnitude has also increased significantly when compared to that when the solution was only exposed to atmospheric concentrations of O_2. This suggested that the post-peak was dependent on the concentration of O_2 in the solution and that the bulk peak is not affected by the presence of O_2. From this finding, a theory was proposed that perhaps the post-peak represented the oxidation of oxygen to ozone. One problem with this theory was that normally oxygen is only oxidised to ozone at much greater potentials (2.07V vs. N.H.E. [31]) than are applied here (upper voltage limit is 0.6V). However this discrepancy could be accounted for by assuming that the ferrocene/ferricinium couple acts as a mediator in this oxidation, therefore allowing the oxygen to be oxidised to ozone at a much lower potential. From this, equations were written to represent the possible reaction involved [31]:

$$O_3 + 2H^+ + 2e^- \Leftrightarrow O_2 + H_2O\,; \qquad E^0 = 2.07\,V \qquad 2.1$$

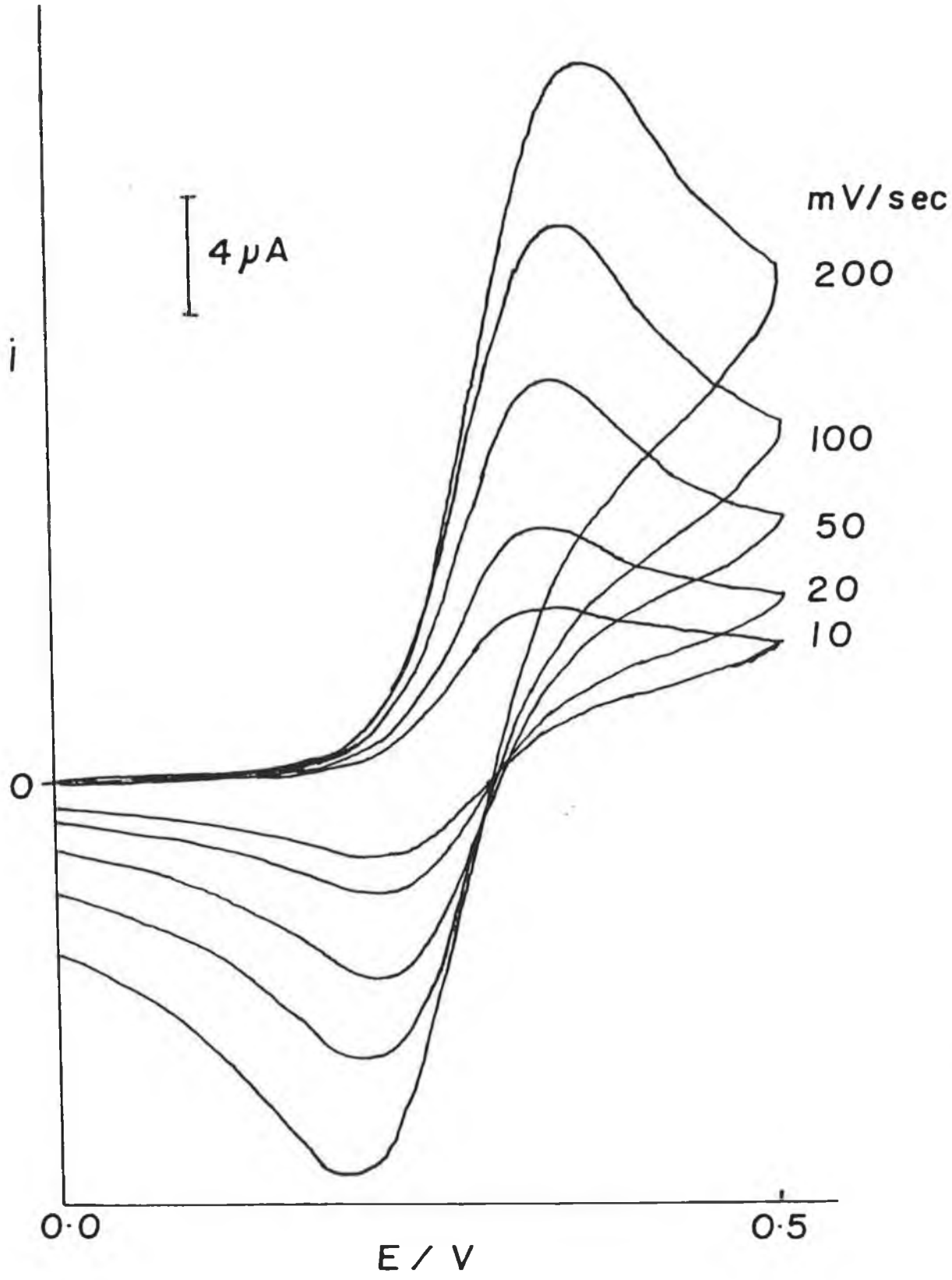

Figure 2.7: Cyclic voltammograms of 2mM FCA in 0.2M Na_2HPO_4/H_2O at a gold electrode, after degassing of the solution with N_2.

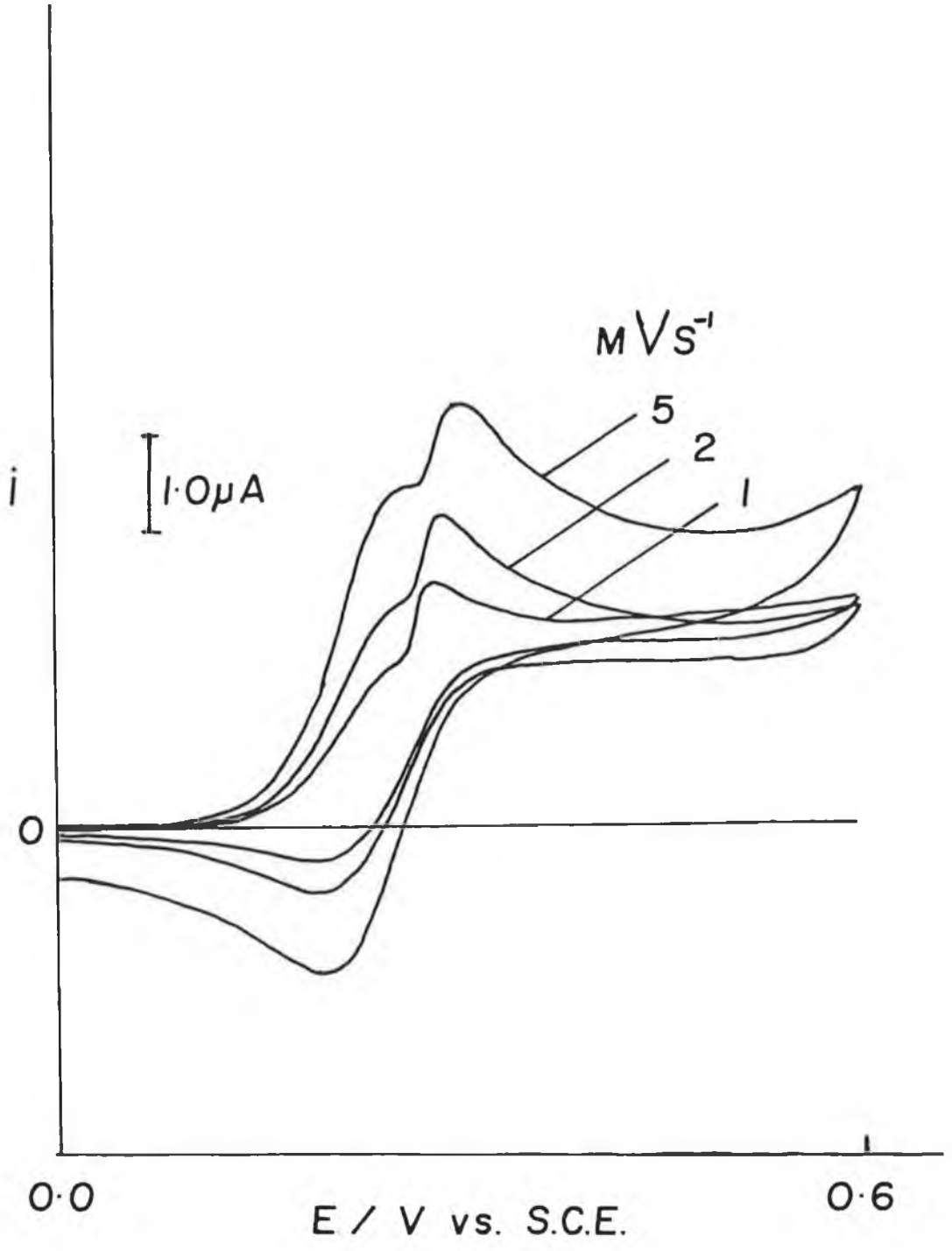

Figure 2.8: Cyclic voltammograms of 2mM FCA in 0.2M Na_2HPO_4/H_2O at a gold electrode, after bubbling the solution with O_2.

$$O_3 + 2H^+(10^{-7}M) + 2e^- \Leftrightarrow O_2 + H_2O;\ E^0 = 2.07\,V \qquad 2.2$$

From equations 2.1 and 2.2, it is clear that the formation of ozone depends on the presence of water. Since the electrochemistry was carried out in water, the conditions would satisfy these equations. However, to ascertain whether or not this equation was truly representative of the reaction involved here, the cyclic voltammetry of FCA was examined in an organic solvent. As can be seen in figures 2.9 and 2.10, there is no evidence of the post-peak either when the solution has been bubbled with N_2 or when the solution has been bubbled with O_2. This was also the case when the electrolyte was changed from $LiClO_4$ to $TBABF_4$. These observations support equations 2.1 and 2.2, in that it appeared water was required as a reagent.

It was then decided to add incremental quantities of water to the organic solution of FCA as it was thought that this might facilitate the oxidation of oxygen to ozone by providing the water necessary for the reactions represented by equations 2.1 and 2.2 to proceed. Firstly this experiment was performed under nitrogen to assess what affect, if any, the addition of water would have on the overall shape of the cyclic voltammogram. The resulting voltammogram is shown in figure 2.11. While the shape of the voltammogram does not change significantly with each addition of water, the peak current decreases and each subsequent voltammogram is also shifted to a lower potential. Since there appeared to be a direct effect on the formal potential of the redox species in solution, from the presence of increasing concentration of water, it was decided to study this. It is not an effect caused by decreasing the resistance of the solution by adding a solvent with a higher dielectric constant, since the cyclic voltammograms are ideal even before the water is added. The following model was then proposed.

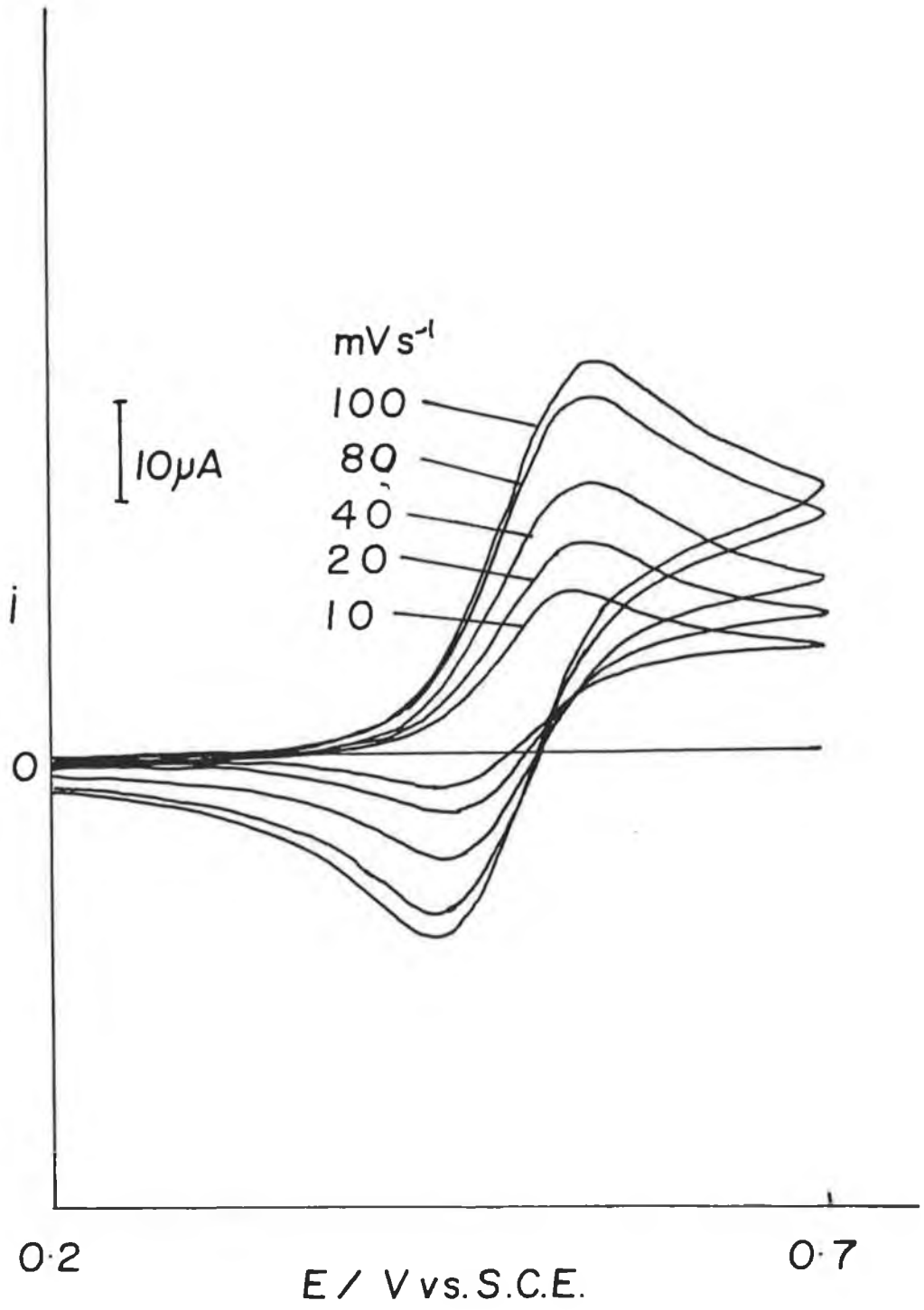

Figure 2.9: Cyclic voltammograms of 1mM FCA in 0.1M $LiClO_4/H_2O$ at a gold electrode, after degassing of the solution with N_2.

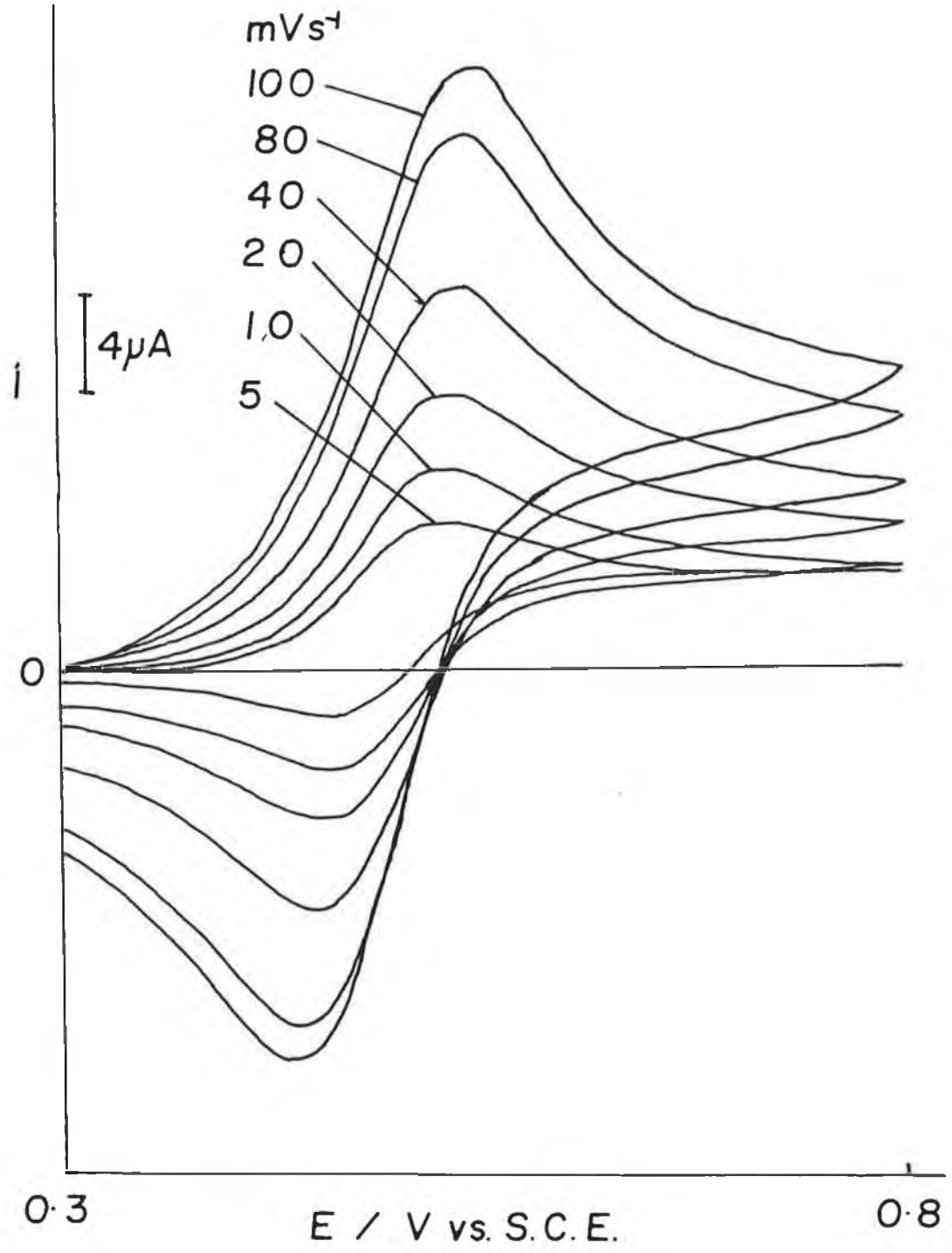

Figure 2.10: Cyclic voltammograms of 1mM FCA in 0.1M $LiClO_4/H_2O$ at a gold electrode, after bubbling the solution with O_2.

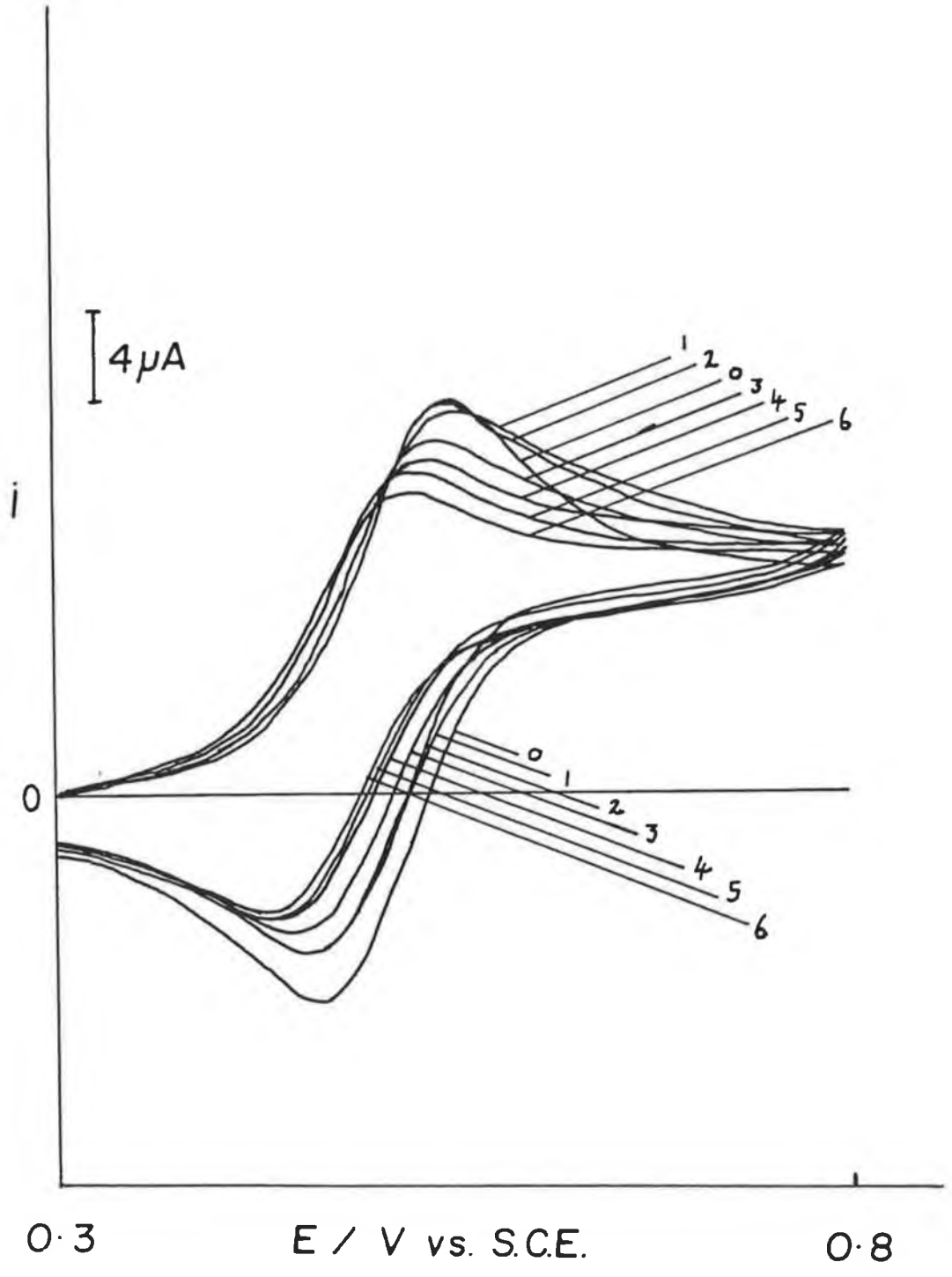

Figure 2.11: Cyclic voltammograms of 1mM FCA in 0.1M $LiClO_4$/ACN with successive 1ml additions of H_2O, at a gold electrode, after degassing of the solution with N_2. Scan rate = 40mVs^{-1}.

Model 2.1

$$mH_2O + FCA^- \rightarrow FCA^0 + e^- + \text{other} \qquad 2.3$$

and

$$E = E^0 + \frac{2.303RT}{nF}\log\left[\frac{[FCA^0]}{[FCA^-][H_2O]^m}\right] \qquad 2.4$$

and

$$E = E^0 + \frac{2.303RT}{nF}\log\left[\frac{[FCA^0]}{[FCA^-]}\right] - \frac{RT2.303m}{nF}\log[H_2O] \qquad 2.5$$

and

$$E = E^{0'} + \frac{2.303RT}{nF}\log\left[\frac{[FCA^0]}{[FCA^-]}\right] \qquad 2.6$$

where

$$E^{0'} = E^0 - \frac{2.303RTm}{nF}\log[H_2O] \qquad 2.7$$

and where m is the amount of water used for hydrating the FCA^-, and all the other symbols have their usual meaning.

Figure 2.12 shows a plot representing the shift in formal potential, measured as $(E^f_p + E^r_p)/2$, with increasing water concentrations that is seen in figure 2.11. From this plot, the slope is -64mV which leads to a value m = 64/59, which results in the approximation that m = 1. This suggests that there is one water molecule stabilising the ferrocene carboxylate.

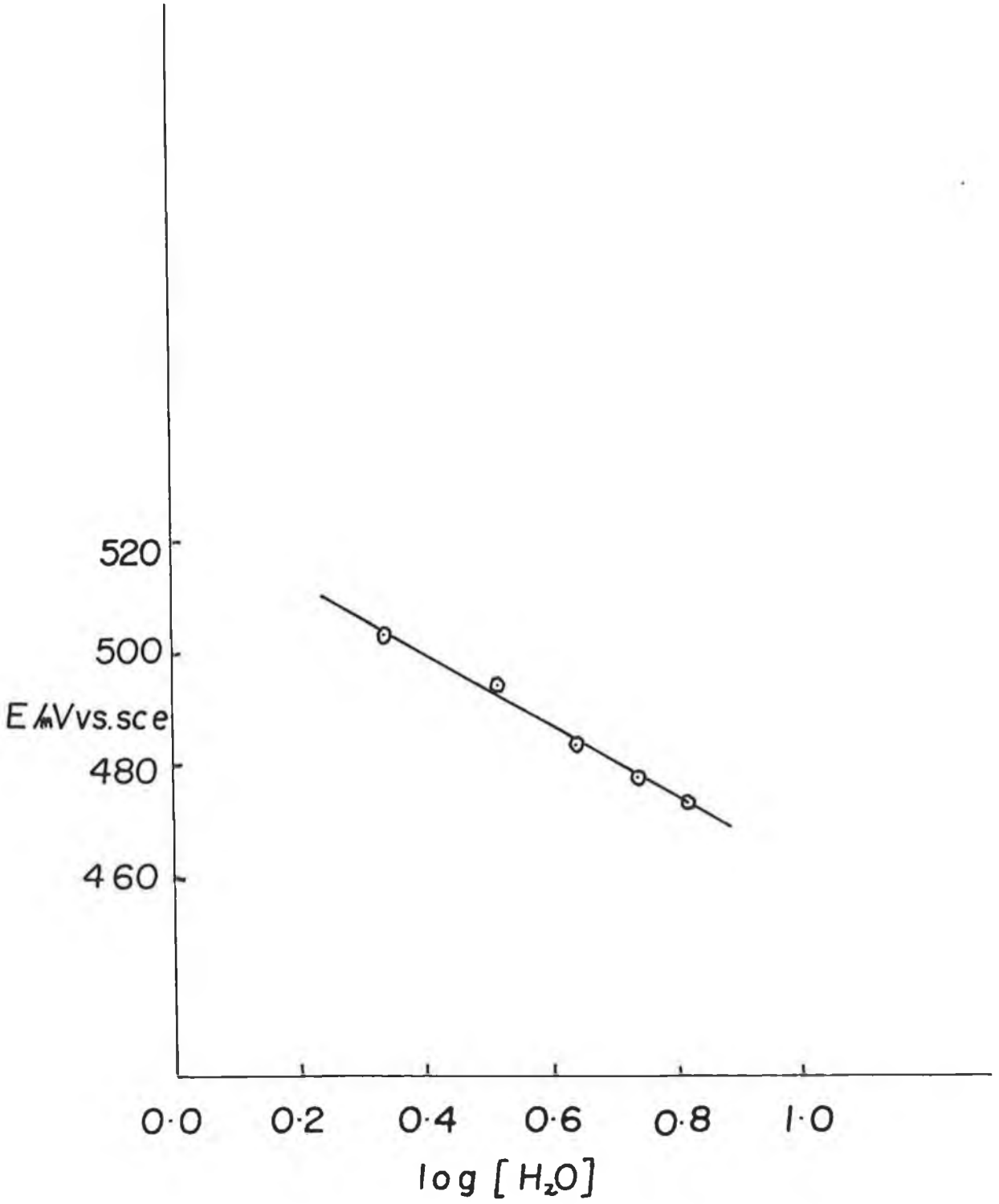

Figure 2.12: Plot representing the shift in formal potential with increasing water concentrations that is seen in figure 2.11.

This experiment was then repeated after bubbling oxygen through the solution of acetonitrile with water deliberately added - see figure 2.13. Contrary to what might have been expected, the post-peak seen after the bulk oxidation of FCA in aqueous solution (figures 2.4, 2.5 and 2.8) did not materialise - even with high concentrations of water present. This of course conflicted with equations 2.1 and 2.2.

Having investigated the difference between two different solvents (water and acetonitrile) with respect to the electrochemical behaviour of FCA, it was decided to revert back to the aqueous solution and look at the effect, if any, of changing the electrolyte. This seemed the logical course of action as when the solvent was changed from H_2O to ACN the electrolyte was also changed from Na_2HPO_4 to $LiClO_4$. This was necessary as Na_2HPO_4 would not dissolve in acetonitrile. Therefore the study of FCA in 0.1M KCl/H_2O was carried out.

As can be seen in figure 2.14, the post-peak does not appear when FCA is scanned in 0.1M KCl/H_2O. As the pH of this solution (pH = 5-6) is lower than when the Na_2HPO_4 buffer is used (pH = 9.2), the FCA is less soluble in it. To increase the solubility of the FCA the pH was raised using a boric acid buffer. This not only had the effect of increasing the solubility of the FCA, but the post-peak also appeared in the presence of oxygen (figure 2.15). Therefore it was thought that rather than the possible oxidation of O_2 to O_3 being dependent on the presence of H_2O, it was dependent on $[OH^-]$. This assumption led to the following equation for the formation of O_3 [32]:

$$O_3 + H_2O + 2e^- \Leftrightarrow O_2 + 2OH^- \qquad E° = 1.24V \qquad 2.8$$

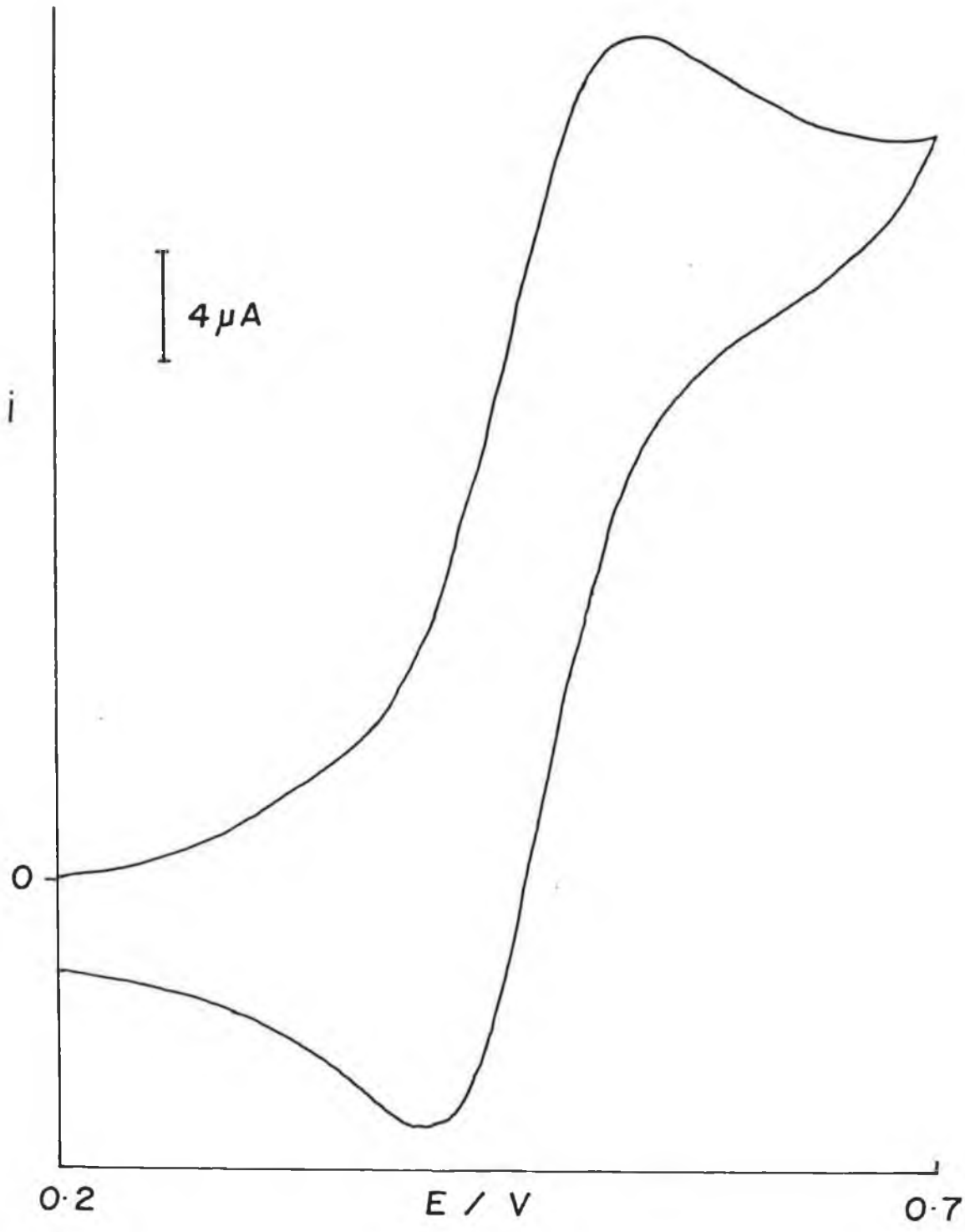

Figure 2.13: Cyclic voltammogram of 1mM FCA in 0.1M $LiClO_4$/ACN after a 3ml addition of H_2O, at a gold electrode, after bubbling the solution with O_2. Scan rate = $40mVs^{-1}$.

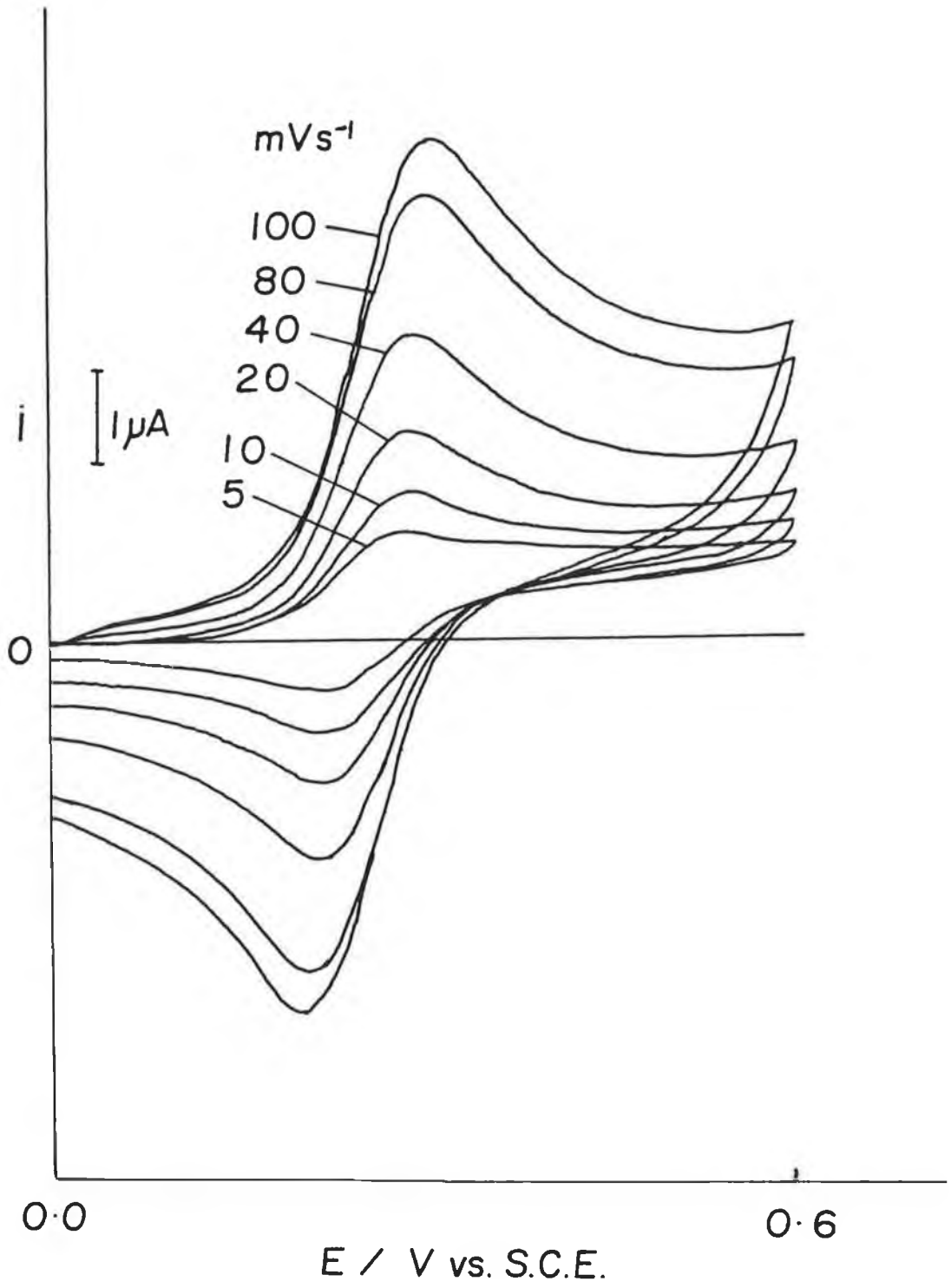

Figure 2.14: Cyclic voltammograms of a saturated solution of FCA (<1mM) in 0.1M KCl/H_2O, (pH = 5-6) at a gold electrode, in the presence of O_2.

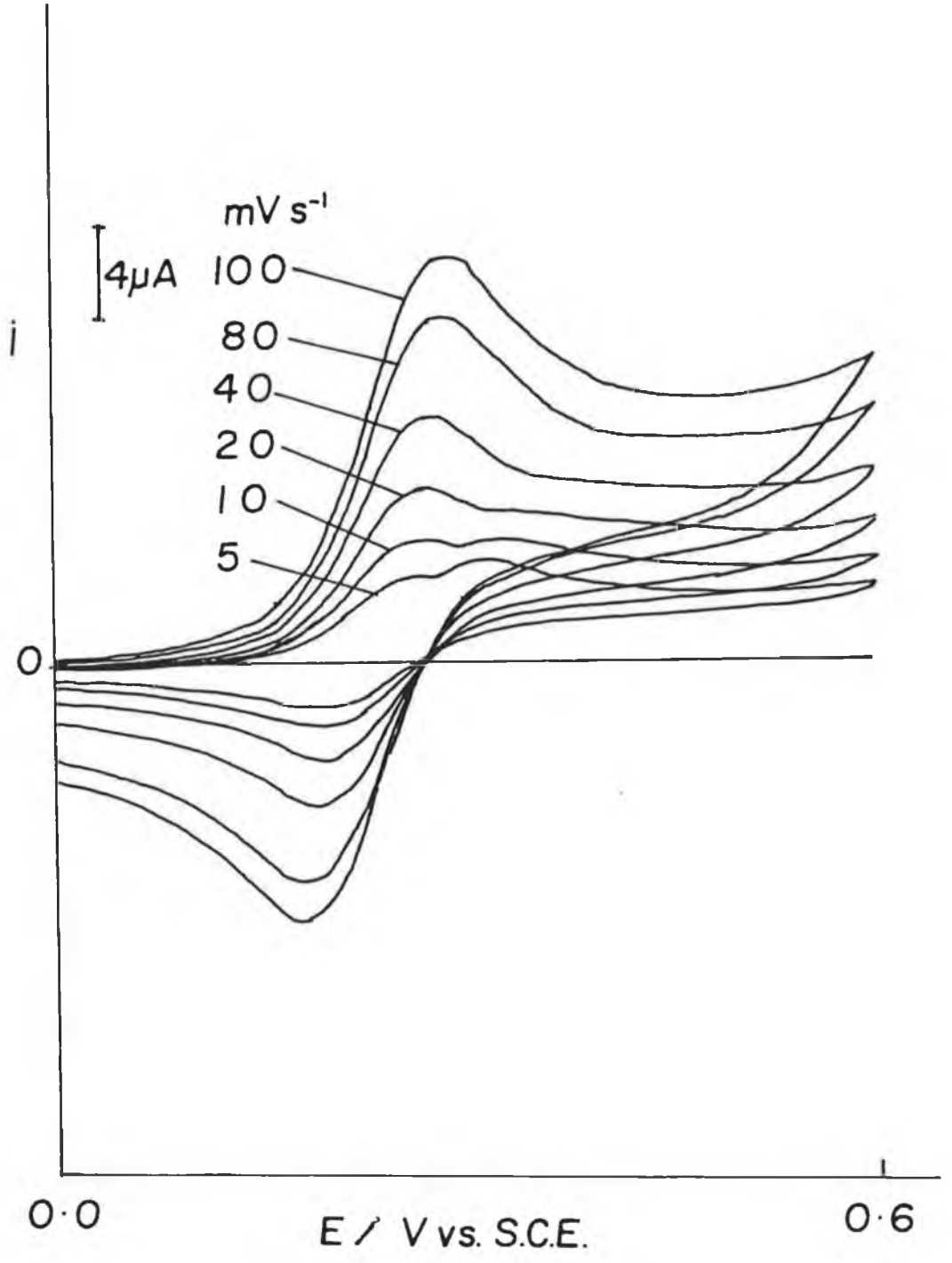

Figure 2.15: Cyclic voltammograms of a saturated solution of FCA (<1mM) in 0.1M boric acid/0.1M KCl/H_2O, (pH = 10) at a gold electrode, in the presence of O_2.

Having seen the effect of changing the pH of the solution, again it was decided to revert back to the original solution and perform a pH study on it. This study showed clearly that the appearance and magnitude of the post-peak depended on both the pH of the solution and the presence of oxygen. The best example of this is shown in figures 2.16(A) and 2.16(B): In figure 2.16(A) the dotted line represents the voltammogram of a saturated solution of FCA in 0.2M Na_2HPO_4/H_2O (pH = 10.2) after being bubbled with N_2 for 30 minutes. There is no trace of a post-peak present. The solid line represents the same solution after being bubbled with O_2 for 30 minutes. Here, in stark contrast to the same solution under N_2, a large sharp peak occurs almost immediately after the bulk oxidation peak. While this comparison shows the influence of O_2 on the electrochemical behaviour of FCA, figures 2.16(A) can also be compared to figure 2.16(B) to illustrate the influence of pH: Figure 2.16(B) represents the voltammogram of the same solution as figure 2.16(A), but at pH 8.2. Although this solution has been bubbled with O_2 for 30 minutes, the change to a lower pH has caused the post-peak to almost completely disappear. From this it is clear that the post-peak will only occur at a high pH and when there is O_2 present. The comparisons drawn from figures 2.16(A) and (B) would support equation 2.2. Also, when combining this information with that gained from the concentration study performed earlier, it is clear that higher concentrations of FCA require higher concentrations of O_2 present for the post-peak to appear.

2.3.2 The electrochemistry of FCA at the microelectrode

After studying the electrochemistry of FCA using cyclic voltammetry, the microelectrode was employed as an extra analytical tool to look at the difference in electrochemistry between the oxygenated and deoxygenated solutions of FCA at a

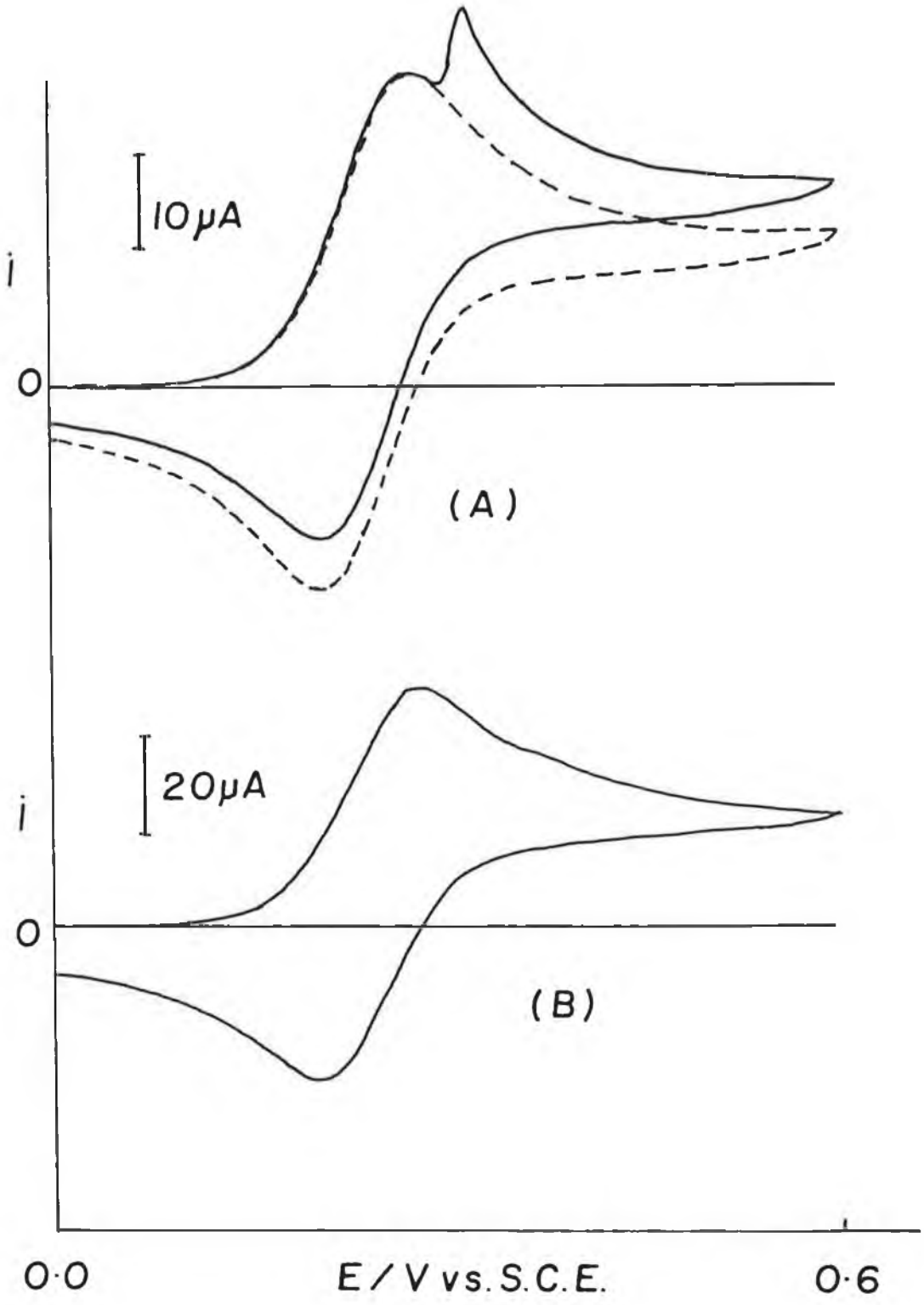

Figure 2.16: The dotted line in (A) represents the cyclic voltammogram of a saturated solution of FCA in 0.2M Na_2HPO_4/H_2O (pH = 10.2) after being bubbled with N_2 for 30 mins. The solid line in (A) represents the cyclic voltammogram of the same solution after being bubbled with O_2 for 30 mins. The cyclic voltammogram shown in (B) represents the same solution as in (A), also after being bubbled with O_2 for 30 mins, but at a lower pH (8.2). The scan rate in each case is 10 mVs^{-1}.

high pH. The microelectrode responses for a solution of FCA at pH = 10, bubbled first with N_2 and then with O_2 are shown in figure 2.17. Surprisingly the current is slightly smaller when the solution is oxygenated.

2.3.3 Infrared and UV - Vis spectroelectrochemistry of FCA

The infrared spectroelectrochemistry of FCA was carried out in the cell described in the experimental section of this chapter. Although this cell has previously been successful in gaining information about the electrochemical intermediates and products of ferrocyanide [33], among other systems, the technique was unsuccessful when looking at saturated solutions of FCA in 0.2M Na_2HPO_4/H_2O. This was due to the fact that although the solutions were saturated, they were not concentrated enough for the redox processes of FCA to be detectable by the infrared beam. The reason for this is that FCA has a low solubility in water, even when saturated (<10mM). It was hoped that this technique could be used to offer spectral proof of the electrochemical formation of ozone in the presence of oxygen and at high pH's. It was thought that by taking a background infrared scan at a potential just after the bulk oxidation of FCA but before the potential at which the post-peak occurs, and then taking the sample infrared scan at the potential after where the post-peak occurs, that the resulting difference spectrum might show a peak representing the formation of ozone, since O_3 absorbs in the infrared region at 1135, 716 and 1089cm^{-1} [34]. Unfortunately, due to the aforementioned reason it was not possible to carry out this experiment successfully.

Having been unsuccessful in an attempt to detect the electrochemical formation of ozone in the infrared region, spectral confirmation of its formation was sought in the UV - Vis region: This involved the bulk electrolysis of FCA, where the potential was

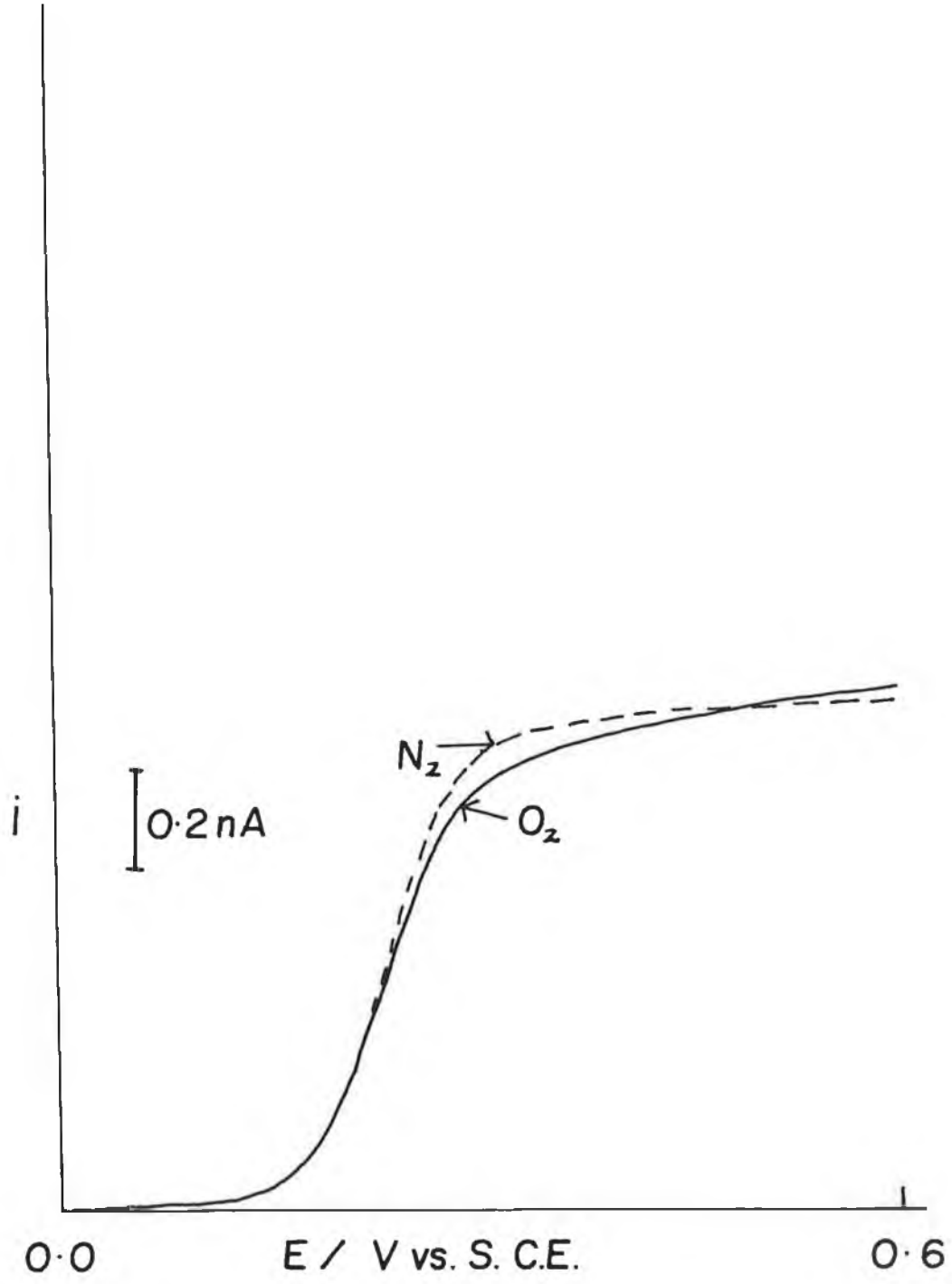

Figure 2.17: Microelectrode responses for a solution of 1mM FCA in 0.1M boric acid/0.1M KCl/H_2O (pH = 10) bubbled first with N_2 and then with O_2.

held at 0.6V for 2 hours in order to convert as much of the neutral compound to its oxidation products as possible (the solution turns from yellow to green). In doing so, it was hoped to maximise the amount of O_3 formed, to allow for its detection in the UV - Vis spectrometer.

Although O_3 absorbs strongly at 250nm [35] so do many other species and therefore it was not possible to detect this characteristic absorbance. However, there were two peaks associated with the FCA observed at 430nm (reduced form) and 630nm (oxidised form) (figure 2.18). It is clearly seen that over time (once the potential is no longer being applied to the solution) the ferricinium ion reconverts to the neutral ferrocene. This is represented by the decrease in absorbance of the peak at 630nm, and the simultaneous increase in absorbance of the peak at 430nm. Also the solution's colour changes from green back to yellow.

Experiments were performed, using UV-Vis spectroscopy, to look at the half-life of ferricinium in the absence and presence of oxygen at high pH. This was done in an effort to confirm the medation reaction between ferricinium and O_2, but the results were inconclusive. Pseudo first order rate constants for ferricinium decay were similar, in the absence and presence of O_2.

Although neither spectroelectrochemical technique was able to provide confirmation of the presence of O_3 as one of the oxidation products, neither technique could provide evidence to the contrary either.

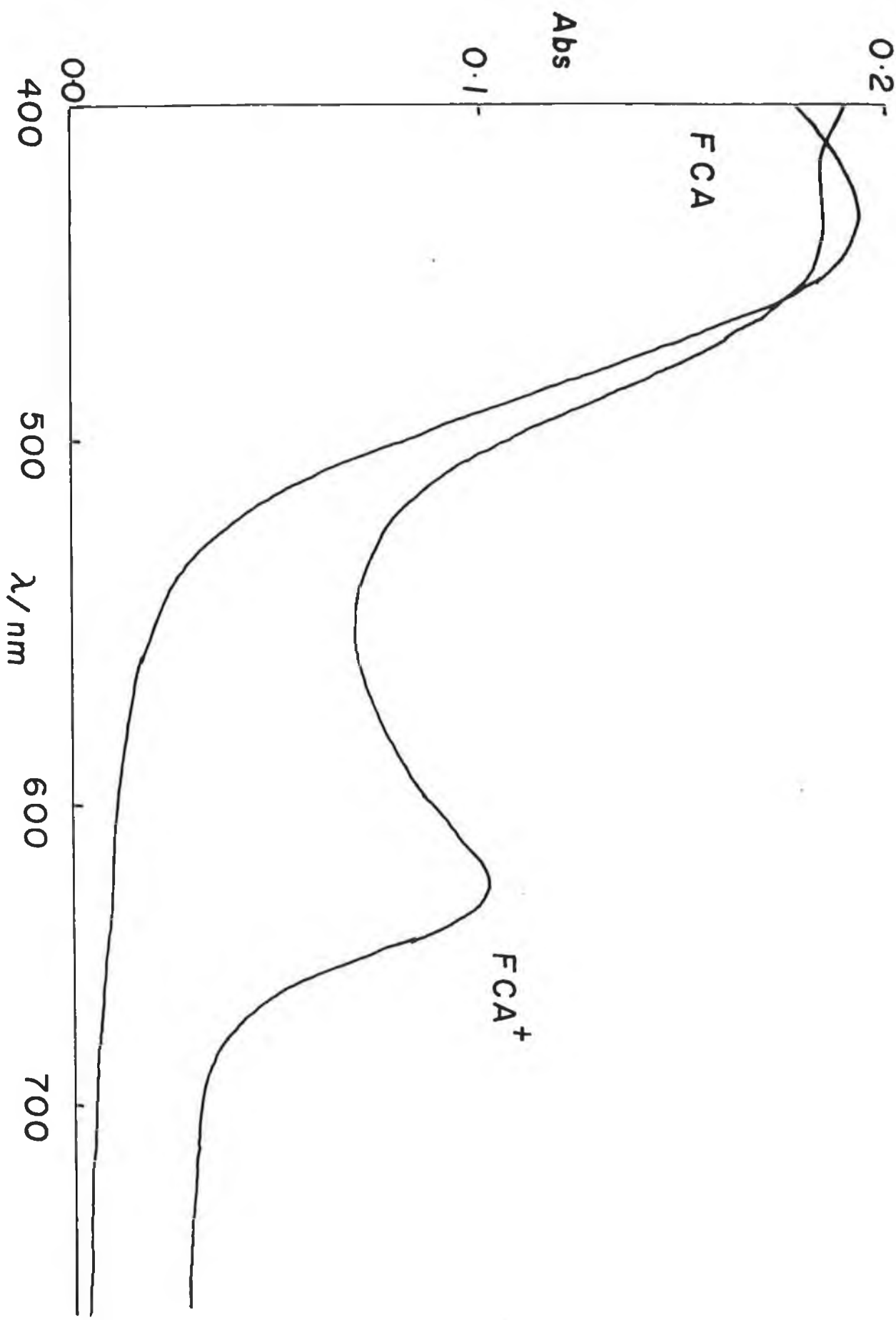

Figure 2.18: UV-Vis spectra of 1mM FCA after bulk electrolysis at 0.6V for 1 hour in 0.2M Na_2HPO_4.

2.3.4 Oxidation of ascorbic acid at a rotating disk electrode; using electrodes coated with PVP layers and loaded with FCA

Several attempts were made to form consistent, reproducible layers of PVP on platinum and carbon disk electrodes. Finally, the conclusion was reached that the best method of doing this was to use hot air to simultaneously blow most of the methanol from the applied drop of the PVP in methanol/1,6 dibromohexane solution off the electrode, while drying the remainder onto the electrode surface. This layer was then cured in the oven at 90°C for 8 hours [36].

Figure 2.19 shows the oxidation of ascorbic acid at the rotating disk electrode at different rotation rates where the electrode used was a platinum disk. The oxidation proceeds very sluggishly which is illustrated by the gradual rise in current as the potential applied increases. The oxidation seems to begin at approximately 0.4V but it is difficult to assess where it achieves a plateau, if indeed it does in this potential range. Consequently, it is hard to extrapolate values for the limiting currents, and from these values calculate the current associated with each oxidation. Unfortunately, this is a problem frequently encountered when looking at the oxidation of ascorbic acid at the rotating disk electrode [37].

Figure 2.20 shows the oxidation of ascorbic acid at the rotating disk electrode at different rotation rates where the electrode used was a platinum disk coated with PVP and loaded with FCA. In this case the oxidation of ascorbic acid at each rotation rate is sharper than the corresponding oxidation at the bare platinum electrode. Here the oxidation also begins earlier (at approximately 0.25V) compared to figure 2.19. This makes it easier to extrapolate limiting current values and calculate oxidation currents.

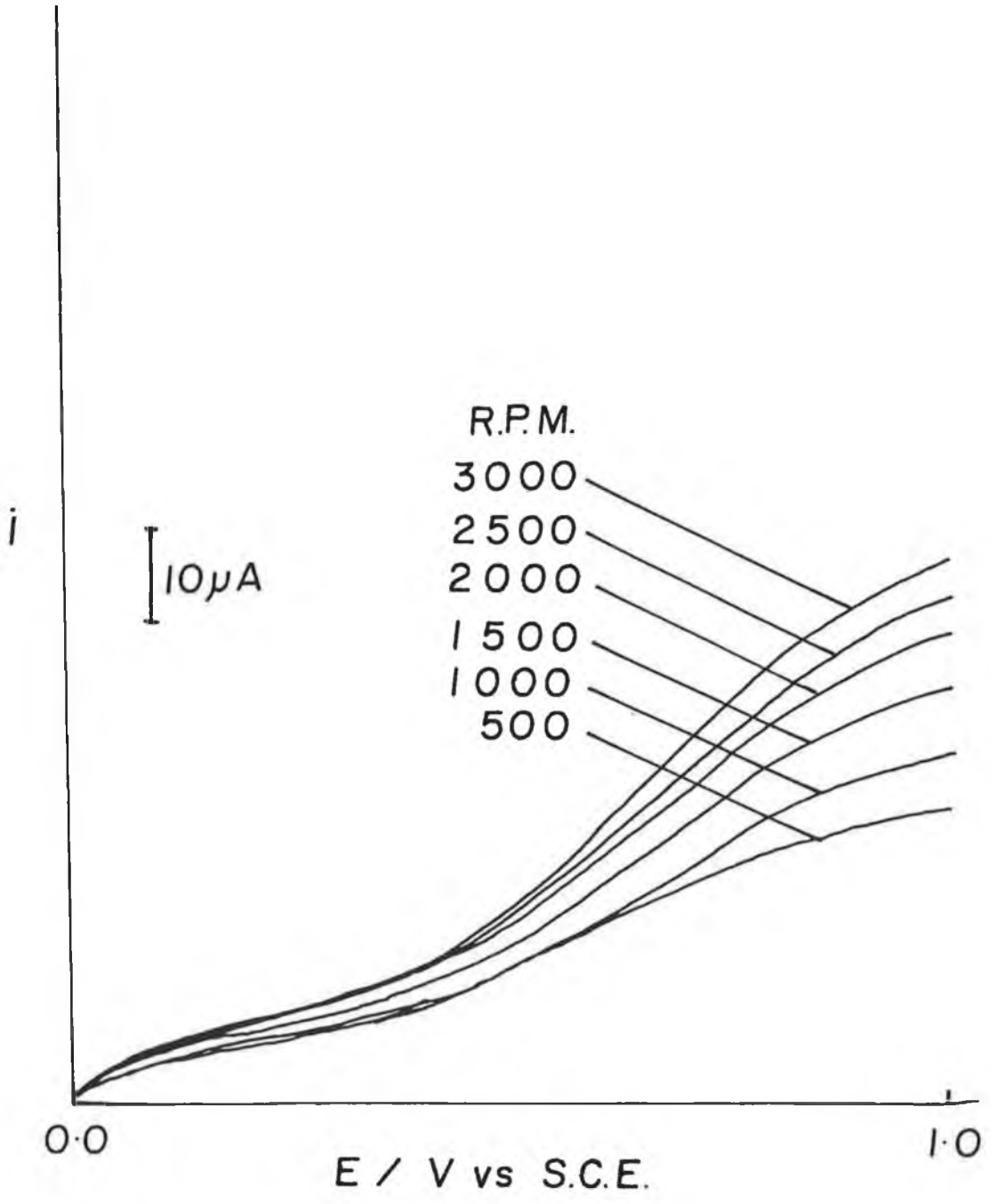

Figure 2.19: Oxidation of 0.5mM ascorbic acid in 0.1M KCl/H_2O at the RDE at different rotation rates. The electrode used here was a platinum disk.

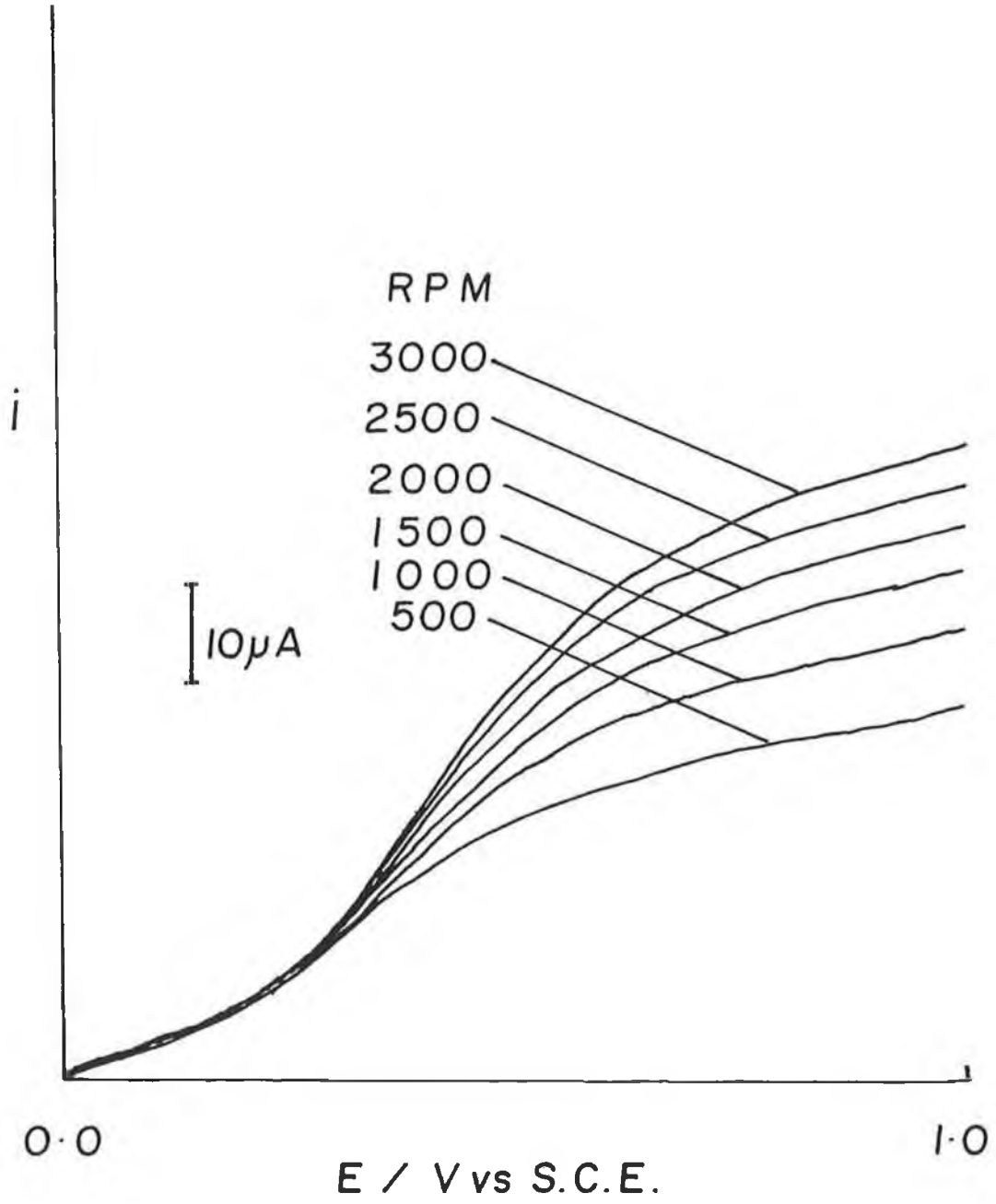

Figure 2.20: Oxidation of 0.5mM ascorbic acid in 0.1M KCl/H_2O at the RDE at different rotation rates. The electrode used here was a platinum disk coated with PVP and loaded with FCA.

The reason for the differences between figures 2.19 and 2.20 is that the oxidation of ascorbic acid is being mediated and therefore enhanced by the oxidation of the neutral ferrocene to the ferricinium ion. The reaction mechanism involved is represented by the following equation pair of equations.

$$Fc \rightarrow Fc^{+} + e^{-} \qquad 2.9$$

$$Fc^{+} + AA \rightarrow Fc + DHA \qquad 2.10$$

where AA stands for ascorbic acid and DHA stands for dehydroascorbate. The ascorbic acid will be oxidised at a lower potential and so in an amperometric method there would be less chance of other species interfering. This mediation could be harnessed for use in the detection of ascorbic acid in fruit juices etc., as its oxidation current is directly proportional to concentration.

2.4.5 Cyclic voltammetry of ferrocene dicarboxylic acid

The structure of ferrocene dicarboxylic acid (FCDA) differs only from that of FCA in that it has a carboxylic acid group on each cyclopentadienyl ring. Therefore it was thought that perhaps, when under the same conditions as one exists for FCA, it may also exhibit a post-peak. However, as can be seen in figure 2.21 - where the pH > 10 and the solution has been oxygenated, this was not the case. Therefore it is suggested that this phenomenon is exclusive to FCA.

There is a difference between the absence and presence of O_2 in that there is a bulk mediation effect as can be seen in figures 2.21 and 2.22. This suggests there is mediation in bulk solution.

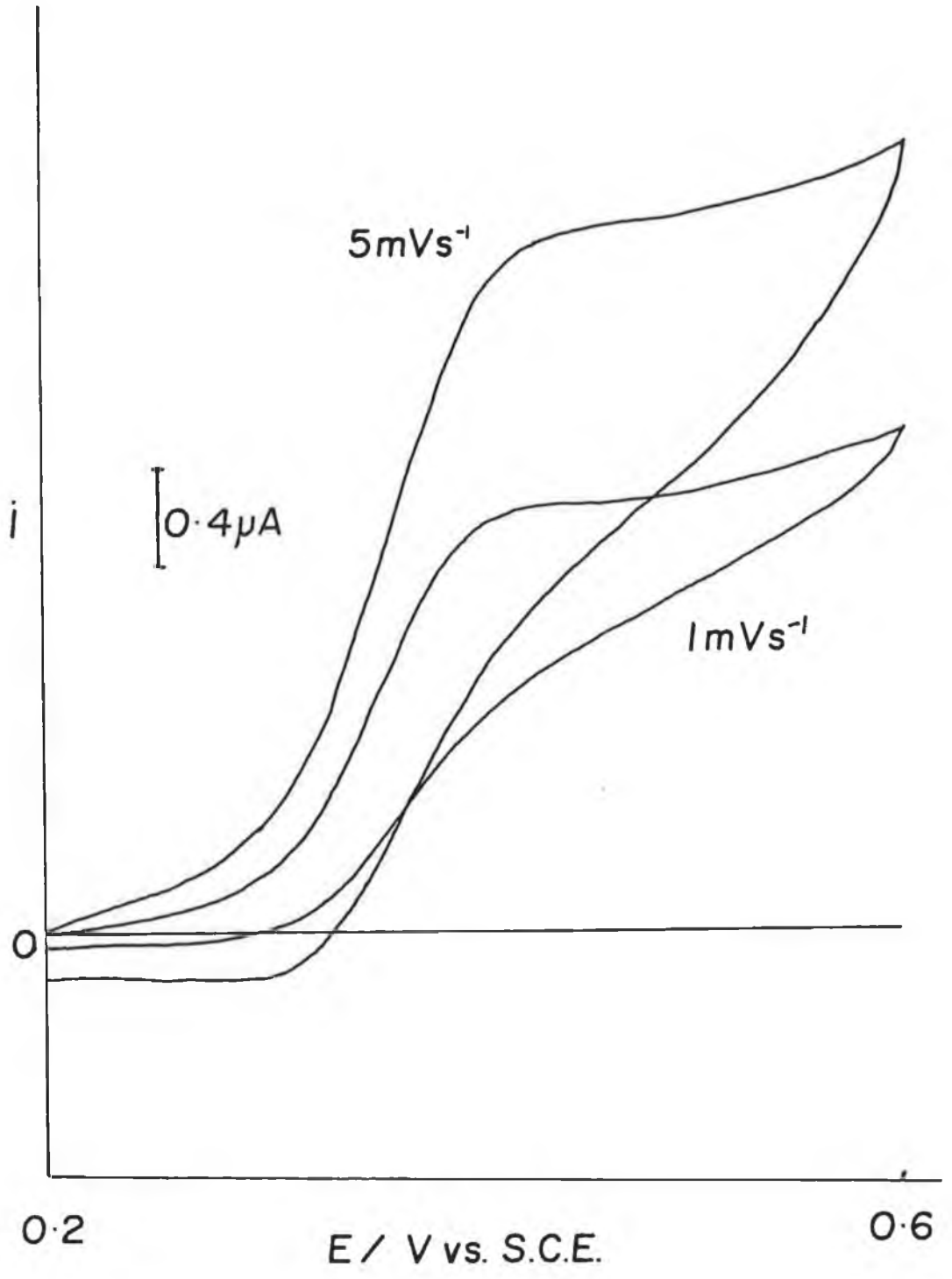

Figure 2.21: Cyclic voltammograms of 1mM FDCA in 0.2M Na_2HPO_4 /H_2O, (pH > 10) at a gold electrode, after bubbling the solution with O_2.

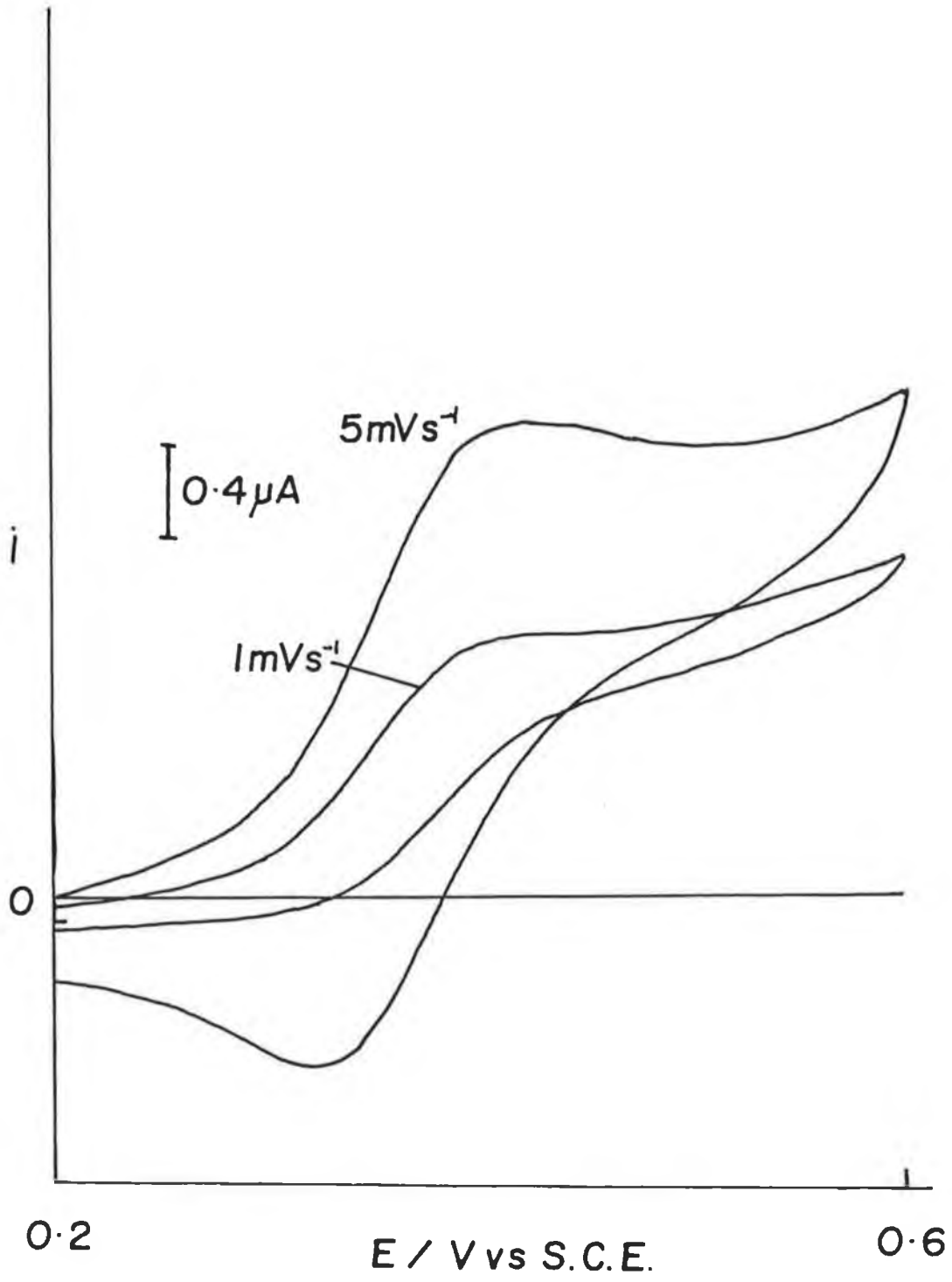

Figure 2.22: Cyclic voltammograms of 1mM FDCA in 0.2M Na_2HPO_4 /H_2O, (pH > 10) at a gold electrode, after degassing the solution with N_2.

2.4 Conclusion

After performing various voltammetric studies on the ferrocene carboxylic acid molecule, under a combination of anaerobic/aerobic and non-aqueous/aqueous conditions, it is proposed that the observed oxidation post-peak corresponds to the oxidation of oxygen to ozone. It is also proposed that this oxidation is facilitated through the action of FCA as a mediator in the reaction represented by equation 2.3. This equation is preferred to equations 2.1 and 2.2 as, from the results it is clear that changing the pH of the solution has a direct effect on the magnitude of the post-peak in the presence of oxygen, whereas the addition of water to the non-aqueous solutions of FCA studied (also in the presence of O_2) did not result in the appearance of the post-peak. Unfortunately, all attempts to gain evidence of the presence of ozone in the solutions studied were unsuccessful.

The ability of FCA to mediate in the oxidation of ascorbic acid was demonstrated at the rotating disk electrode. This is just another example of the multiple existing and potential applications of ferrocenes and their derivatives as electron transfer agents.

Although, as mentioned in section 2.1, ferrocene monocarboxylic acid is widely used as an electrochemical system, it is suggested that it not be used for this purpose under conditions where the solution is both at a high pH and exposed to oxygen. This suggestion is made on the basis of results in this work, which found FCA to exhibit non-ideal behaviour under these conditions.

2.5 References

1. B.J. Coe, C.J. Jones, J.A. McCleverty, D. Bloor, P.V. Kolinsky, and R.J. Jones, J. Chem. Soc. Chem. Comm., (1989), 1485.

2. A. Houlton, J.R. Miller, J. Silver, N. Jasim, M.T. Ahmet, T.L. Axon, D. Bloor, and G.H. Cross, Inorg. Chim. Acta, (1993), **205**, 65.

3. J.S. Miller, A.J. Epstein, and W.M. Reiff, Chem. Res., (1988), **88**, 201.

4. T.J. Meyer, Pure Appl. Chem., (1986), **56**, 1193.

5. W. Schuhmann, Biosens. Bioelectron., (1993), **8**, 191.

6. E.I. Iwuoha, and M.R. Smyth, Analyst, (1994), **119**, 265.

7. T. Osa, Y. Kashiwagi, and Y. Yanagisawa, Chem. Lett., (1994), **2**, 367.

8. A.V. Barmin, A.V. Eremenko, I.N Kurochkin, and A.A. Sokolovsky, Electroanalysis, (1994), **6**, 107.

9. C. Bourdillon, C. Demaille, J. Gueris, J. Moiroux, and J.M. Saveant, J. Am. Chem. Soc., (1993), **115**, 12264.

10. J.K. Harkness, O.J. Murphy, and G.D. Hitchens, J. Electroanal. Chem. (1993),**357**, 261.

11. M.A.T. Kilmartin, J.P. Hart, and B.J. Birch, Analyst, (1994), **119**, 243.

12. D.M. Fraser, S.M. Zakeeruddin, and M. Gratzel, J. Electroanal. Chem., (1993), **359**, 125.

13. A.A. Shulga, H. Koudelkahep, N.F. Derooij, and L.I. Netchiporouk, Anal. Chem., (1994), **66**, 205.

14. J.M. Dicks, M.F. Cardosi, A.P.F. Turner, and I. Karube, Electroanalysis, (1993), **5**, 1.

15. S.P. Hendry, M.F. Cardosi, A.P.F. Turner, and E.W. Neuse, Anal. Chim. Acta, (1993), **281**, 453.

16. S.E. Creager, and G.K. Rowe, J. Electroanal. Chem., (1994), **370**, 203.

17. Y. Degani, and A. Heller, J. Am. Chem. Soc., (1988), **110**, 2615.

18. W. Schuhmann, T.J. Ohara, H.L. Schmidt, and A. Heller, J. Am. Chem. Soc., (1991), **113**, 1394.

19. A. Badia, R. Carlini, A. Fernandez, F. Battaglini, S.R. Mikkelsen, and A.M. English, J. Am. Chem. Soc., (1993), **115**, 7053.

20. O. Traverso, and F. Scandola, Inorg. Chim. Acta, (1970), **4**, 493.

21. A.M. Tarr, and D. Wiles, Canadian J. Chem., (1968), **46**, 2725.

22. J.D. Coyle, and G. Marr, J. Organomet. Chem., (1973), **60**, 153.

23. L.H. Ali, A. Cox, and T.J. Kemp, J. Chem. Soc. Dalton Trans., (1970), 1468.

24. P.N. Bartlett, and K.F.E. Pratt, J. Electroanal. Chem., (1995), **397**, 53.

25. J. Davis, D.H. Vaughan, M.F. Cardosi, Electroanalysis, (1997), **9**, 650.

26. T. Kuwana, and W. Heineman, Acc. Chem. Res., (1976), **9**, 241.

27. W. Heineman, F. Hawkridge, and H. Blount, "Spectroelectrochemistry at Optically Transparent Electrodes." In 'Electroanalytical Chemistry, Vol. 13, ed. A.J. Bard (Marcel Dekker, New York, 1986).

28. J. Wang, 'Analytical Electrochemistry', VCH New York, (1994), p174.

29. J.D.E. McIntyre, Adv. In Electrochem. and Electrochem. Eng., (1973), **9**, 61.

30. S. McCormac, N.R. Russell, and J.C. Cassidy, Electrochim. Acta, (1992), **37**, 1939.

31. F.A. Cotton, and G. Wilkinson, 'Advanced Inorganic Chemistry,' 3rd edition, Interscience, New York, (1972), p.410.

32. F.A. Cotton, and G. Wilkinson, 'Advanced Inorganic Chemistry,' 3rd edition, Interscience, New York, (1972), p.411.

33. J. O'Gorman, Unpublished Work, (1995).

34. A. Barbe, C. Secroun, and P. Jouve, J. Mol. Spectrosc., (1974), **49**, 171.

35. S.R. Radel, and M.H. Navidi, 'Chemistry,' 2nd edition, West Publishing Co., Minneapolis, p.394.

36. J.F. Cassidy, and K. Tokuda, J. Electroanal. Chem., (1990), **285**, 287.

37. M.E.G. Lyons, W. Breen, and J.C. Cassidy, J. Chem. Soc. Faraday Trans., (1991), **87**, 115.

3 Differential Pulse Voltammetry at a Microelectrode

3.1 Introduction

Microelectrodes have been cited to have many advantages over conventional electrodes [1-3]. As only extremely small currents are involved (sometimes as little as 10^{-17}A) when using microelectrodes, the addition of supporting electrolyte may be avoided. This may be necessary in an experiment where the potential limits extend to a region where the electrolyte is oxidised/reduced, thus obscuring the oxidation/reduction waves of the analyte. There may also be no need to introduce an auxiliary electrode as a 'current sink', as the current may not be large enough to have a disruptive effect on the reference electrode. The small currents drawn by microelectrodes, together with their tiny dimensions, makes *in vivo* analysis a real possibility [4]. They can be used to characterise short-time processes in living cells. They can be used in arrays, where potential control of a multi-electrode system is required when probing the cell.

Although the microelectrode has become a powerful analytic tool, it does have its drawbacks. Microelectrodes are fragile and have an inability to measure small quantities of current without noise interference. Also, while the effect of double layer charging at the microelectrode is diminished compared to that at a macroelectrode, it is still present. However the main disadvantage is that use of a microelectrode in a direct mode potential sweep experiment results in a sigmoidal output, which is difficult to interpret at low analyte concentrations. The aim of this work is to characterise the response from the application of a differential pulse voltammetric waveform to a microelectrode.

3.2 Theory

In postulating the theory behind differential pulse voltammetry at a microelectrode the following assumptions are made [5]:

1. When a pulse is applied at the microelectrode, the Cottrell equation may be used for characterisation of the current response at short time periods.

2. The DC component of the current follows the traditional microelectrode behaviour with a potential dependent component.

3. DC and pulse terms are additive for a reversible system, thus;

$$i_1 = \frac{nFA\sqrt{DC}}{\sqrt{\pi\delta}}\left[\frac{(1-\sigma^2)\varepsilon_1}{(1+\varepsilon_1)(1+\sigma^2\varepsilon_1)}\right] \qquad 3.1$$

$$i_2 = \frac{4nFrDC}{1+\varepsilon_1} \qquad 3.2$$

$$i_3 = \frac{4nFrDC}{1+\varepsilon_2} \qquad 3.3$$

where i_1 is the current contribution from pulse, i_2 is the DC current before the pulse is applied, i_3 is the DC current at the end of the pulse, and ε_1, ε_2 and σ^2 may be expressed as follows;

$$\varepsilon_1 = \exp\left(\frac{nF(E_1 - E^{0'})}{RT}\right) \qquad 3.4$$

$$\varepsilon_2 = \exp\left(\frac{nF(E_2 - E^{0'})}{RT}\right) \qquad 3.5$$

$$\sigma^2 = \exp\left(\frac{nF\Delta E}{RT}\right) \qquad 3.6$$

where E_1 is the potential prior to pulse (at a time τ), E_2 is the potential after the pulse is applied (at a time $\delta + \tau$). τ is the time at which the current is sampled before the pulse is applied and $(\delta + \tau)$ is the time at which the current is sampled after the pulse is applied. ΔE is the pulse amplitude and all the other symbols have their usual meaning. The instrumental differential current output is represented as follows:

$$i = i_1 + i_3 - i_2 \qquad 3.7$$

3.3 Experimental Procedure

All experiments were carried out using an Edt potentiostat Model ECP 100, and at room temperature. A J.J.Lloyd X-Y chart recorder Model PL3 was used to chart the response. A three electrode one compartment system was used where; the working electrode was a platinum microelectrode (EG&G), the reference was a saturated calomel electrode and the auxiliary was a carbon rod. All chemicals used were of reagent grade and all solutions were prepared using de-ionised water. The simulations were calculated using a computer program coded in FORTRAN.

3.4 Results and Discussion

From the limiting current, i_L, of the voltammetric response obtained by scanning 1×10^{-3}M ferrocyanide using the microelectrode, the electrode radius can be found, since:

$$i_L = 4nFrDC. \qquad 3.8$$

From experiment, $i_L = 5.6\times10^{-9}$ A. Therefore $r = 4.46\times10^{-6}$ m, taking D for $\left[Fe(CN)_6\right]^{4-}$ to be 6.5×10^{-6} cm^{2}sec^{-1}, as quoted by Sawyer and Roberts [6]. This compares with the nominal radius of 5×10^{-6} m.

When the differential waveform was applied to the microelectrode, the following analyses were carried out; the peak current, i_p, was studied at different values of ΔE and the effects of varying the scan rate and drop time were also studied. Experimental results show that varying the scan rate or the drop time only serves to distort the peaks, making them more elongated the faster the scan rate (>0.05Vsec^{-1}) or the longer the drop time (>1sec). The optimum values for both the scan rate and drop time were found to be 1×10^{-2} Vsec^{-1} and 1 sec respectively.

Figure 3.1 shows the differential peak current as a function of pulse amplitude (ΔE). The starting point of each plot was manually shifted upwards for clarity. The peak current occurs at the formal potential of the $\left[Fe(CN)_6\right]^{4-}/\left[Fe(CN)_6\right]^{3-}$ couple, and the instrument defines this. The peak width at half height shows no significant variation with ΔE.

Figure 3.2 shows a simulated differential current (eq. 3.7) as a function of pulse amplitude taking the experimental parameters from figure 1. It can be seen that there is little correlation, as in figure 3.2 the peaks broaden with increasing ΔE, and the magnitude of i_p is much less than that for the experimental. Thus in comparing figures 3.1 and 3.2, there seems to be a discrepancy with the theory.

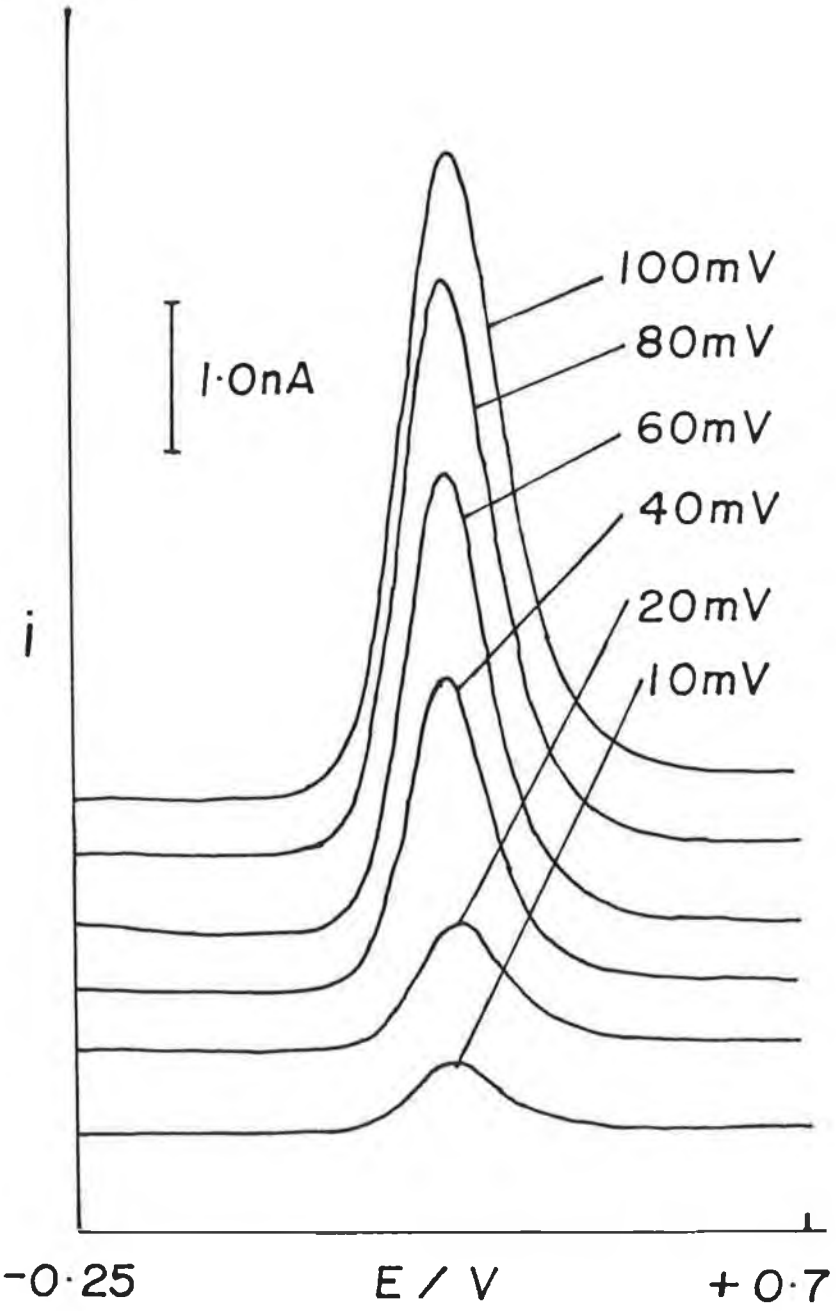

Figure 3.1: Differential pulse response for $\left[Fe(CN)_6\right]^{4-}$ (5×10^{-3}M) in aqueous KCl (0.1M). Platinum microelectrode, radius $=4.46\times10^{-6}$m, scan rate $=1\times10^{-2}$Vsec^{-1}, time constant = 1 sec, drop time ($\delta+\tau$) = 1 sec, pulse width (δ) = 5.5×10^{-2}sec. Pulse amplitudes are indicated in the figure.

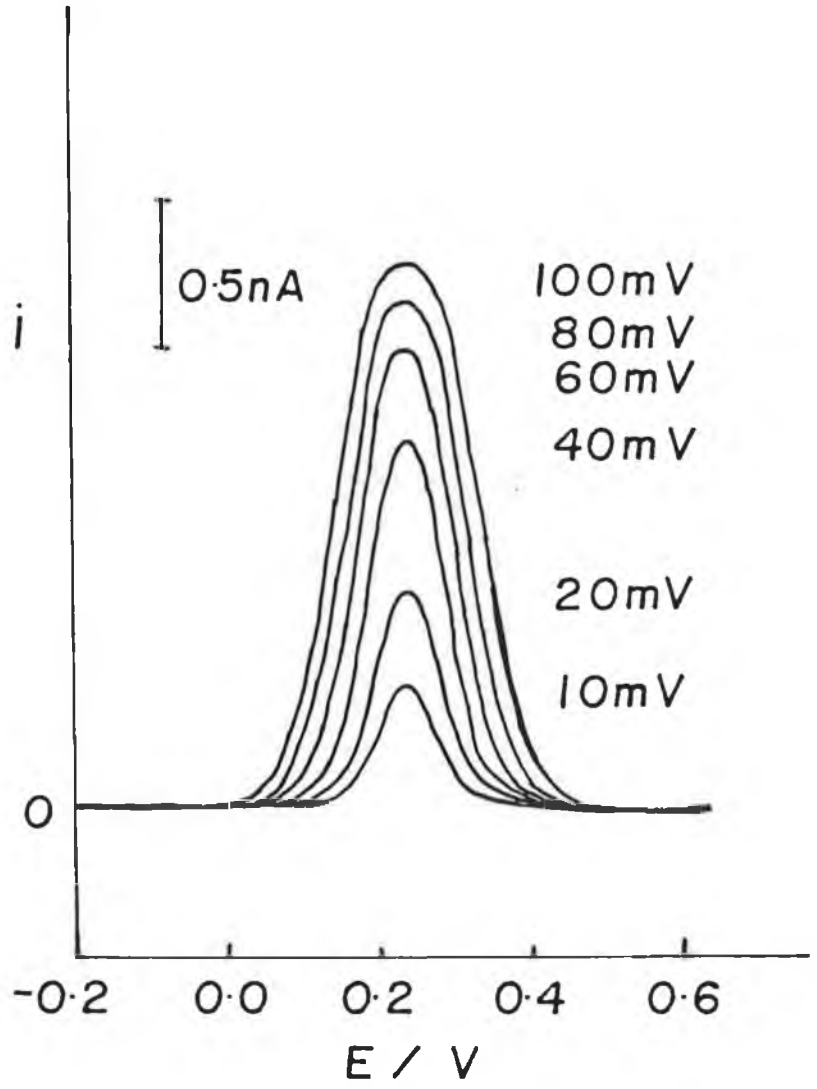

Figure 3.2: Simulated differential current using eq.7. $E^{0'}$ = 0.235V, scan rate = 1×10^{-2} Vsec^{-1}, D = 6.5×10^{-6} cm^{2}sec^{-1}, r = 4.46×10^{-6} m, concentration = 1×10^{-3} M, $(\delta+\tau)$ = 1 sec, (δ) = 5.5×10^{-2} sec. Pulse amplitudes are indicated in the figure.

The diffusion layer thickness, *d*, for ferrocyanide oxidation within the pulse width, can be calculated from the following equation;

$$d = \sqrt{\pi Dt} = \sqrt{3.14\left(6.5\times10^{-6}\right)\left(5.5\times10^{-2}\right)} = 1.06\times10^{-5}\,\mathrm{m} \qquad 3.9$$

where t = pulse width = 5.5×10^{-2} sec. This thickness is of the same order of magnitude as the microelectrode diameter. Therefore there is a considerable 'edge - effect' which leads to a steady state current within the pulse width. By modifying the theory, the differential current, i`, may be calculated as follows;

$$i` = i_4 - i_2 \qquad 3.10$$

where

$$i_4 = \frac{4nFrDC}{1+\varepsilon_3} \qquad 3.11$$

where

$$\varepsilon_3 = \exp\left(\frac{nF\left(E_2 + \Delta E - E^{0'}\right)}{RT}\right) \qquad 3.12$$

This modified theory allows for steady state current to occur before and after the pulse. Figure 3.3 shows the modified simulation of the differential pulse current, i`, plotted as a function of pulse amplitude. It can be seen that there is a good correlation between the magnitudes and shapes of the experimental (figure 3.1) and simulated peaks (figure 3.3). It was found that the sensitivity of the experimental technique was $8.1\times10^{-7}\,\mathrm{AM^{-1}}$, while that predicted from the simulations was $8.4\times10^{-7}\,\mathrm{AM^{-1}}$. For a separate run over a range of concentrations between 5×10^{-4} M and 5×10^{-5} M, a

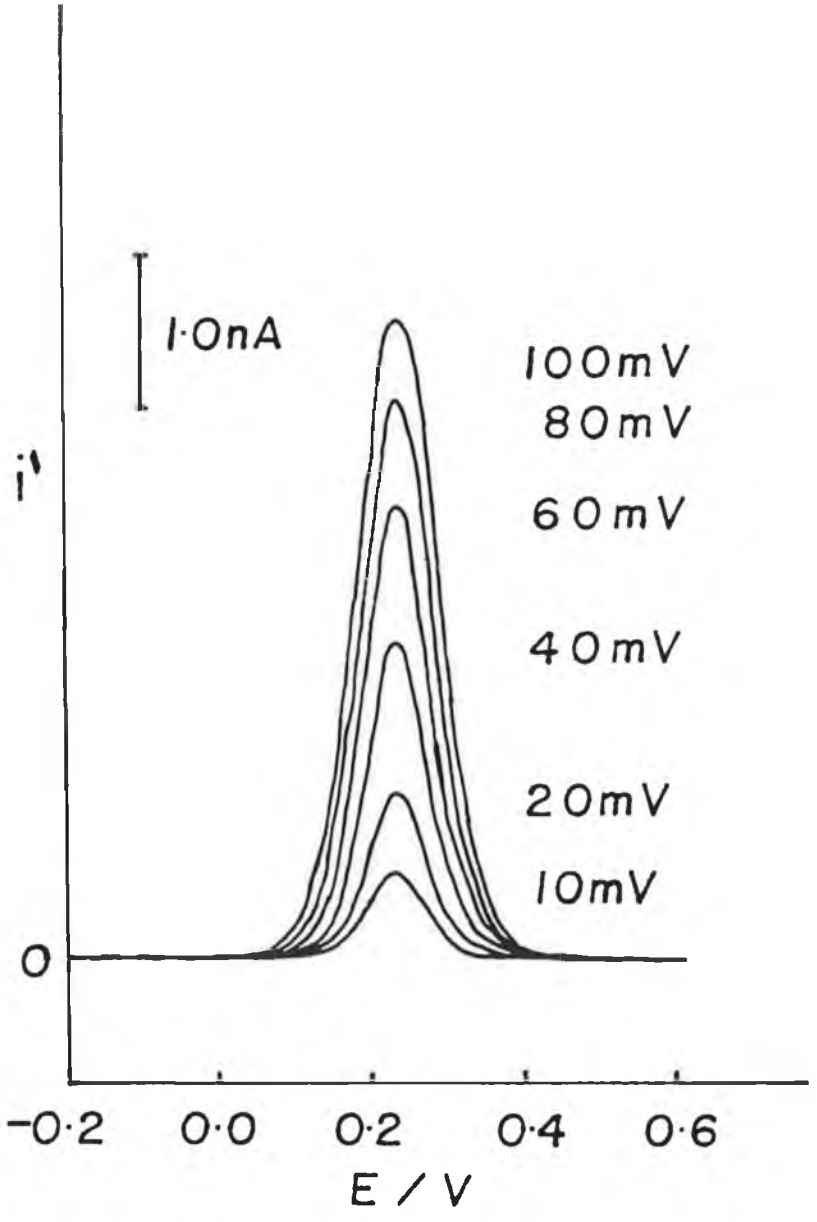

Figure 3.3: Simulated differential current calculated using eq. 3.9. Parameters are the same as in figure 3.2.

straight line of slope $1.07\times10^{-6}AM^{-1}$ and intercept of $-0.02\times10^{-9}A$ was determined with R = 0.989, (n = 5).

A distinct advantage of applying a differential pulse to a microelectrode can be seen at lower concentrations. This is evident in figure 3.4 where the response at the microelectrode is shown both for direct current and after applying a differential pulse. The direct response is very difficult to interpret and therefore almost useless in providing information about any electrochemical reactions taking place. However for the differential pulse response, there is useful information to be gained as a peak is clearly seen at the potential at which the electrochemical reaction in question is known to occur. This has the effect of lowering the limit of detection relative to the direct current experiments. Also a peaked response is more desirable as a baseline can be drawn enabling, peak current to be easily determined. This is in stark contrast to the difficulties encountered, when attempting to measure limiting current from a direct current microelectrode experiment at sub-millimolar concentrations.

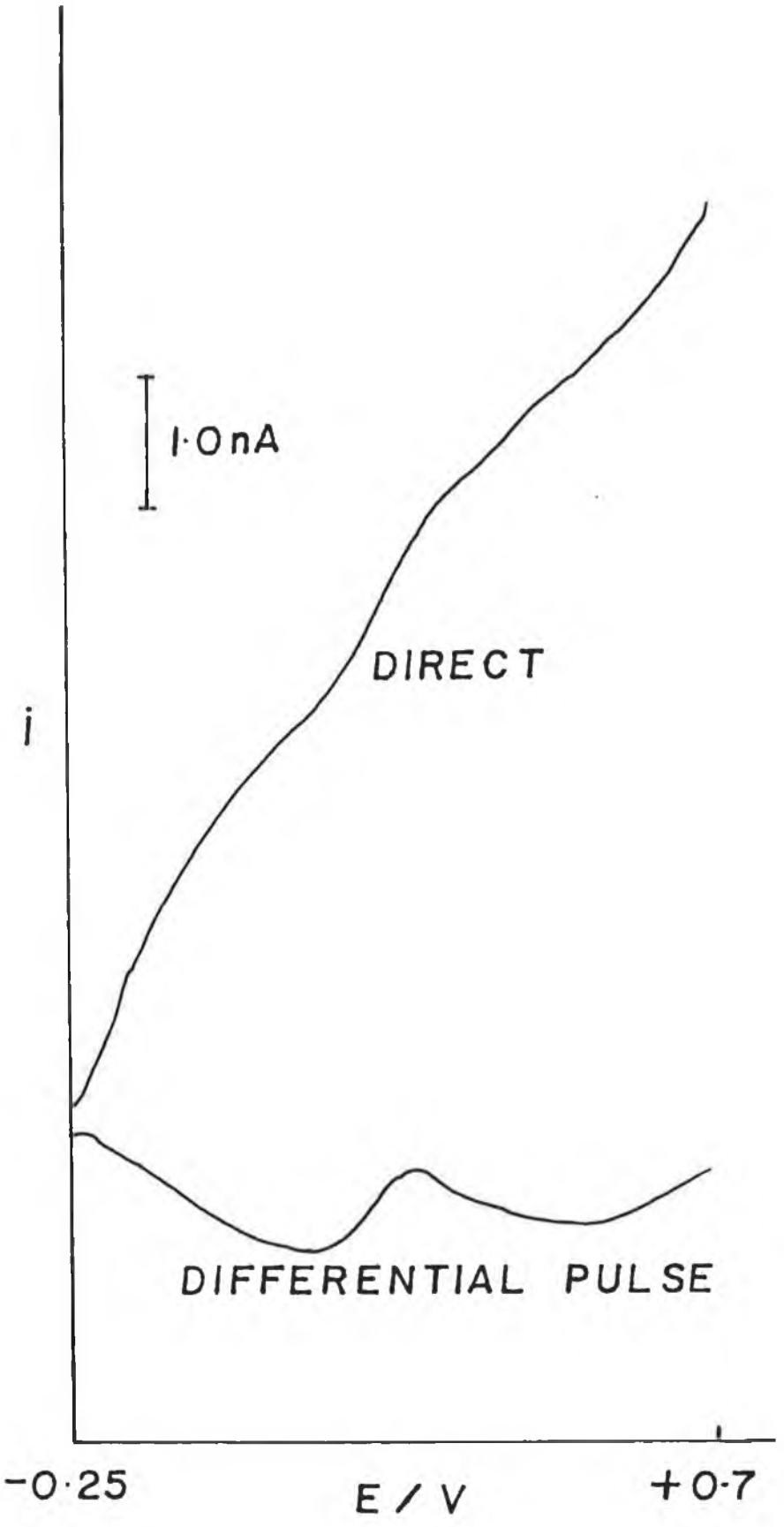

Figure 3.4: Experimental voltammetry for a solution of $\left[Fe(CN)_6\right]^{4-}$ $(5\times10^{-5}M)$ in aqueous KCl (0.1M). Pulse amplitude = 0.1V. The other conditions for the differential pulse signal are as in Fig.1. Direct current signal scan rate = $1\times10^{-2}Vsec^{-1}$.

3.5 Conclusion

As the differential current depends on the diffusion layer thickness, which in turn depends on both the pulse width and the electrode radius, both sets of theory postulated here would hold, but for different conditions. Indeed while the results in this case seemed to correlate well with the modified theory, it would be expected that the shorter the pulse width, the more the experiment would be governed by the original theory. This original theory applies for pulse widths $< \frac{r^2}{25\pi D}$ to ensure that the diffusion layer thickness is less than one tenth the electrode diameter. The modified theory applies for pulse widths $> \frac{4r^2}{\pi D}$ to ensure that the diffusion layer thickness is of the same magnitude as the electrode diameter. From the experimental results it is clear that applying a differential pulse to a microelectrode has obvious advantages for the electrochemist and could prove to be a powerful electroanalytic technique.

3.6 References

1. R.M. Wightman, and D.O. Wipf, in Electroanalytical Chemistry - A Series of Advances, ed. Bard, A.J., Marcel Decker, New York, Vol 15, (1988).

2. S. Pons, and M. Fleischmann, Anal. Chem., (1987), **59**, 1391A.

3. R.M. Wightman, Science, (1988), **240**, 415.

4. J.F. Cassidy, and M.B. Foley, Chemistry in Britain, (1993), **9**, 764.

5. J.E. Anderson, A.M. Bond, and R.D. Jones, Anal. Chem., (1981), **53**, 1016.

6. D.T. Sawyer, and J.L. Robertson, Experimental Electrochemistry for Chemists, Wiley, New York, (1974), p.77.

4 Differential Pulse Voltammetry at a Rotating Disk Electrode

4.1 Introduction

Until the mid-1940's, physical electrochemistry was primarily based around the dropping mercury electrode. However, Levich [1] was to show that rotating a disk-shaped electrode in a solution renders it uniformly accessible to diffusion, yet the hydrodynamics of the liquid flow are solvable and the kinetic equations are relatively simple. In addition, in contrast to the case of a stationary planar electrode, the current at a rotating disk electrode (R.D.E.) rapidly attains a steady-state value. The rotating disk electrode is now a popular system for kinetic and mechanistic studies [2-4]. It combines ease of construction and use, with the ability to control and vary the rate of mass transfer over a wide range.

One drawback however, is that the sigmoidal response of the R.D.E. can sometimes be rather difficult to interpret, especially at low analyte concentrations. One way to solve this problem is to apply a differential pulse to the R.D.E., which converts the sigmoidal response to a peaked voltammogram. This makes the signal easier to interpret, but also introduces additional theoretical considerations [5].

The aim of this work is to characterise the response obtained from applying a differential pulse waveform to an R.D.E., in a solution of a standard reversible electrochemical system; namely potassium ferrocyanide.

4.2 Theory

A ramp potential waveform is applied as the underlying waveform, on top of which a series of pulses of width δ, which are separated by a time interval, τ, are applied to a rotating disk electrode in a solution of a reversible couple.

Two straightforward models are proposed here. Model 1 assumes that the current subsequent to the pulse dominates, while Model 2 assumes that the pulse width is sufficiently long to allow a steady-state current to exist during the pulse width.

Model 1

A differential pulse waveform of pulse width δ, where the interval between pulses is τ, is applied to a rotating disk electrode. The resulting differential current, i, is a combination of the current sampled before the pulse, i_2, and just before the end of the pulse; $i_1 + i_3$. The differential current is;

$$i = i_1 + i_3 - i_2 \qquad 4.1$$

where the current associated with the pulse, i_1, is taken to be independent of the underlying current;

$$i_1 = \frac{nFA\sqrt{DC}}{\sqrt{\pi\delta}}\left[\frac{(1-\sigma^2)\varepsilon_1}{(1+\varepsilon_1)(1+\sigma^2\varepsilon_1)}\right] \qquad 4.2$$

where

$$\sigma = \exp\left(\frac{-nF\Delta E}{RT}\right) \qquad 4.3$$

and

$$\varepsilon_1 = \exp\left(\frac{-nF(E_1 - E^{0'})}{RT}\right) \qquad 4.4$$

where ΔE = pulse amplitude, E_1 is the potential before the pulse is applied and all the other symbols have their usual meaning.

The current before the pulse is applied, i_2, depends on E_1 and is represented as follows;

$$i_2 = \frac{0.62nFAD^{2/3}\omega^{1/2}\nu^{-1/6}C}{(1+\varepsilon_1)} \qquad 4.5$$

and the current at the end of time δ, if the pulse were not applied would be;

$$i_3 = \frac{0.62nFAD^{2/3}\omega^{1/2}\nu^{-1/6}C}{(1+\varepsilon_2)} \qquad 4.6$$

where

$$\varepsilon_2 = \exp\left(\frac{-nF(E_2 - E^{0'})}{RT}\right) \qquad 4.7$$

where E_2 is the potential magnitude at time δ after the time when the voltage is E_1 without the pulse being applied. The contribution of the current from the pulse is i_1. i is plotted against $E_1+\Delta E$, where E_1 is the base potential.

Model 2

For a pulse width, δ, of 55msec and when D = 6.5×10^{-6} cm^2sec^{-1} [6] the diffusion layer thickness d_1, where $d_1 \cong (\pi Dt)^{-1}$, is 1×10^{-3}cm. From R.D.E. theory [7], the effective diffusion layer thickness, $d_2 = 1.61D^{1/3}\omega^{-1/2}\nu^{1/6}$ at f = 2000rpm, then d_2 =

0.98×10^{-3} cm, and so a steady state response can arise within the timescale of the pulse width. The resulting differential pulse current, *i*', is as follows;

$$i` = i_4 - i_2 \qquad 4.8$$

where

$$i_4 = \frac{0.62nFAD^{2/3}\omega^{1/2}\nu^{-1/6}C}{(1+\varepsilon_3)} \qquad 4.9$$

where

$$\varepsilon_3 = \exp\left(\frac{-nF(E_2 + \Delta E - E^{\circ'})}{RT}\right) \qquad 4.10$$

$i`$ is plotted against $E + \frac{\Delta E}{2}$.

An important aspect of equations 4.1 and 4.8 is that the differential currents in each case are directly related to the concentration of substrate.

4.3 Experimental Procedure:

All experiments were carried out using an Edt potentiostat Model ECP 100, and at room temperature. A J.J.Lloyd X-Y chart recorder Model PL3 was used to chart the response. A three electrode one compartment system was used where; the working electrode was a platinum disk rotated using a Metrohm 628-10 system, the reference was a saturated calomel electrode and the auxiliary was a carbon rod. All chemicals used were of reagent grade and all solutions were prepared using de-ionised water. The electrode area was determined from limiting current measurements. The

simulations were calculated using a computer program coded in FORTRAN on a personal computer.

4.4 Results and Discussion

Figures 4.1 and 4.2 show the experimental differential pulse voltammograms at a rotating disk electrode (D.P.R.D.E.), as a function of pulse amplitude for two rotation rates. It can be clearly seen that the peak height increases with both pulse amplitude and rotation rate. Model 1 does not apply in this case as, under the experimental conditions, it predicts that peak height does not increase with increasing rotation rate.

Simulated plots are shown in figure 4.3 for the experimental conditions in figures 4.1 and 4.2 using Model 2 (equation 4.8). There is good agreement between figures 4.1 and 4.3, in that the peak width at half height does not vary with ΔE and the peak current magnitudes are similar. Model 2 depends on the diffusion layer, thickness d_2, extending out to achieve steady-state conditions within the pulse width. However, the experimental plots do not fully return to baseline, since the potentiostat allowed only one pulse width which may not be long enough to ensure that the experimental conditions comply fully with the Model 2 assumptions. There is also an increasing background signal that changes with pulse amplitude, which is more dominant at the low rotation rate.

In figure 4.2 the peak widths at half height are 158 ± 20mV for the range of pulse amplitudes. For the Model 2 responses (figure 4.3), the peak width at half height is about 100mV and does not change with pulse amplitude.

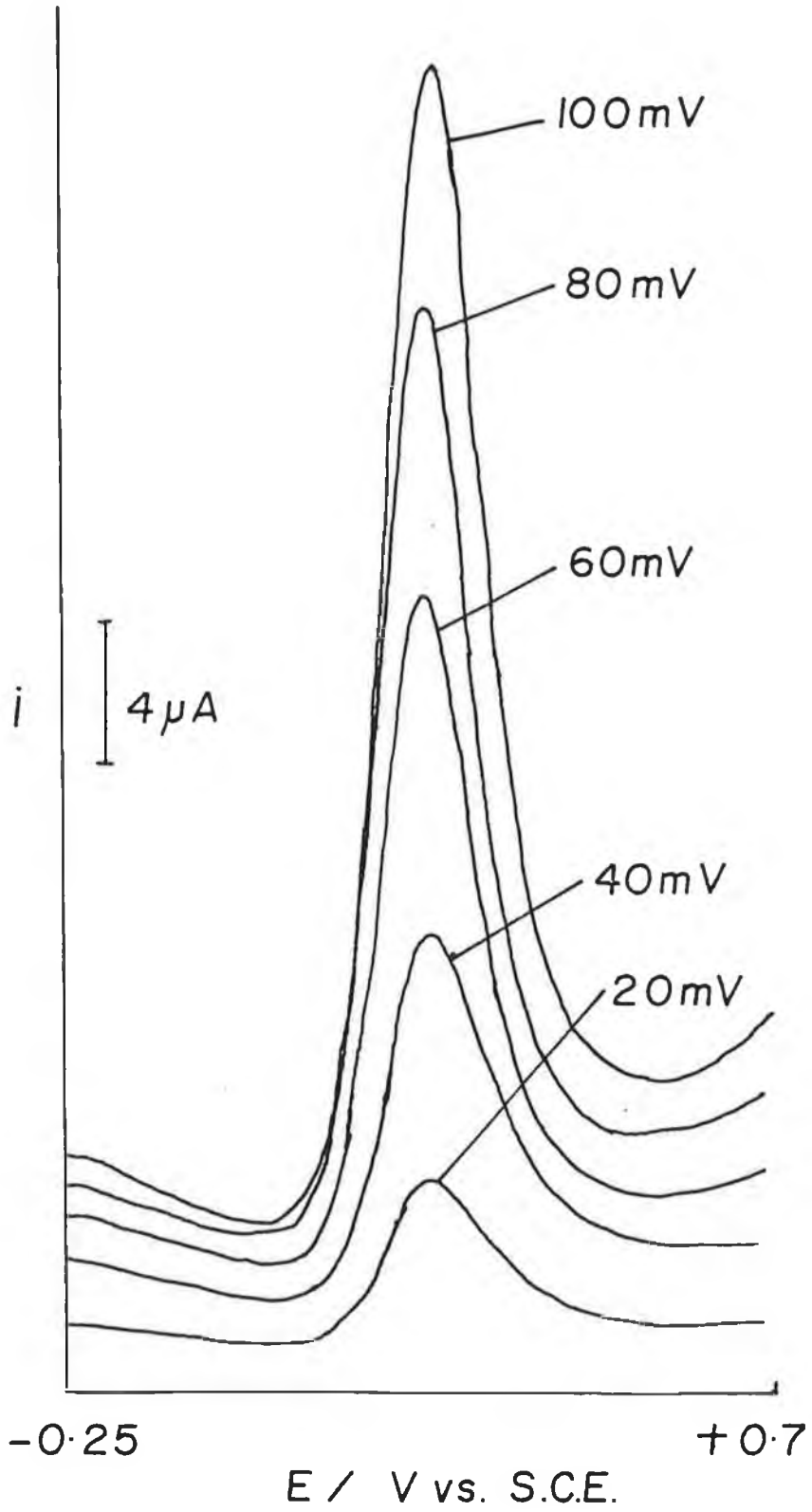

Figure 4.1: D.P.R.D.E. response for $\left[Fe(CN)_6\right]^{4-}$ (1×10^{-3}M) in aqueous KCl (0.1M). Platinum electrode (area = 0.051cm^2), scan rate =1×10^{-2}Vsec^{-1}, f = 3000rpm, time constant = 1 sec, drop time ($\delta+\tau$) = 1 sec, pulse width (δ) = 5.5×10^{-2}sec. Pulse amplitudes are indicated in the figure.

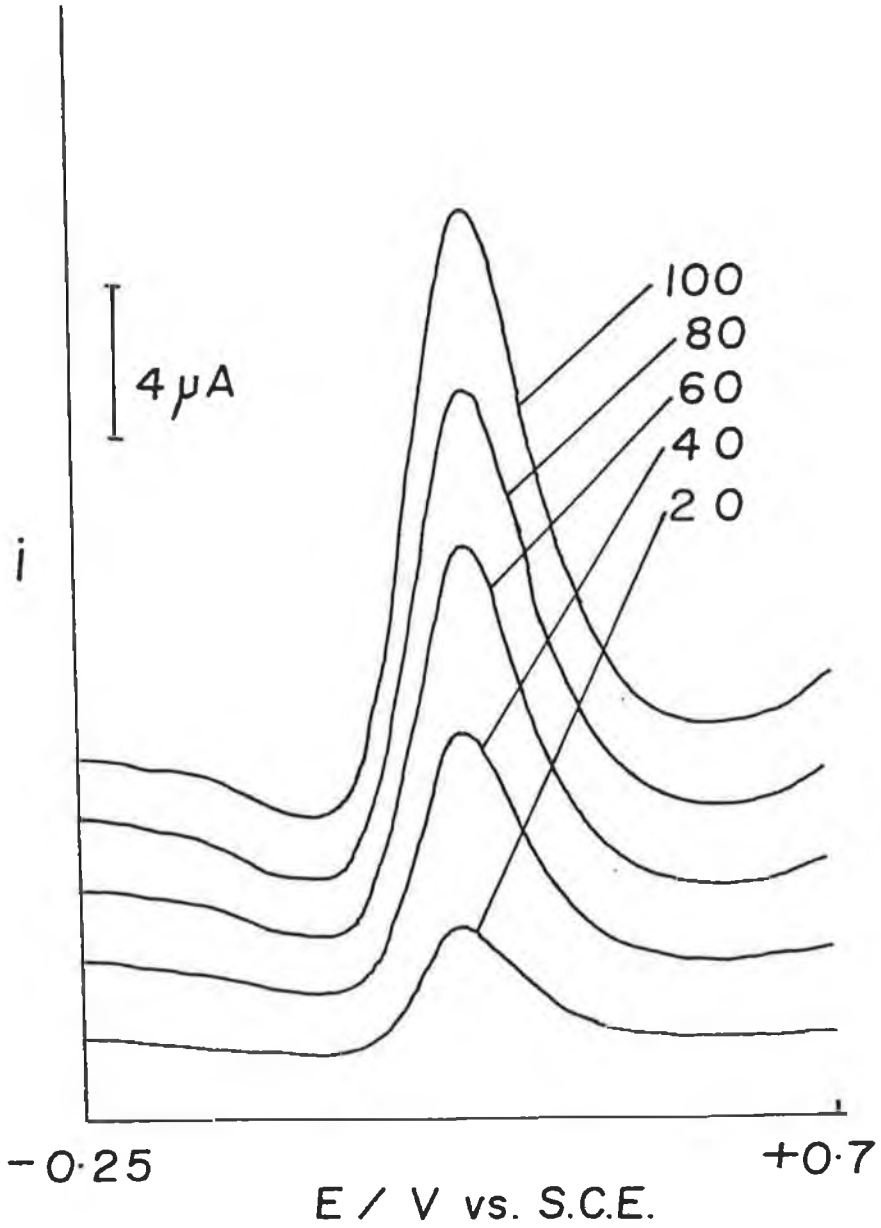

Figure 4.2: D.P.R.D.E. response for $\left[Fe(CN)_6\right]^{4-}$ (1×10^{-3}M) in aqueous KCl (0.1M). Platinum electrode (area = 0.051cm^2), scan rate = 1×10^{-2} Vsec^{-1}, f = 500rpm, time constant = 1 sec, drop time ($\delta+\tau$) = 1 sec, pulse width (δ) = 5.5×10^{-2} sec. Pulse amplitudes are indicated in the figure.

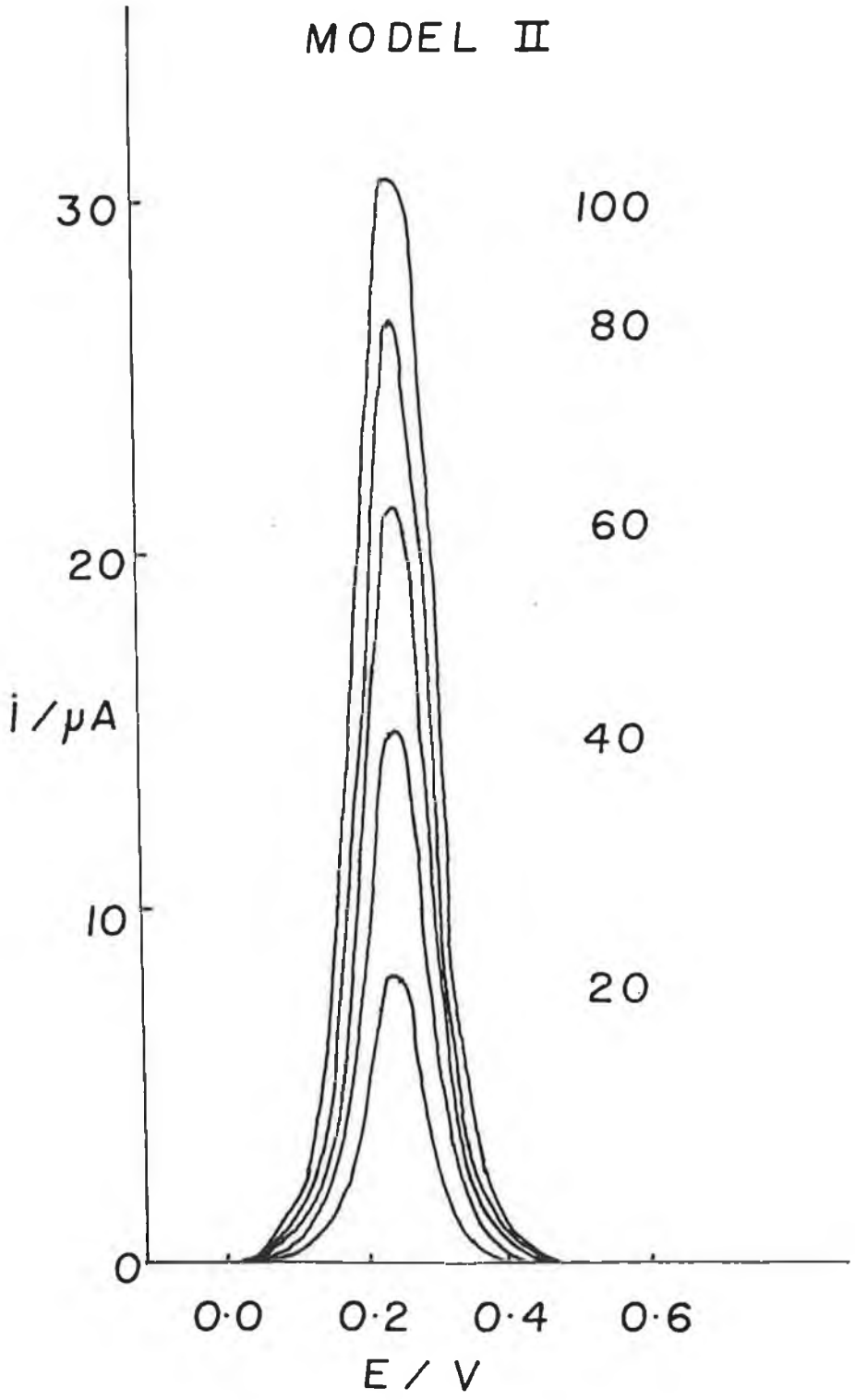

Figure 4.3: Simulated D.P.R.D.E. response using Model 2. $E^{0'} = 0.235V$, scan rate = $1\times10^{-2}\,Vsec^{-1}$, $D = 6.5\times10^{-6}\,cm^2sec^{-1}$, area = $0.051cm^2$, concentration = $1\times10^{-3}\,M$, $(\delta+\tau) = 1$ sec, $(\delta) = 5.5\times10^{-2}$ sec, kinematic viscosity = $0.01cm^2\,sec^{-1}$, $f = 3000$rpm. Pulse amplitudes are indicated in the figure.

Figures 4.4 and 4.5 show the effect of rotation rate experimentally, for two different pulse amplitudes. It can be seen that the background current and background current magnitudes vary more with rotation rate when ΔE is smaller. Under these conditions the diffusion layer thickness associated with the pulse, $d_1 = 1.1 \times 10^{-3}$cm, and the effective diffusion layer thicknesses, d_2, are 0.80×10^{-3}cm, 0.98×10^{-3}cm and 1.38×10^{-3}cm for 3000, 2000 and 1000rpm respectively.

On first glance it is curious that the background behaviour should be different for figures 4.4 and 4.5, since the rotation rates are similar and that Model 2 is more relevant than Model 1. The key to the behaviour lies in the magnitude of the pulse amplitude, which is the driving force of the reaction. The nominal diffusion layer thicknesses associated with the pulse, d_1, and the rotation rates, d_2, are similar in magnitude. In figure 4.4 the pulse amplitude is small, so the response is dominated by the concentration profiles from the underlying ramp sweep rather than the pulse and varies with ω. In figure 4.5, where ΔE = 100mV, the response is dominated by the pulse component of the waveform, as there is a greater driving force for the reaction and since the magnitude of d_1 is similar to that of d_2.

This behaviour is also reflected in figures 4.1 and 4.2, where the background is seen to vary more greatly with ΔE at low rotation rate, than at high rotation rate.

Models 1 & 2 are limiting models and the experimental results constitute a region of mixed control where because of the fixed pulse width and limited rotation rates, $d_1 \approx d_2$. Model 2 fits the experimental results better than Model 1 as can be seen from figure 4.6; where conditions similar to figure 4.5 were employed in the calculations

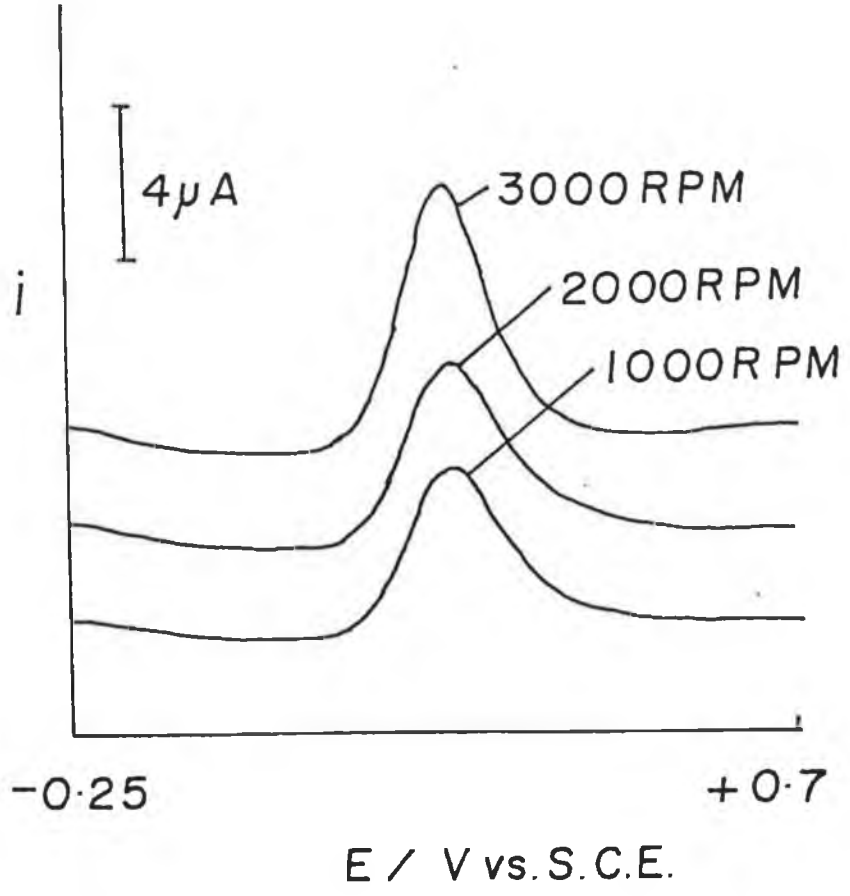

Figure 4.4: D.P.R.D.E. response for $\left[Fe(CN)_6\right]^{4-}$ (1×10^{-3}M) in aqueous KCl (0.1M). Platinum electrode (area = 0.051cm^2), scan rate =1×10^{-2}Vsec^{-1}, time constant = 1 sec, drop time ($\delta+\tau$) = 1 sec, pulse width (δ) = 5.5×10^{-2}sec, pulse amplitude = 20mV, rotation rates are shown in figure.

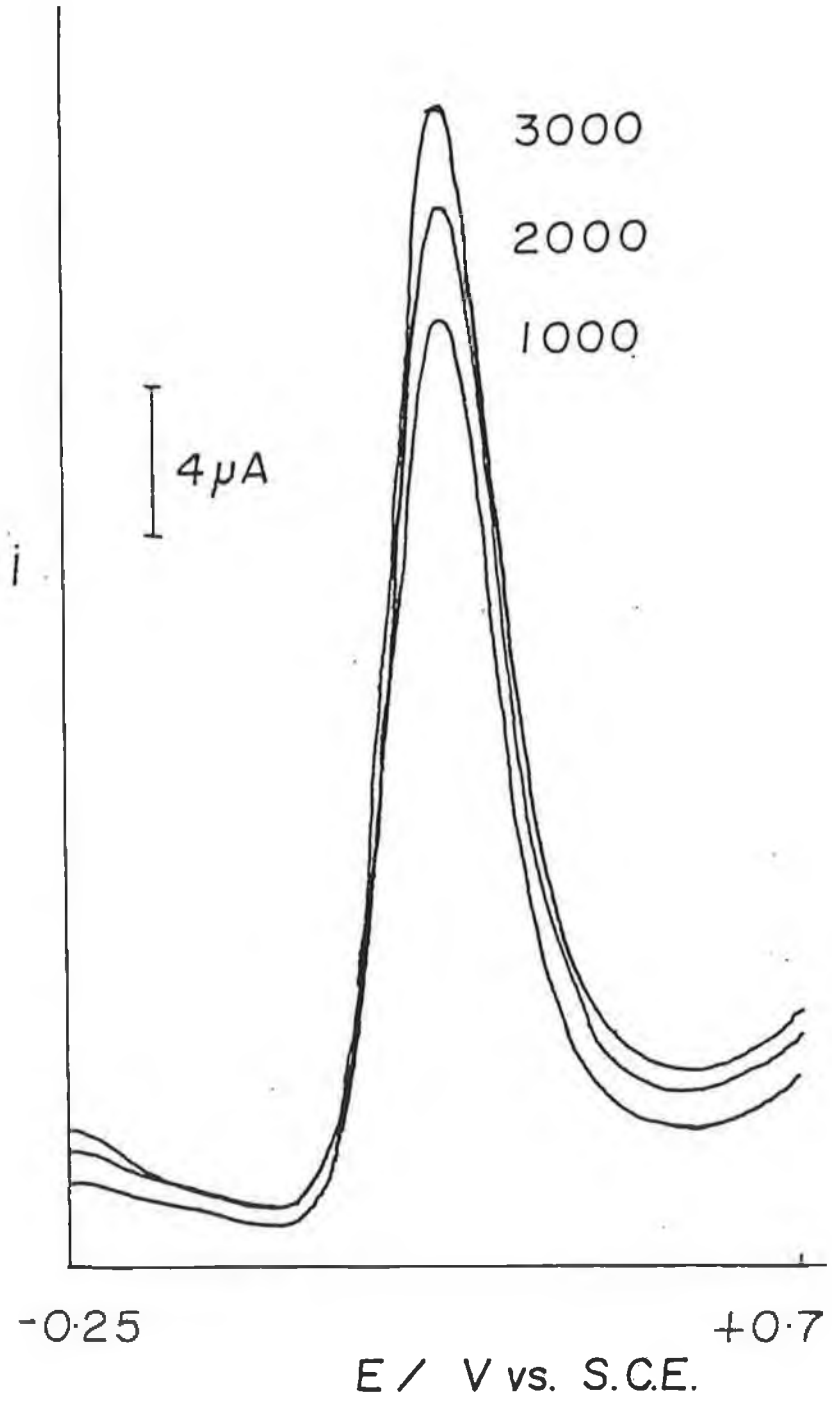

Figure 4.5: D.P.R.D.E. response for $\left[Fe(CN)_6\right]^{4-}$ (1×10^{-3}M) in aqueous KCl (0.1M). Platinum electrode (area = 0.051cm^2), scan rate =1×10^{-2}Vsec^{-1}, time constant = 1 sec, drop time ($\delta+\tau$) = 1 sec, pulse width (δ) = 5.5×10^{-2}sec, pulse amplitude = 100mV, rotation rates are shown in figure in rpm.

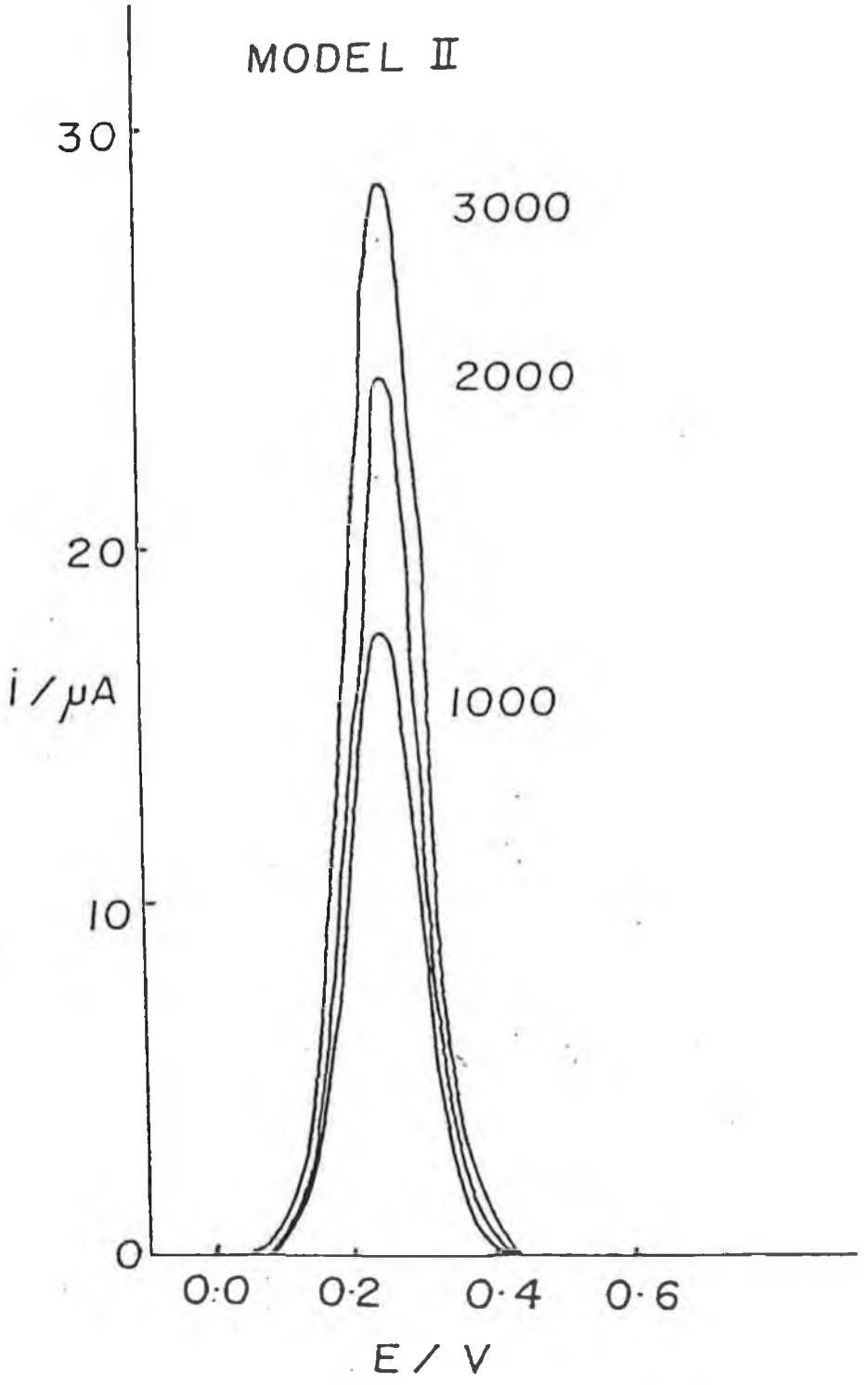

Figure 4.6: Simulated D.P.R.D.E. response using Model 2. $E^{0'} = 0.235V$, scan rate = 1×10^{-2} Vsec^{-1}, D = 6.5×10^{-6} cm^{2}sec^{-1}, area = 0.051cm^2, concentration = 1×10^{-3} M, $(\delta+\tau)$ = 1 sec, (δ) = 5.5×10^{-2} sec, kinematic viscosity = 0.01cm^2 sec^{-1}, pulse amplitude = 100mV and *f* values are shown in figure in rpm.

and similar behaviour was observed. However, a limitation of the models is reflected in the inability of the peaks to return to baseline, as can be seen in figures 4.4 and 4.5.

Figure 4.7 shows that at lower concentrations there is an increase in the background signal for higher pulse amplitudes, even though the analytically useful response also increases. The dashed line represents the background D.P.R.D.E. sweep, which has a U-shaped curve, which may be used to determine the point of zero charge of a solid electrode. There is a small peak present which may be due to a prussian blue impurity between the disk and the insulator. However, it can be seen that the analytical usefulness of the technique is limited by the double layer charging, current which is responsible for this background shape. The pulse amplitude affects the magnitude of this background response as well as the magnitude of the analyte signal.

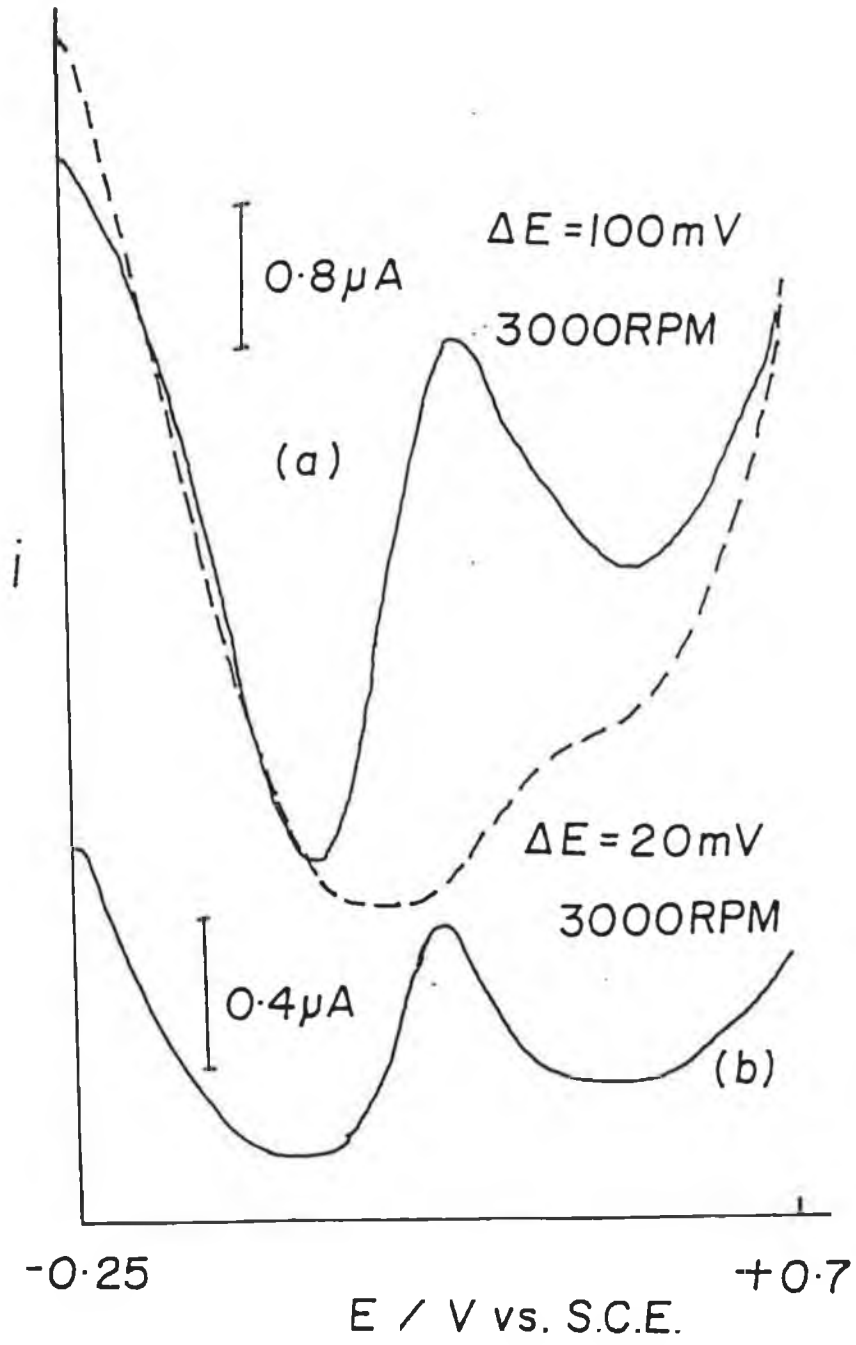

Figure 4.7(a): D.P.R.D.E. response for $\left[Fe(CN)_6\right]^{4-}$ (1×10^{-3}M) in aqueous KCl (0.1M) pulse amplitude = 100mV. Platinum electrode (area = 0.051cm^2), scan rate = 1×10^{-2}Vsec^{-1}, time constant = 1 sec, drop time ($\delta+\tau$) = 1 sec, pulse width (δ) = 5.5×10^{-2}sec, f = 3000rpm. Dashed line is background in absence of $\left[Fe(CN)_6\right]^{4-}$.

(b): As (a) but pulse amplitude = 20mV.

4.5 Conclusion

As the differential current depends on the diffusion layer thickness, which in turn depends on both the pulse width and the rotation rate, both models postulated here would hold, but for different conditions. Indeed while the results in this case seemed to coincide with an overlapping of both models, it would be expected that the shorter the pulse width and/or the greater the pulse amplitudes and/or the slower the rotation rate, the more the experiment would be governed by Model 1. From the experimental results it is clear that applying a differential pulse to an R.D.E. has an obvious advantage for the electrochemist. A peaked D.P.R.D.E. response is far more useful than a sigmoidal wave for obtaining information about a system. However, in order for the technique to be analytically useful, background correction would be necessary.

4.6 References

1. V.G. Levich, Physicochemical Hydrodynamics, Prentice Hall, Englewood Cliffs, New Jersey, (1962).

2. G. Lalande and G. Faubert, J. Power Sources, (1996) , **61**, 227.

3. S.M. Golabi and J.B. Raoof, J. Electroanal. Chem., (1996), **416**, 75.

4. Q. Wu and M. Maskus, Anal. Chem., (1996), **68**, 3688.

5. J.E. Anderson, A.M. Bond and R.D. Jones, Anal. Chem., (1981), **53**, 1016.

6. D.T. Sawyer and J.L. Roberts, Experimental Electrochemistry for Chemists, Wiley, New York, (1974), p.77.

7. A.J. Bard and L.R. Faulkner, Electrochemical Methods - Fundamentals and Applications, Wiley, NewYork, (1980), pp. 283-299.

5 Other Techniques for Electroanalysis

This chapter deals with two different electroanalytical methods and as a result it is broken into two different sections. Section 5.1 is concerned with the semidifferentiation of cyclic voltammograms of FCA, while in section 5.2 the effect of an applied differential pulse on the response from a HPLC electrochemical detector is studied for ascorbic acid.

5.1 Semidifferentiation of Cyclic Voltammograms of FCA

5.1.1 Introduction

A principle difficulty with the use of dynamic electrochemistry as a quantitative technique is the problem of overlapping waves. This is of particular importance in linear sweep voltammetry (lsv) and anodic stripping voltammetry (asv) at a stationary mercury electrode because of the very broad, asymmetric nature of the peaks. Another difficulty is that the current – potential relationship is not describable by an analytical function. These problems are particularly unfortunate since lsv instrumentation is easy to use and is relatively inexpensive.

One technique that can be used to solve this problem of resolution of overlapping waves is semidifferentiation. By using a data acquisition system and a computer program to semidifferentiate the resulting digitised voltammograms, the resolution of electrochemical peaks can be vastly improved.

The equation used here in the semidifferentiation of cyclic voltammograms is as follows [1];

$$m'(t) = \frac{2}{\left(\sqrt{\pi\Delta}\right)}\left\{\sum_{j=1}^{t/\Delta}\left[i(j\Delta) - i(j\Delta - \Delta)\right]\left[\sqrt{t/\Delta - j + 1} - \sqrt{t/\Delta - j}\right]\right\} \qquad 5.1$$

where m`(t) denotes the semiderivative of the current, i, measured as a function of time, j is the counter, and Δ denotes the time interval, which should be constant.

5.1.2 Experimental Procedure

All chemicals employed were of reagent grade, and were used without further purification. All voltammetric experiments were carried out in air and at room temperature in a single compartment, three-electrode cell. A saturated calomel electrode (SCE) was employed as the reference electrode, the auxiliary was a carbon rod and each of three working electrodes was used at different stages during this work. These were glassy carbon, platinum and gold and were polished thoroughly with alumina, and rinsed with de-ionised water prior to use.

A ramp generator (HB Thompson 16 bit), an Edt potentiostat (Model ECP 100) and an X-Y chart recorder (J.J. Lloyd PL3) were used for cyclic voltammetry. A "Pasco Data Monitor" was used as a data acquisition program [2]. A fortran program was used to semidifferentiate the digitised voltammograms, and "Microsoft EXCEL" was used to plot the outputs. Digital simulation of the voltammetry was done using collocation [3].

5.1.3 Results and Discussion

Figure 5.1 shows a simulated cyclic voltammogram (full line -) and the corresponding semiderivative output (dotted line - m`(t)) for a series of species with different formal potentials and relative concentrations of 1:2:3:4. As illustrated in

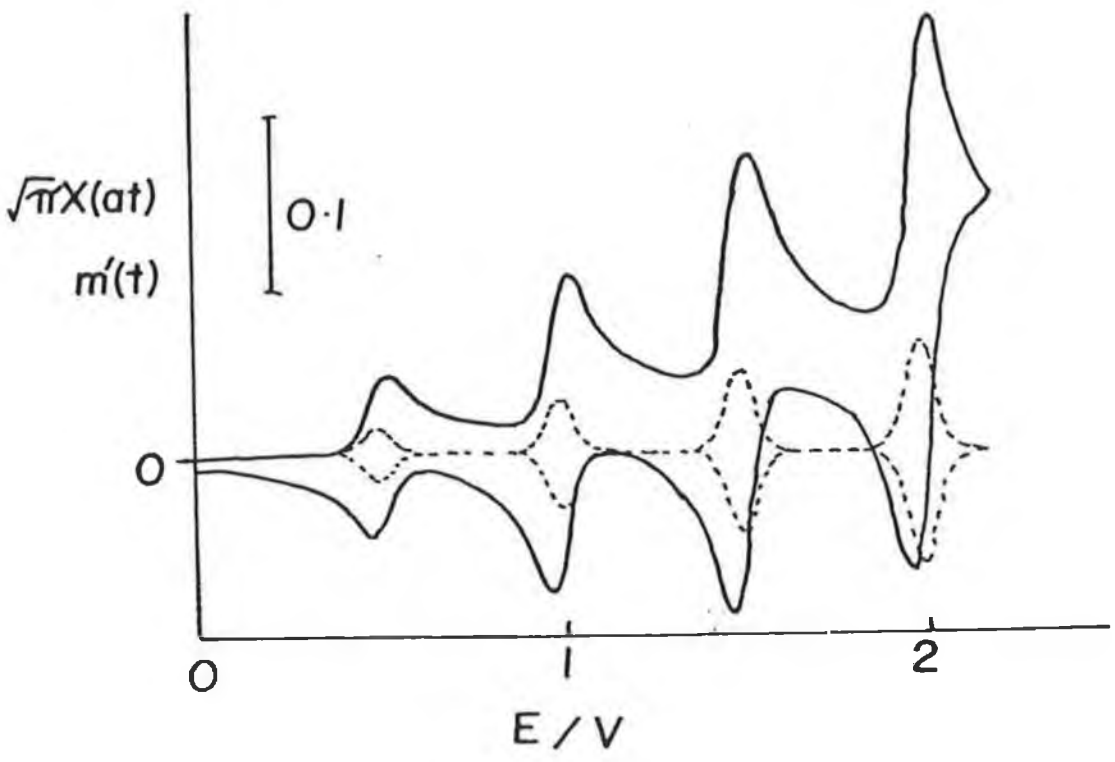

Figure 5.1: Simulated cyclic voltammogram (full line) of a series of species with formal potentials equal to 0.5, 1.0, 1.5, and 2.0V and relative concentrations of 1:2:3:4 respectively along with the corresponding semiderivative output (dotted line). The y axes have dimensionless units $((\pi)^{1/2}\chi(at))$ for the cyclic voltammogram and have units of $s^{-1/2}$ in the case of the semiderivative.

figure 5.1, there are many advantages in semidifferentiating cyclic voltammograms. These advantages are listed below.

1. Semidifferentiation results in baseline resolution of the redox processes occurring. This results in better separation of redox couples and eliminates the problems associated with the evaluation of individual peak currents from cyclic voltammograms of multi-redox processes.

2. There is a direct increase in peak height with concentration for the semiderivative, so that the last peak is 4 times the magnitude of the first peak. This is not evident with the cyclic voltammogram.

3. For the semiderivative the oxidation and reduction peaks occur at the same potential, which simplifies the task of estimating the formal potential of a particular species.

A disadvantage is that the actual signal magnitude for the semiderivative is smaller than that of the cyclic voltammogram.

Figure 5.2 shows the cyclic voltammogram (full line) and the semiderivative (dotted line - m`(t)) for a real system (ferrocyanide). The response is similar to theory in that despite the practical double layer charging current, this does not appear in the semiderivative plot. This system was investigated at low scan speeds, in order to verify the semidifferentiation procedure. Comparing figure 5.2 to figure 5.1, it is clear that the ferrocyanide system exhibits behaviour very close to that of an ideal system.

Figure 5.3 shows a cyclic voltammogram (full line) of ferrocene carboxylate (dotted line) and its semiderivative. The post-peak discussed in chapter 2 can be seen clearly

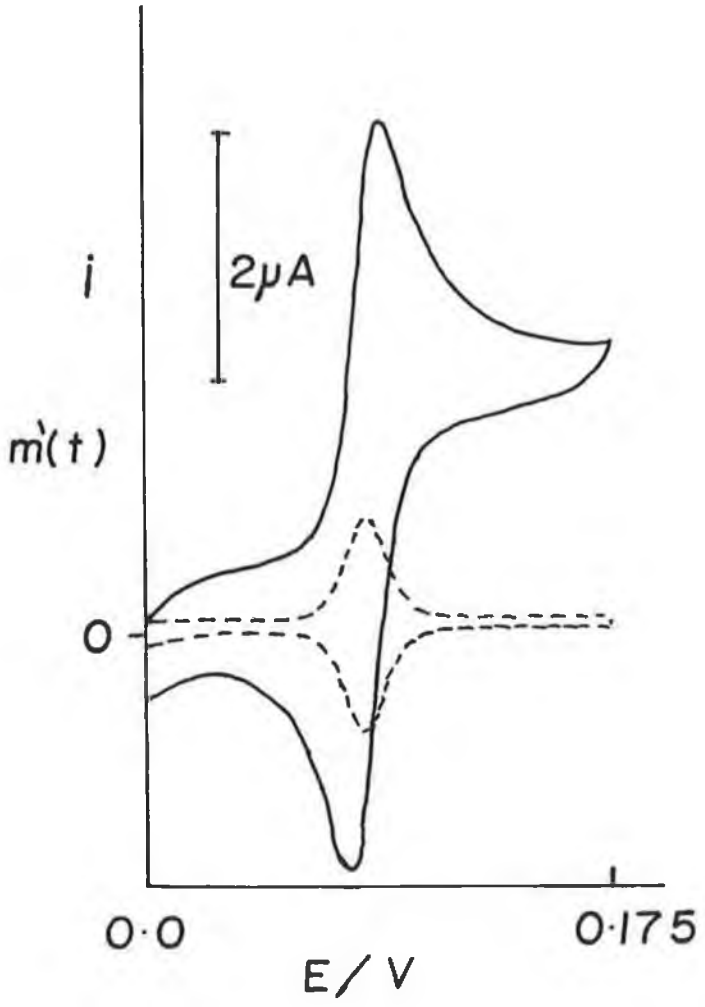

Figure 5.2: Experimental cyclic voltammogram (full line) for a solution of 1mM $K_4Fe(CN)_6$ in 0.1M KCl. Sweep rate = 5 mVs^{-1} at a C electrode vs SCE. The units for the dashed semiderivative plot are in $As^{-1/2}$.

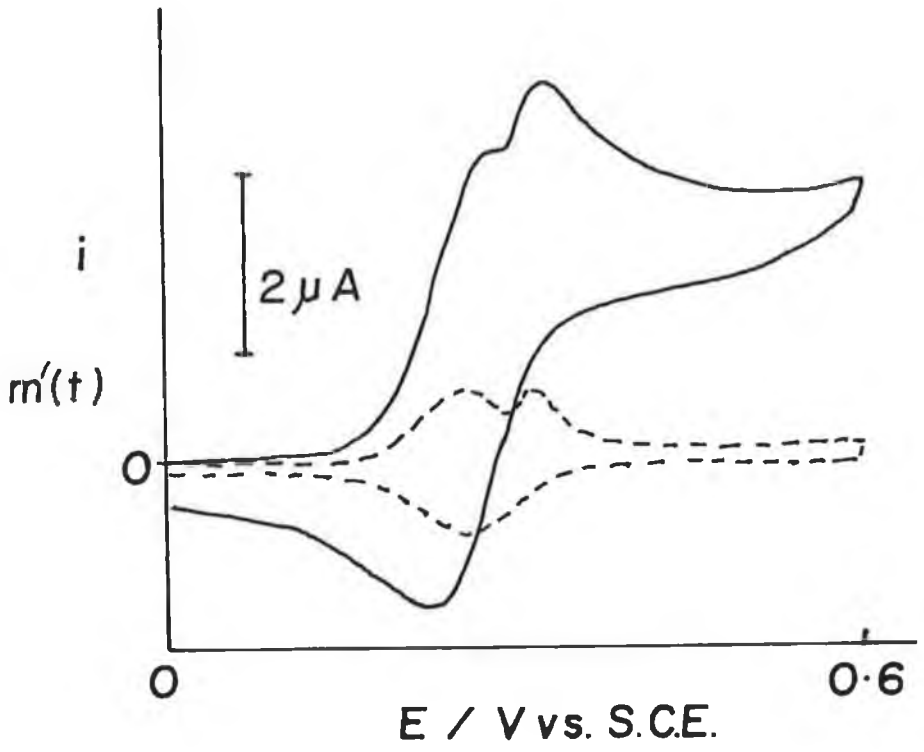

Figure 5.3: Experimental cyclic voltammogram of a solution of 1mM ferrocene carboxylate in phosphate buffer (pH = 9), at an Au electrode vs SCE. Sweep rate = 5 mVs^{-1}. The units for the dashed semiderivative plot are in $As^{-1/2}$.

on both plots. The reverse peak is a little smaller than the forward peak in the cyclic voltammogram, although this may be a result of the post-peak perhaps enhancing the forward peak. The semiderivative shows both peaks having the same magnitude.

It was hoped to discount the theory that the post-peak was due to adsorption, by looking at the semiderivative of a thin-layer system. Figure 5.4 shows the semiderivative (dotted line) of a thin layer simulated cyclic voltammogram (full line). There is an asymmetric hysteresis present, which is not seen in figure 5.3. This tends to indicate that the post-peak is not due to a surface confined species.

Figure 5.5 shows experimental cyclic voltammograms and semiderivatives as a function of two different concentrations of FCA. It can be seen that there is a change in the formal potential for the system as a function of concentration. This could be due to a fault with the data acquisition software used, since this effect is not seen on a chart recorder. The post-peak may be seen more clearly in the semiderivative plots.

Simulations were carried out to look at an EC mechanism as a possible system for the post-peak, based on the following equations:

$$Fc \rightarrow Fc^{+} + e^{-} \qquad 5.2$$

$$Fc^{+} + A \xrightarrow{k} Fc + B \qquad 5.3$$

Cyclic voltammograms were simulated for the system, and the semiderivatives were calculated. Figure 5.6 shows an example of this simulation for an intermediate value of k. It can be seen that although the cyclic voltammogram is affected by the subsequent reaction, the semiderivative is less affected. It is interesting to note that there is still a reverse peak in the case of the semiderivative – which implies that the

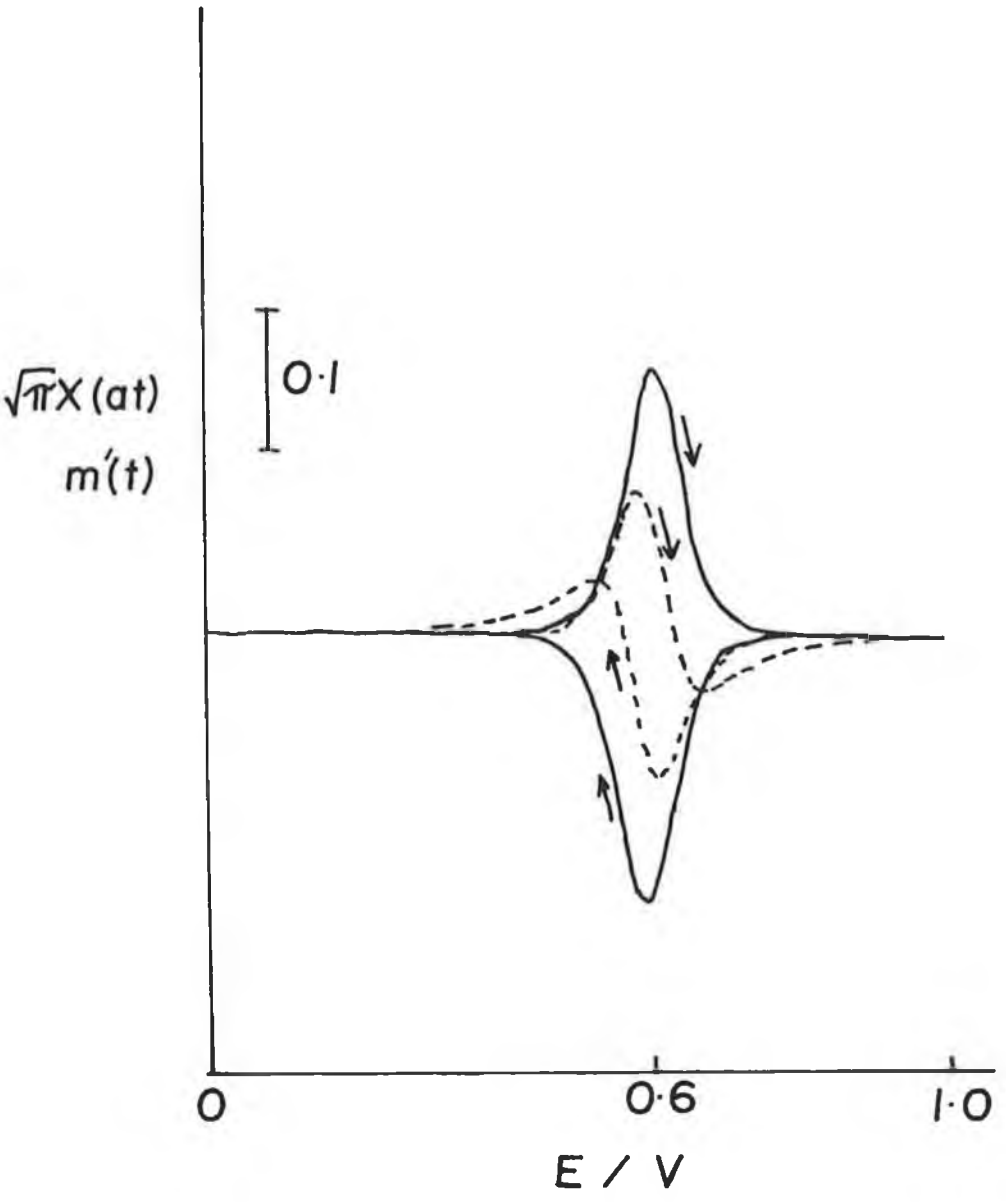

Figure 5.4: Simulated cyclic voltammogram (full line) of a thin layer species and the corresponding semiderivative (dashed line). E_O is 0.6V, layer thickness = 1.2×10^{-3}cm, sweep rate = $20mVs^{-1}$, D = $2\times10^{-6}cm^2sec^{-1}$, concentration = 3mM.

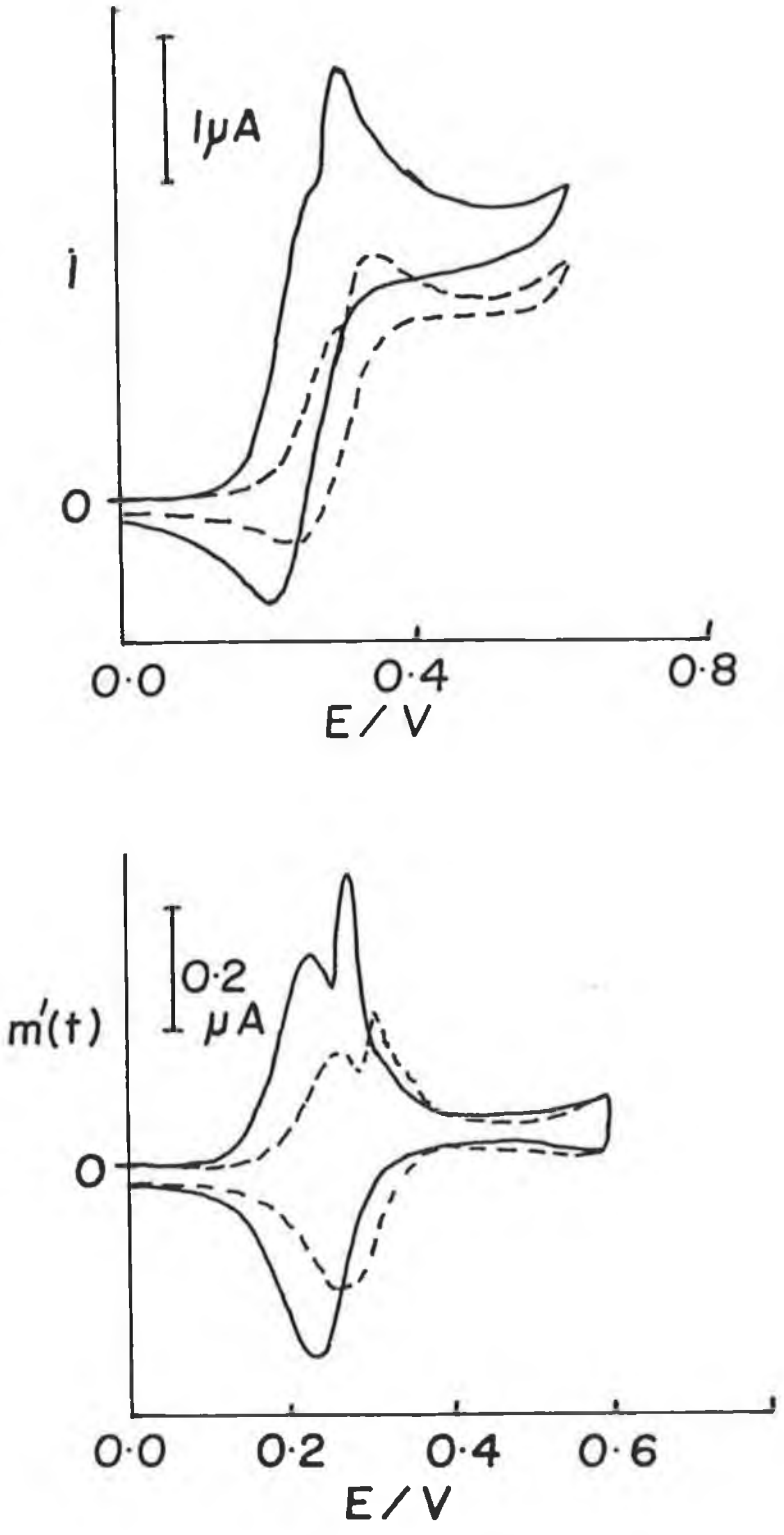

Figure 5.5: Cyclic voltammogram and semiderivative for a solution of FCA when the concentrations were 2mM and 1mM, at a gold electrode vs SCE. Sweep rate=2mVs^{-1}.

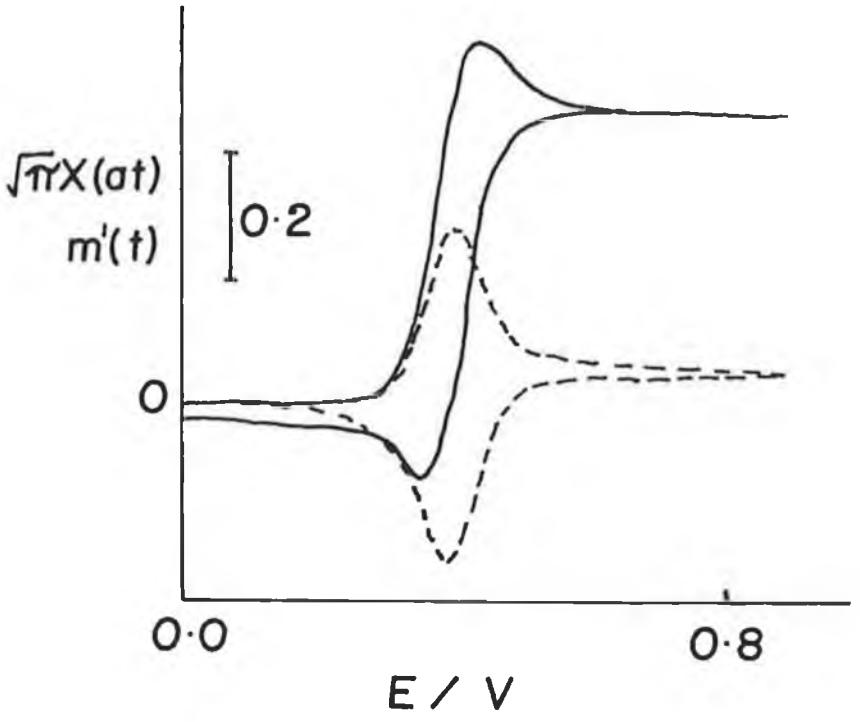

Figure 5.6: Simulated cyclic voltammogram for an EC mechanism where k = 0.15, D = 3×10^{-6}cm^{2}sec^{-1}, concentration = 3mM, and sweep rate = 20mVs^{-1}.

subsequent reaction is seen in the semiderivative plot as a change in baseline after the peak.

Figure 5.7 shows a situation when the subsequent reaction rate is large – leaving a sigmoidal-shaped cyclic voltammogram. The semiderivative takes the shape of a reversible cyclic voltammogram. This implies that the semiderivative ignores, to a certain extent, the subsequent reaction.

In an effort to simulate the ferrocene carboxylate system, a model consisting of a bulk species, followed by a surface confined species was examined as shown in figure 5.8. The corresponding semiderivative, where the concentration of the confined species is increased, is shown in figure 5.9. It can be seen that the semiderivative in figure 5.9 does not resemble any of the experimental semiderivative outputs. This indicates that the post-peak is not due to a confined layer.

Figure 5.10 shows a simulation for a reversible bulk species with a subsequent irreversible system and this appears to model the experimental outputs from the ferrocene carboxylate system (figure 5.5) best. The limitation of the simulation is that the same plot may be obtained by adjusting a number of different parameters.

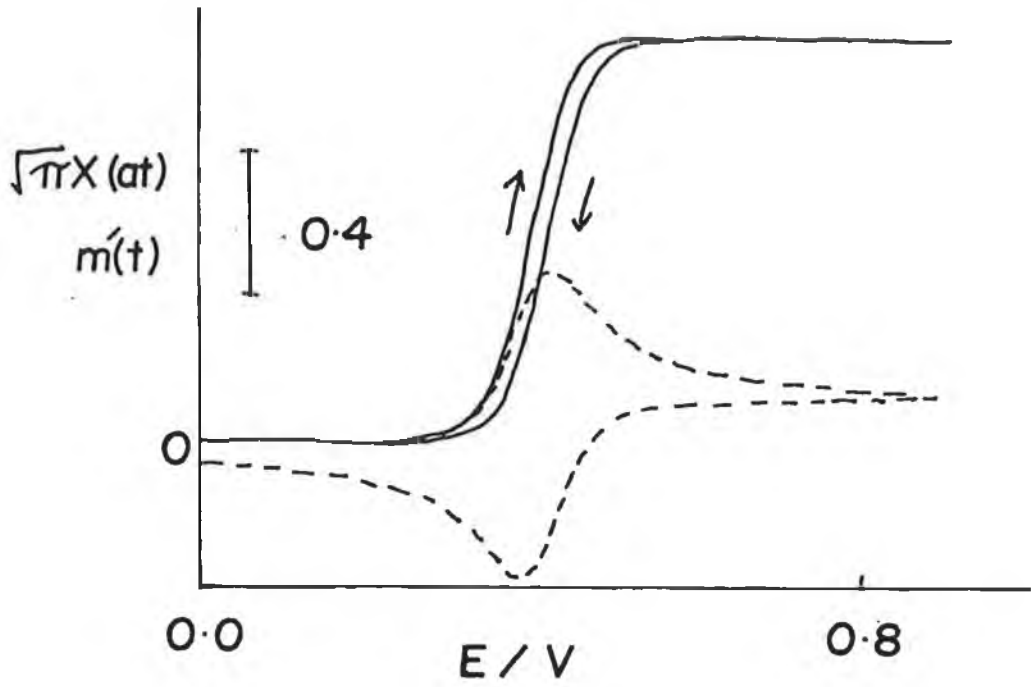

Figure 5.7: Simulated cyclic voltammogram for an EC mechanism where k = 0.99, D = 3×10^{-6}cm^{2}sec^{-1}, concentration = 3mM, and sweep rate = 20mVs^{-1}.

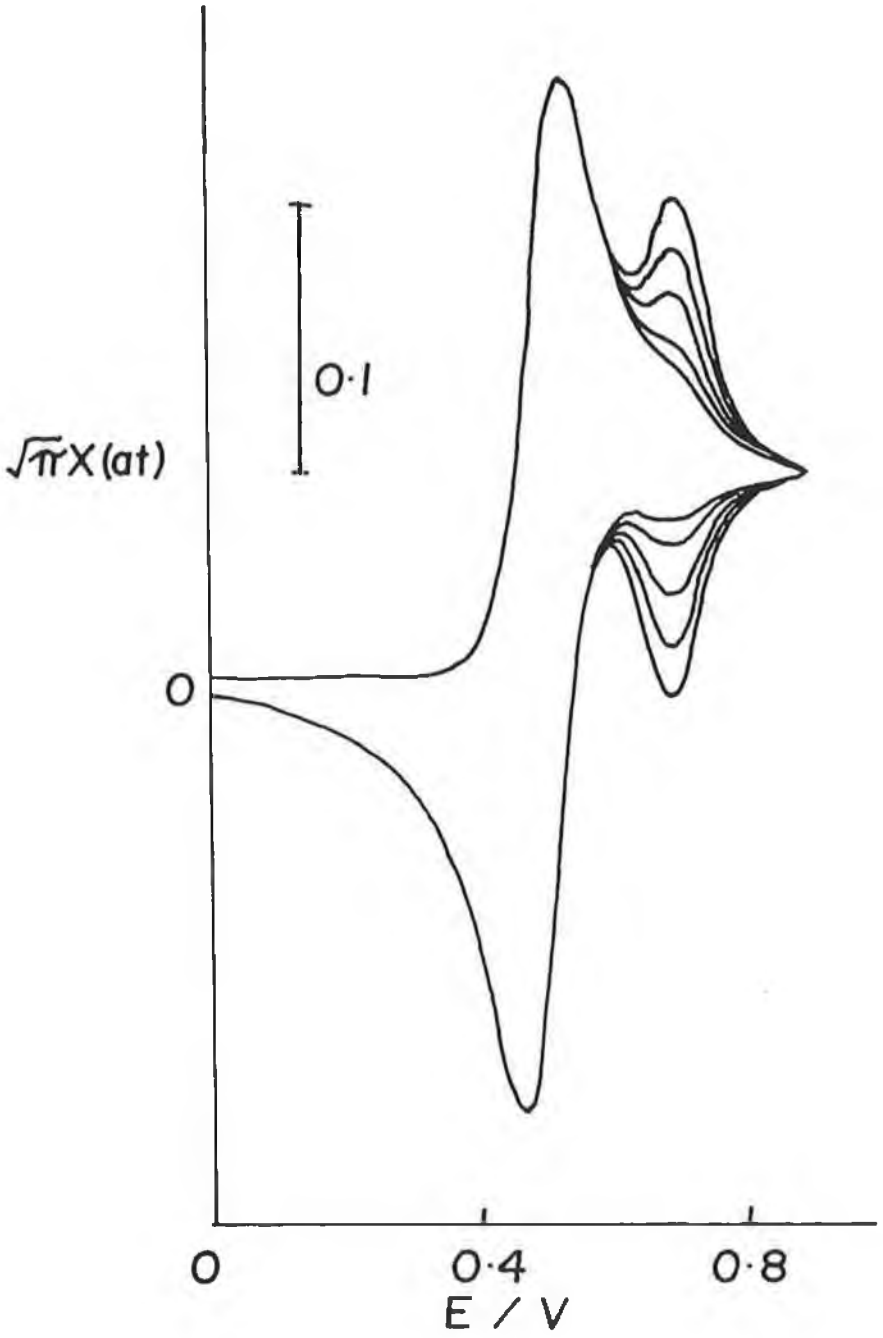

Figure 5.8: Simulated cyclic voltammogram for 2 redox couples - one bulk species ($E^{0'}$ = 0.5V) and one surface confined species ($E^{0'}$ = 0.7V). Sweep rate = 20mVs^{-1}, D = 2×10^{-6}cm^{2}sec^{-1}, C_{Total} = 3mM, layer thickness = 1.2×10^{-3}cm, fraction of total concentration, C, is C_{bulk} = 0.5, and fraction of total concentration of confined species is 0.1, 0.2, 0.3, 0.4, and 0.5.

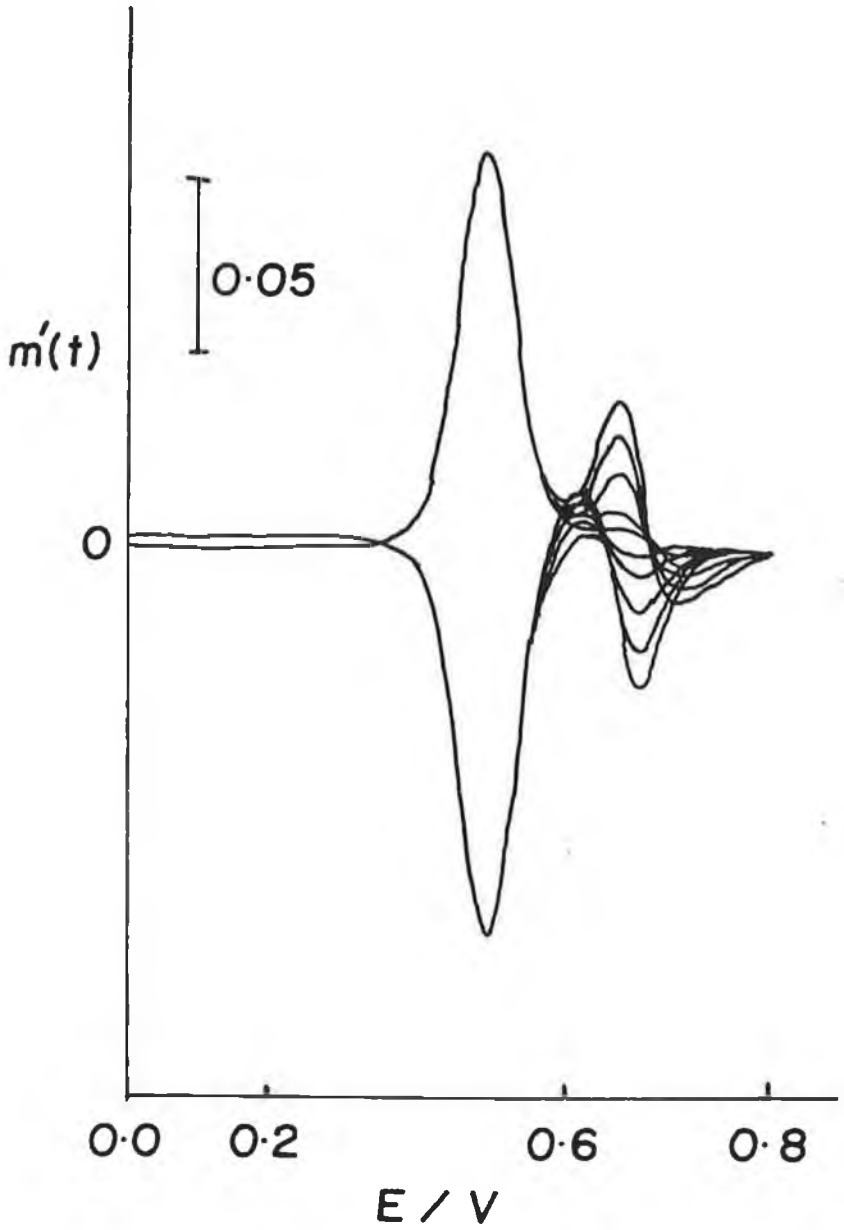

Figure 5.9: Simulated semiderivative for 2 redox couples - one bulk species ($E^{0'}$ = 0.5V) and one surface confined species ($E^{0'}$ = 0.7V). Sweep rate = 20mVs^{-1}, D = 2×10^{-6}cm^{2}sec^{-1}, C_{Total} = 3mM, layer thickness = 1.2×10^{-3}cm, fraction of total concentration, C, is C_{bulk} = 0.5, and fraction of total concentration of confined species is 0.1, 0.2, 0.3, 0.4, and 0.5.

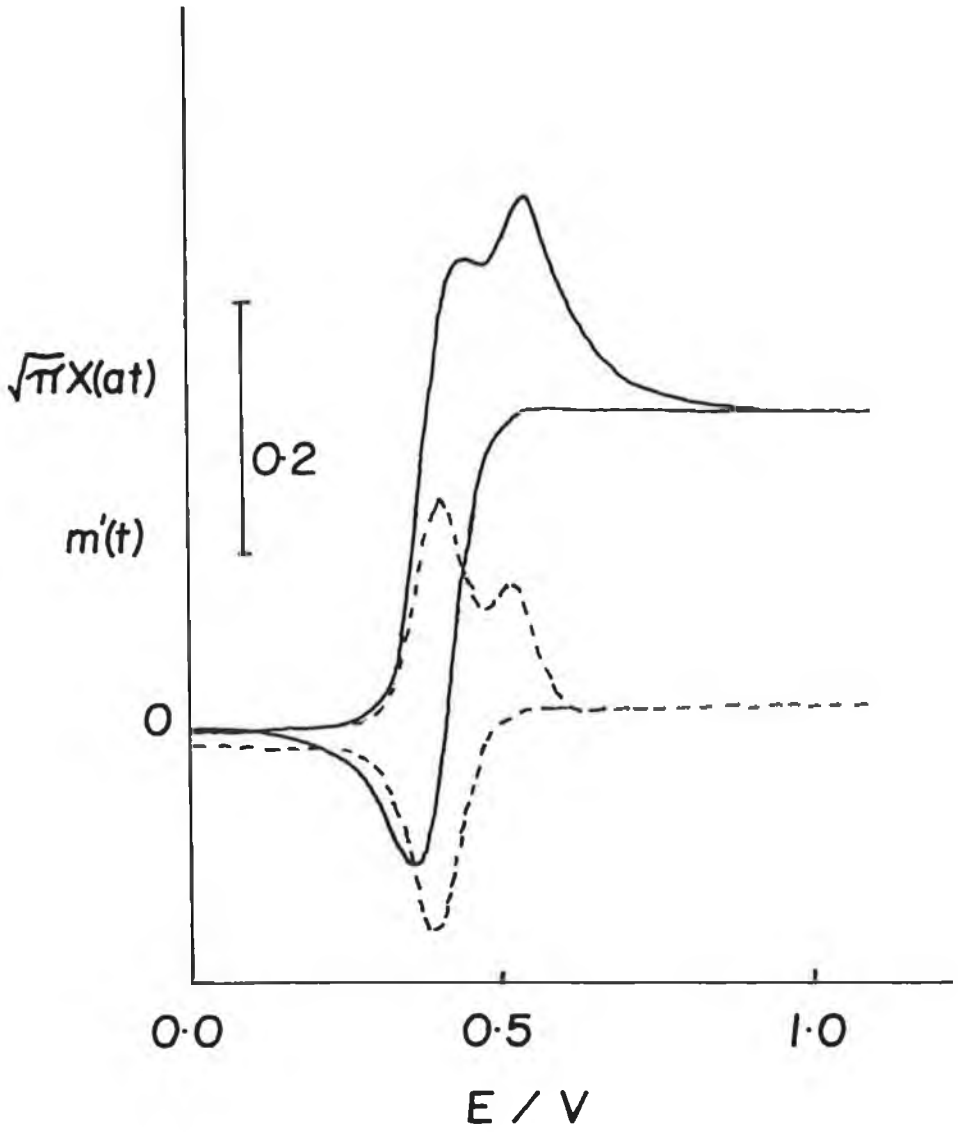

Figure 5.10: Simulated cyclic voltammogram (full line) and semiderivative (dotted line) for a bulk species with a subsequent catalytic current and an irreversible adsorbed species. The ratio of amounts is 7:3 for the bulk to surface species respectively. Sweep rate = $20mVs^{-1}$, D = $2\times10^{-6}cm^2sec^{-1}$, and the catalytic rate constant = $0.1s^{-1}$. The formal potential for the bulk species = 0.4V, and 0.55V for the adsorbed species. The thickness of the adsorbed layer = 4.2×10^{-3}cm.

5.1.4 Conclusion

The semidifferentiation of cyclic voltammograms has many advantageous, analytically useful features. As a function of its symmetrical shape, it provides a powerful analytical tool to the electrochemist in the calculation of peak currents and formal potentials of individual redox processes in multi-redox couple systems.

The information gained from the simulated and experimental semiderivatives of cyclic voltammograms of FCA indicated that the post-peak is not due to a surface confined species.

5.2 HPLC of Ascorbic Acid with Electrochemical Detection

5.2.1 Introduction

Having seen the benefits of applying a differential pulse at a microelectrode (see chapter 3) and at a rotating disk electrode (see chapter 4), the idea of applying a differential pulse at a HPLC electrochemical detector for the enhanced detection of ascorbic acid appeared reasonable.

It was surmised that using a pulsed method of detection would compare favourably to the direct current approach to electrochemical detection. It was expected that as a number of ascorbic acid samples passed through the column the magnitude of the peak corresponding to ascorbic acid elution would decrease, when direct current detection was employed. This effect would, in theory, be caused by a fouling of the electrode by ascorbic acid oxidation intermediates, which would decrease the current response, thus causing a decrease in peak magnitude. Conversely, it was thought that

applying a differential pulse to this electrode would instantaneously desorb any ascorbic acid oxidation intermediates attempting to adsorb onto the electrode and therefore give a constant response, independent of the number of consecutive samples analysed.

In an effort to prove these theories true, experiments were carried out for both the direct current and differential methods – the results are given below in section 5.2.3.

5.2.2 Experimental Procedure

All chemicals used were of reagent grade and were used without further purification. An Edt potentiostat (Model ECP 100) was used to apply both the direct and differential pulse waveforms. The ascorbic acid samples were analysed on a HPLC, C^{18} column fitted with a Shimadzu electrochemical detector. The mobile phase consisted of a 0.1M acetic acid/sodium acetate solution.

5.2.3 Results and Discussion

Five consecutive samples of ascorbic acid were analysed for both the direct current and the differential pulse methods of detection and the results are shown in table 5.1.

Table 5.1: Comparison of direct current and differential pulse detection methods

Direct Current				Differential Pulse			
Att	rt(mins)	Sample No.	Peak Area	Att	rt(mins)	Sample No.	Peak Area
5	2.972	1	216404	0	2.923	1	733
5	2.97	2	220101	0	2.928	2	792
5	2.96	3	213334	0	2.922	3	801
5	2.972	4	188133	0	2.93	4	787
5	2.965	5	171482	0	2.928	5	783

As can be seen in table 5.1, the magnitude of the peaks for the direct current experiments are far greater than the magnitudes of the differential pulse peaks. This may be due to the fact that, while in the direct current experiments the electrode is held at a constant potential of 0.5V, the differential pulse technique subtracts the current before the pulse from the current after the pulse. Also the differential pulse peaks occur slightly earlier. The reason for this is unknown.

It is also clear from table 5.1 that the direct current peak areas decrease in magnitude with increasing number of samples analysed. This agrees with the theoretical predictions. On the other hand the peak magnitudes for the differential pulse remain relatively constant. This is due to the cleaning nature of the pulsed waveform.

In an attempt to characterise the response from the differential pulse, the applied pulse parameters were varied for the analysis of samples of ascorbic acid of the same concentration. The resulting outputs are shown in figure 5.11(b) – (e), where they are shown in contrast to the direct current output in figure 5.11(a). Figure 5.11(b) shows the bipolar differential current output associated with a pulse drop time of 1 second. As this drop time is shortened to 0.5 sec and 0.1 sec in figures 5.11(c) and 5.11(d) respectively, the response becomes less bipolar. While figure 5.11(e) has the same drop time as figure 5.11(d), the pulse amplitude in figure 5.11(e) is 20mV whereas the pulse amplitude in figure 5.11(d) is 100mV. This decrease in pulse amplitude has the effect of making the output more bipolar again. Therefore, care is needed when choosing the drop time and pulse amplitude.

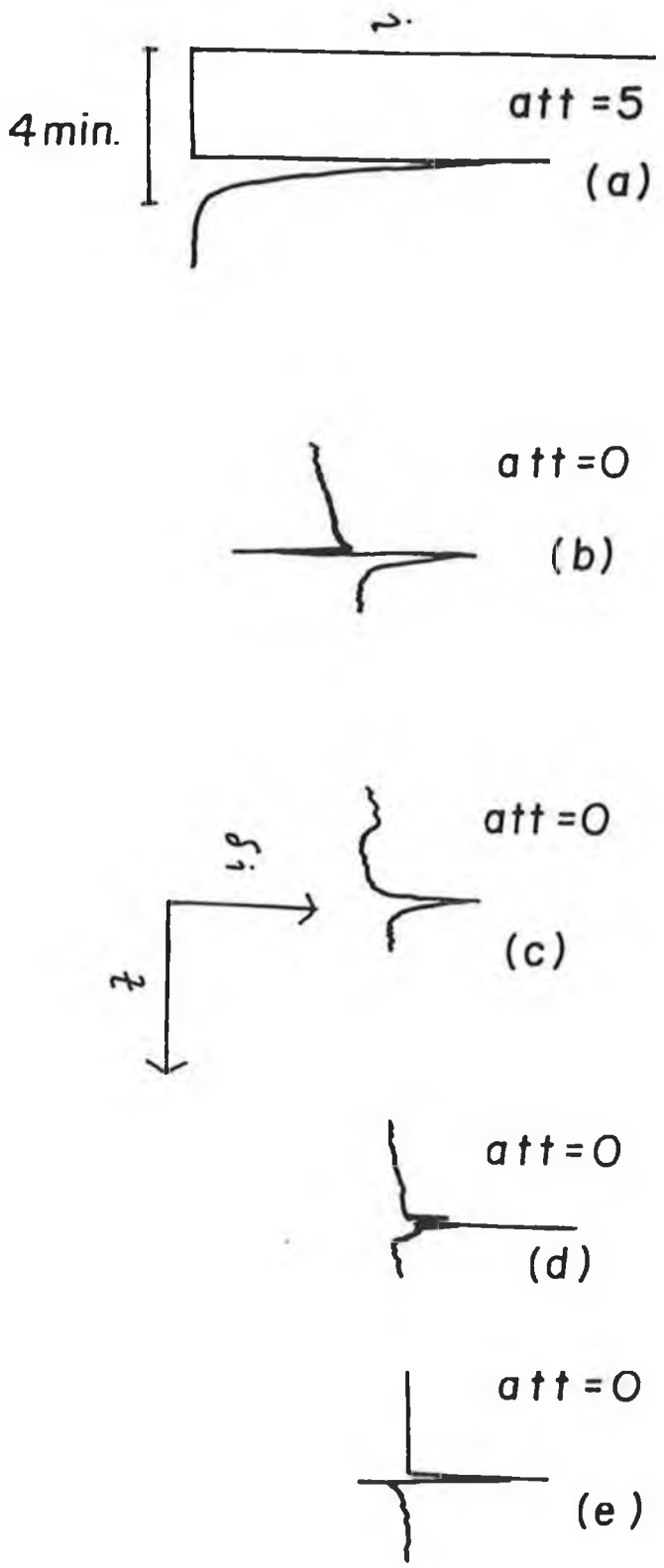

Figure 5.11: (a) Direct current HPLC output where the potential was stepped from 0V to 0.5V. (b)-(e) Differential pulse HPLC outputs where pulse drop times are 1, 0.5, 0.1 and 0.1sec respectively, and pulse amplitudes are 100, 100, 100, and 20mV respectively.

5.2.4 Conclusion

While the differential current output was shown to be relatively consistent, it is suggested that it is not as analytically useful as the direct current outputs due to the large decrease in sensitivity encountered when using the differential pulse technique. However there are also faults with the direct current responses as illustrated in the asymmetrical shape of the peaks, and the trend shown in table 5.1 of decreasing peak area with increasing sample number.

5.3 References

1. M. Grennes, and K.B. Oldham, Anal. Chem., (1972), **44**, 1121.

2. PASCO scientific, 10101 Foothills Blvd., Roseville, California.

3. J.F. Cassidy in, Electroactive Polymer Chemistry Part 2 – Fundamentals and Applications, ed. M.E. Lyons, Plenum Press (1996), p79.